



UNIVERSITEIT•STELLENBOSCH•UNIVERSITY  
jou kennisvennoot • your knowledge partner

# Mesh Termination Schemes for the Finite Element Method in Electromagnetics

by

André Young



*Thesis presented at the University of Stellenbosch in partial  
fulfilment of the requirements for the degree of*

Master of Science in Engineering

Department of Electrical Engineering  
University of Stellenbosch  
Private Bag X1, 7602 Matieland, South Africa

Study leader: Prof D.B. Davidson

December 2007

# Declaration

I, the undersigned, hereby declare that the work contained in this thesis is my own original work and that I have not previously in its entirety or in part submitted it at any university for a degree.

Signature: .....

A. Young

Date: .....

# Abstract

The finite element method is a very efficient numerical tool to solve geometrically complex problems in electromagnetics. Traditionally the method is applied to bounded domain problems, but it can also be forged to solve unbounded domain problems using one of various mesh termination schemes.

A scalar finite element solution to a typical unbounded two-dimensional problem is presented and the need for a proper mesh termination scheme is motivated. Different such schemes, specifically absorbing boundary conditions, the finite element boundary integral method and infinite elements, are formulated and implemented. These schemes are directly compared using different criteria, especially solution accuracy and computational efficiency.

A vector finite element solution in three dimensions is also discussed and a new type of infinite element compatible with tetrahedral vector finite elements is presented. The performance of this infinite element is compared to that of a first order absorbing boundary condition.

# Opsomming

Die eindige element metode is 'n baie effektiewe numeriese metode om probleme in elektromagnetika op te los wat ingewikkelde geometrië bevat. Oorspronklik is die metode gebruik om eindige gebied probleme op te los, maar dit kan ook gebruik word om oneindige gebied probleme op te los indien die eindige element maas behoorlik afgesluit word.

'n Skalaar eindige element metode word geïmplementeer om 'n tipiese oneindige gebied probleem in twee dimensies op te los en die behoefte aan 'n behoorlike maas afsluiting metode word gemotiveer. Verskeie sulke afsluiting metodes, spesifiek absorberende randvoorwaardes, die eindige element grensintegraal metode en oneindige elemente, word bespreek en geïmplementeer. Hierdie metodes word ook direk met mekaar vergelyk, veral op grond van akkuraatheid en effektiwiteit.

'n Vektor eindige element oplossing in drie dimensies word ook bespreek en 'n nuwe oneindige element wat versoenbaar is met tetraheder vektor eindige elemente word ten toon gestel. Die gebruik van hierdie oneindige element word vergelyk met die gebruik van 'n eerste orde absorberende randvoorwaarde.

# Acknowledgements

I would like to express my sincerest gratitude toward the following people and organisations for their contribution to the success of this project.

- Prof. D.B. Davidson for introducing me to this exciting field of research and for his excellent academic leadership
- The other CEMAGG members: M.M. Botha, N. Marais, J.P. Swartz, R. Marchand and E. Lezar for various insightful ideas and for providing a rich learning environment
- My family for a valuable education and their unconditional love and support
- Big thanks to all my friends, however obscure their involvement in this project, and especially to those who had absolutely nothing to do with it!
- Special thanks to the occupants of E206 for accommodating the odd one out: S. Schulze, D.I.L. de Villiers, D.M.P. Smith, T. Stander and M. van der Walt
- D.N.J. Els for the US-Thesis Package and C.J.P. Brand for the easy installation instructions
- The University of Stellenbosch and specifically the Department of Electrical and Electronic Engineering for outstanding quality of education
- The NRF for financial support granted

# Contents

<b>Declaration</b>	<b>i</b>
<b>Abstract</b>	<b>ii</b>
<b>Opsomming</b>	<b>iii</b>
<b>Acknowledgements</b>	<b>iv</b>
<b>Contents</b>	<b>v</b>
<b>List of Figures</b>	<b>vii</b>
<b>List of Tables</b>	<b>ix</b>
<b>1 Introduction</b>	<b>1</b>
<b>2 A Finite Element Solution in 2D</b>	<b>3</b>
2.1 Background . . . . .	3
2.2 The Scattering Problem in 2D . . . . .	4
2.3 Finite Element Solution . . . . .	5
2.4 Conclusion . . . . .	17
<b>3 Mesh Termination Schemes in 2D</b>	<b>18</b>
3.1 Background . . . . .	18
3.2 Absorbing Boundary Conditions . . . . .	19
3.3 Finite Element Boundary Integral Method . . . . .	25
3.4 Infinite Elements . . . . .	40
3.5 Comparison of Mesh Termination Schemes . . . . .	52
3.6 Conclusion . . . . .	58

<b>4</b>	<b>A Finite Element Solution in 3D</b>	<b>59</b>
4.1	Background . . . . .	59
4.2	Unbounded Problems in 3D . . . . .	60
4.3	A Finite Element Solution . . . . .	62
4.4	Conclusion . . . . .	70
<b>5</b>	<b>Infinite Elements in 3D</b>	<b>71</b>
5.1	Background . . . . .	71
5.2	Infinite Element Solution Formulation . . . . .	72
5.3	Discretisation . . . . .	73
5.4	The 3D Infinite Element . . . . .	75
5.5	Results . . . . .	83
5.6	Conclusion . . . . .	90
<b>6</b>	<b>General Conclusion</b>	<b>91</b>
6.1	Recommendations . . . . .	92
	<b>Appendices</b>	<b>93</b>
<b>A</b>	<b>Special Functions</b>	<b>94</b>
A.1	Bessel and Related Functions . . . . .	94
A.2	$En$ -Function . . . . .	96
A.3	Legendre Polynomials . . . . .	98
<b>B</b>	<b>The Green Function and Integral Equations</b>	<b>99</b>
B.1	Integral Equation Derivation . . . . .	99
B.2	Integration over the Green Function Singularity . . . . .	101
B.3	Integrating over the Green Function Derivative Singularity . . . . .	103
<b>C</b>	<b>2D Infinite Element Integrals</b>	<b>106</b>
C.1	Elemental Integrals - Galerkin Weighted . . . . .	106
C.2	Elemental Integrals - Complex Conjugate Weighted . . . . .	109
<b>D</b>	<b>3D Infinite Element Integrals</b>	<b>113</b>
D.1	Integrand Evaluations . . . . .	113
D.2	Gauss-Legendre Quadrature on Triangular Elements . . . . .	119
D.3	Integration of Singular Functions . . . . .	122
	<b>Bibliography</b>	<b>124</b>

# List of Figures

2.1	Description of two-dimensional scattering problem. . . . .	4
2.2	The two-dimensional finite element domain. . . . .	6
2.3	Coordinate rotation on a boundary edge. . . . .	15
3.1	An approximate curvature radius is calculated locally for an edge. . . . .	22
3.2	Scattered electric near-field computed using absorbing boundary conditions. . . . .	24
3.3	Echo width of perfectly electrical conducting cylinder computed using absorbing boundary conditions. . . . .	24
3.4	Subdivision of segments to integrate the Green function more accurately. . . . .	31
3.5	Scattered electric near-field computed using the finite element boundary integral method. . . . .	33
3.6	Echo width of perfectly conducting electrical cylinder computed using the finite element boundary integral method. . . . .	33
3.7	Total electric near-field computed using the total field formulation of the finite element boundary integral method. . . . .	37
3.8	Susceptibility of the finite element boundary integral method to interior resonances. . . . .	38
3.9	Interior resonances at higher frequencies. . . . .	39
3.10	Effect of loss on the solution accuracy for the finite element boundary integral method near an interior resonance. . . . .	40
3.11	The infinite element domain for the scattering problem in two dimensions. . . . .	41
3.12	Compatibility between finite and infinite elements. . . . .	47
3.13	Placement of radial nodes for higher order infinite elements. . . . .	48



3.14	Scattered electric near-field computed using infinite elements with various orders of radial expansions. . . . .	49
3.15	Echo width of perfectly electrical conducting cylinder computed using infinite elements with a third order radial expansion. . . . .	50
3.16	Scattered electric near-field computed using complex conjugate weighted infinite elements. . . . .	51
3.17	Effect of mesh fineness on the error for different mesh termination schemes. . . . .	53
3.18	Effect of outer boundary radius on the error for different mesh termination schemes. . . . .	54
4.1	Description of the three-dimensional scattering problem. . . . .	61
4.2	Description of the radiating current filament problem. . . . .	62
5.1	The shape of the three-dimensional infinite element. . . . .	76
5.2	Node numbers for a higher order infinite element. . . . .	82
5.3	Scattered field computed using a first order absorbing boundary condition. . . . .	84
5.4	Scattered field computed using a first order infinite element. . . . .	85
5.5	Radiated field computed using a first order absorbing boundary condition and first order infinite element. . . . .	86
5.6	Effect of mesh fineness on accuracy of absorbing boundary condition and infinite element solutions. . . . .	87
5.7	Effect of boundary radius on accuracy of absorbing boundary condition and infinite element solutions for a coarse mesh. . . . .	88
5.8	Effect of boundary radius on accuracy of absorbing boundary condition and infinite element solutions for a fine mesh. . . . .	88
5.9	Effect of boundary radius on accuracy of absorbing boundary condition and infinite element solutions for a fine mesh. The infinite element scheme rotates each infinite element toward the equator. . . . .	90
B.1	Integration paths near a singularity of the derivative of the Green function. . . . .	104
D.1	Mapping from arbitrary triangle to standard triangle. . . . .	120
D.2	Mapping from standard triangle to standard square. . . . .	120

# List of Tables

3.1	Computational costs for different mesh termination schemes. . . . .	56
4.1	Local edge numbers for a tetrahedral element. . . . .	69
4.2	Local edge numbers for a triangular face. . . . .	69
5.1	First order basis function numbers and associated nodes. . . . .	82
5.2	Comparison of accuracy and computational costs of the first order absorbing boundary condition and different orders of infinite elements.	85
D.1	Accuracy of Gauss-Legendre quadrature over a triangle with a sin- gularity at a vertex. . . . .	123

# Chapter 1

## Introduction

Since the formulation of the Maxwell equations governing electromagnetic phenomena, these equations have been applied to solve a wide range of problems in the field of electromagnetics. However, due to the complexity of these formulae an exact analytic solution is not necessarily obtainable, especially when the geometry of the problem becomes complicated. By using appropriate numerical methods these equations can be wielded into a very useful tool for analysing many different electromagnetic structures.

Depending on the problem at hand an appropriate form of the Maxwell equations are chosen and a suited numerical solution is applied to yield any of the various well established methods in computational electromagnetics. For instance, to calculate the voltage on a transmission line for an arbitrary input pulse, the differential form of the Maxwell equations can be solved using the Finite Difference Time Domain (FDTD) method. On the other hand, if a distributed current source in free space is radiating and the far-field patterns are required, an integral equation can be solved using the Method of Moments (MoM). Clearly these problems are vastly different and certain techniques are more efficient to solve a specific type of problem than are other techniques.

Problems in applied electromagnetics can be classified according to different criteria such as electrical size, geometrical complexity, whether it is to be solved in the frequency or the time domain, and so on. One such classification divides problems into bounded domain and unbounded domain problems. The former typically includes problems such as determining the resonant frequencies of cavities and the magnetic field distribution in electric motors, whereas the latter typically includes determining the radiation pattern of an antenna

or the scattering characteristics of an object.

As a technique widely applied to problems in structural and continuum mechanics, the Finite Element Method (FEM) is typically used to solve bounded problems. Equivalently the method is in many instances used for bounded problems in electromagnetics, such as determining waveguide modes. When it is used to solve unbounded problems a special treatment of the method is required to ensure that the physics of such unbounded problems are modelled correctly. Such adaptations have been developed using rather different approaches, such as the use of infinite elements or Perfectly Matched Layers (PML). It is the focus of this project to compare some of these approaches.

In Chapter 2 a typical unbounded problem in two dimensions is presented and a scalar finite element solution is formulated without consideration of the necessary adaptations to model the unbounded domain accurately. This formulation is then used as the foundation for Chapter 3 where different approaches are used to model the unbounded nature of the problem. Specifically the use of Absorbing Boundary Conditions (ABC), the Finite Element Boundary Integral (FEBI) method and Infinite Elements (IE) are considered.

In Chapter 4 an unbounded problem in three dimensions is presented and a vector finite element solution is formulated, again without consideration for the mesh termination scheme. Then an infinite element termination is developed for this finite element solution in Chapter 5.

Finally, some concluding remarks and recommendations for future work are given in Chapter 6.

## Chapter 2

# A Finite Element Solution in 2D

Here a finite element solution to an unbounded two-dimensional problem is presented. First some background concerning the development of the finite element method is discussed. Then a classic unbounded electromagnetic problem is given along with an analytic solution. Finally the finite element solution is formulated and some implementation issues are also discussed.

### 2.1 Background

The finite element method in its current form can be credited to Courant who presented an application of variational methods to potential theory in a publication dating back to 1943 [1]. In this publication by Courant [2] a few two-dimensional problems are solved using linear approximation functions on a set of triangles, which the author called “elements”. Only about a decade later in the 1950s the finite element method was applied to engineering problems [3], specifically for designing and analysing aircraft structures. From there use of the method became widespread in the field of structural mechanics.

Adoption of the finite element method into the electrical engineering community followed in the 1960s, an early example being the application to waveguide problems in [4]. Soon the method was applied to other problems in electromagnetics, ranging from magnetostatics to wire antennas, and the method grew in popularity.

Many textbooks devoted to the finite element method and its applications to structural and continuum mechanics have been written since, especially [5] is often cited. It was only in 1983 when the first textbook presenting the

finite element method within the context of electrical engineering appeared [6]. Further advances in the application of the finite element method to electromagnetics continued and especially application to high-frequency problems warranted the appearance of another well-known text [3].

Today the finite element method in electromagnetics is a very rich and specialised field. It has become a powerful numerical tool applicable to a wide range of problems. Advanced topics in the finite element method include hierarchal basis functions, error estimation and mesh adaptation, and the time domain finite element method [7].

## 2.2 The Scattering Problem in 2D

The problem under consideration is fairly simple. Given an infinitely long perfectly conducting cylinder of radius  $\rho_a$ , find the echo width of the cylinder. Calculating the echo width is equivalent to solving for the scattered field in the far-field region around the cylinder when it is illuminated by an incident field. The incident field is assumed to be a plane wave with transverse magnetic polarisation, which means the electric field has only a component parallel to the length of the cylinder. Let the cylinder extend to infinity in the  $z$ -direction. Figure 2.1 describes the problem graphically.

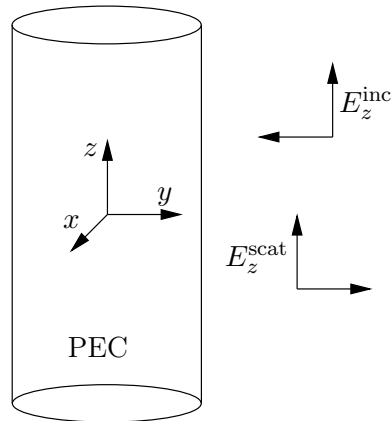


**Figure 2.1:** Description of two-dimensional scattering problem.

Due to the simplicity of the problem an analytic solution in the form of an infinite series can easily be obtained and is presented below.

### 2.2.1 Analytic Solution

A detailed derivation of the solution can be found in [8]. In short, the solution is obtained by expanding the incident field in an infinite series of Bessel functions and approximating the scattered field as a similar infinite series of Hankel functions of which the coefficients are unknown. The solution is obtained by simply forcing the scattered electric field equal to the negative of the incident field on the surface of the cylinder. This is equivalent to forcing the tangential component of the total electric field to be zero, which is the boundary condition at a perfectly conducting surface.

For an incident field given by

$$\mathbf{E}^{\text{inc}} = E_z^{\text{inc}} \hat{i}_z = E_0 e^{jk_0 \rho \cos(\phi)} \hat{i}_z \quad (2.2.1)$$

the scattered electric field is determined as

$$\mathbf{E}^{\text{scat}} = E_z^{\text{scat}} \hat{i}_z = -E_0 \sum_{n=-\infty}^{+\infty} j^{-n} \left[ \frac{J_n(k_0 \rho_a)}{H_n^{(2)}(k_0 \rho_a)} H_n^{(2)}(k_0 \rho) \right] e^{jn\phi} \hat{i}_z \quad (2.2.2)$$

where  $J_n$  is the Bessel function of the first kind and  $H_n^{(2)}$  is the Hankel function of the second kind. Some of the properties of the Hankel and Bessel functions are given in Appendix A.

With the scattered field calculated and the incident field known, the echo width  $\sigma_{2D}$  of the cylinder can be determined using

$$\sigma_{2D} = \lim_{r \rightarrow \infty} 2\pi r \frac{|E_z^{\text{scat}}|^2}{|E_z^{\text{inc}}|^2} \quad (2.2.3)$$

which is the desired result.

## 2.3 Finite Element Solution

For solving electromagnetic problems, the finite element method is typically employed to solve the Laplace differential equation (for static problems) or the Helmholtz differential equation (for dynamic problems). As the scattering problem involves the full-wave dynamics of electromagnetic fields, the finite element method is used here to solve the Helmholtz equation.

A typical starting point is to define the domain in which a solution is sought. The objective is to solve the scattered field in the free space sur-

rounding the cylinder, which means that the solution domain is bounded by the cylinder surface. Since the scattering problem is unbounded, the solution domain is infinite in extent. Equivalently the domain can be seen as bounded at infinity. However, a practical implementation of the finite element method can only find a solution in a finite domain, which means the outer boundary cannot be at infinity but should be at some finite distance.

Figure 2.2 depicts the situation. The finite element domain is  $\Omega_1$  which is enclosed by the boundaries  $\Gamma_1$  (the surface of the cylinder) and  $\Gamma_2$  (the outer boundary). Exterior to the boundary  $\Gamma_2$  lies the rest of the solution domain  $\Omega_2$  which is enclosed by the boundary  $\Gamma_\infty$  at infinity. The problem now becomes clear: to solve the scattering problem a solution has to be found in  $\Omega_1 + \Omega_2$ , but the finite element method can only find a solution in  $\Omega_1$ .

Solving differential equations uniquely requires adequate specification of the boundary conditions. For the solution in the domain  $\Omega_1 + \Omega_2$  this means that appropriate boundary conditions have to be applied at the boundaries  $\Gamma_1$  and  $\Gamma_\infty$ , depending on what is represented by these boundaries. At  $\Gamma_\infty$  the scattered field is required to vanish since the boundary lies at an infinite distance, whereas the total field should be zero at the boundary  $\Gamma_1$ , which represents a perfectly electrical conducting cylinder. The scattered field is therefore simply the negative of the incident field on this boundary.

Since the finite element method aims to solve a differential equation in  $\Omega_1$  boundary conditions are again required to ensure that a unique solution is obtained. Because the boundary  $\Gamma_1$  still represents the conducting cylinder,

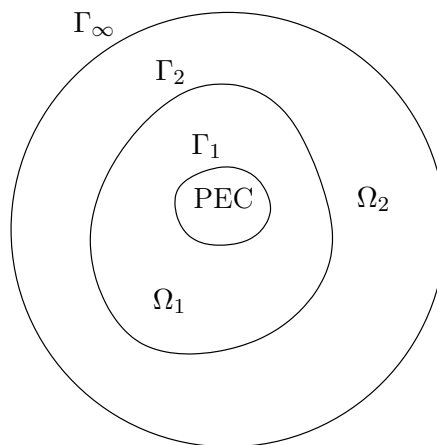


**Figure 2.2:** The two-dimensional finite element domain.



the scattered field should be the negative of the incident field on this boundary. The question is then raised, what does the boundary  $\Gamma_2$  represent? Since both  $\Omega_1$  and  $\Omega_2$  represent free space, this boundary is non-physical. For the scattered field then this boundary should seem transparent. Enforcing this transparent property of the outer boundary and emulating an infinite exterior region is the main goal of using an appropriate mesh termination scheme for the finite element method. Exactly how this is achieved is the subject of Chapter 3 and for now it is sufficient to assume that an appropriate boundary condition is applied at  $\Gamma_2$ .

The above description of the problem can now be stated mathematically and the finite element solution can be formulated using variational principles.

### 2.3.1 Variational Formulation

For a free space region in which no current sources are present the behaviour of the scattered electric field is governed by the homogeneous Helmholtz equation

$$\nabla^2 E + k_0^2 E = 0. \quad (2.3.1)$$

Since the problem domain is two-dimensional the scalar Laplacian  $\nabla^2$  contains only the derivatives with respect to the  $x$  and  $y$  coordinates. Throughout it is assumed that  $E$  represents the  $z$ -directed scattered field.

The boundary condition for the field  $E$  on the surface of the conducting cylinder is simply

$$E = -E^{\text{inc}} \quad (2.3.2)$$

where  $E^{\text{inc}}$  is the field incident on the cylinder. This condition is required so that the tangential component of the total field is zero on the conducting cylinder. Since the field itself is specified on this boundary, this is a Dirichlet boundary condition (or boundary condition of the first kind). Assume that the boundary condition on the fictitious outer boundary of the finite element domain is of the form

$$\nabla E \cdot \hat{i}_n + \gamma E = 0 \quad (2.3.3)$$

where  $\gamma$  is some constant. The unit vector  $\hat{i}_n$  is normally outward directed on the outer boundary. This is a boundary condition of the third kind, as both the field and its derivative are specified.

Now the scattering problem can be stated as a boundary-value problem

$$\begin{aligned} \nabla^2 E + k_0^2 E &= 0 & \text{in } \Omega_1 \\ E &= -E^{\text{inc}} & \text{on } \Gamma_1 \\ \nabla E \cdot \hat{i}_n + \gamma E &= 0 & \text{on } \Gamma_2. \end{aligned} \quad (2.3.4)$$

The solution to this boundary-value problem is obtained by setting the first variation of the functional  $\Pi(E)$  equal to zero [3] where

$$\Pi(E) = \iint_{\Omega_1} \nabla E \cdot \nabla E - k_0^2 E^2 \, d\Omega + \int_{\Gamma_2} E \gamma E \, d\Gamma. \quad (2.3.5)$$

To show the validity of this functional a boundary value problem similar to (2.3.4) is defined

$$\begin{aligned} \nabla^2 F + k_0^2 F &= g & \text{in } \Omega_1 \\ F &= 0 & \text{on } \Gamma_1 \\ \nabla F \cdot \hat{i}_n + \gamma F &= 0 & \text{on } \Gamma_2 \end{aligned} \quad (2.3.6)$$

by letting  $F = E - E_1$  where  $E_1$  is any function that satisfies the boundary conditions stated in (2.3.4). Now define the operator

$$\mathcal{L}(\cdot) = \nabla^2(\cdot) + k_0^2(\cdot) \quad (2.3.7)$$

and the symmetric inner product

$$\langle v, w \rangle = \iint_{\Omega_1} vw \, d\Omega. \quad (2.3.8)$$

Since the boundary conditions for (2.3.6) are homogeneous it can be shown that the operator  $\mathcal{L}$  is symmetric and the solution to the boundary value problem is obtained by rendering the functional

$$\Pi(F) = \langle \mathcal{L}F, F \rangle - 2\langle F, g \rangle \quad (2.3.9)$$

stationary [3]. Substituting the definition of  $F$  the functional becomes

$$\begin{aligned} \Pi(E) &= \langle \mathcal{L}(E - E_1), (E - E_1) \rangle - 2\langle (E - E_1), g \rangle \\ &= \langle \mathcal{L}E, E \rangle - \langle \mathcal{L}E, E_1 \rangle - \langle \mathcal{L}E_1, E \rangle - 2\langle E, g \rangle \end{aligned} \quad (2.3.10)$$

where the terms not containing  $E$  have been discarded since the variation is taken with respect to  $E$ . Noting that  $\mathcal{L}E_1 = -g$ , the functional is further simplified to

$$\Pi(E) = \langle \mathcal{L}E, E \rangle - \langle \mathcal{L}E, E_1 \rangle + \langle \mathcal{L}E_1, E \rangle. \quad (2.3.11)$$

By the definition of the inner product (2.3.8)

$$\Pi(E) = \iint_{\Omega_1} E(\nabla^2 + k_0^2)E \, d\Omega + \iint_{\Omega_1} E\nabla^2 E_1 - E_1\nabla^2 E \, d\Omega. \quad (2.3.12)$$

Using the first and second scalar Green theorems and then applying the boundary conditions applicable to  $E$  and  $E_1$  gives

$$\begin{aligned} \Pi(E) &= \iint_{\Omega_1} -\nabla E \cdot \nabla E + k_0^2 E^2 \, d\Omega + \oint_{\Gamma_1 + \Gamma_2} E(\nabla E \cdot \hat{i}_n) \, d\Gamma \\ &\quad + \oint_{\Gamma_1 + \Gamma_2} E(\nabla E_1 \cdot \hat{i}_n) - E_1(\nabla E \cdot \hat{i}_n) \, d\Gamma \\ &= \iint_{\Omega_1} -\nabla E \cdot \nabla E + k_0^2 E^2 \, d\Omega - \int_{\Gamma_1} E^{\text{inc}}(\nabla E \cdot \hat{i}_n) \, d\Gamma - \int_{\Gamma_2} E\gamma E \, d\Gamma \\ &\quad + \int_{\Gamma_1} E^{\text{inc}}(\nabla E \cdot \hat{i}_n) - E^{\text{inc}}(\nabla E_1 \cdot \hat{i}_n) \, d\Gamma \\ &\quad - \int_{\Gamma_2} E\gamma E_1 - E_1\gamma E \, d\Gamma. \end{aligned} \quad (2.3.13)$$

If  $\gamma$  is symmetric under the integral over  $\Gamma_2$  the last term in this expression is zero. Discarding the term not containing  $E$  results in the integrals over  $\Gamma_1$  to cancel and the following result is obtained

$$\Pi(E) = - \iint_{\Omega_1} \nabla E \cdot \nabla E - k_0^2 E^2 \, d\Omega - \int_{\Gamma_2} E\gamma E \, d\Gamma \quad (2.3.14)$$

which becomes (2.3.5) by simply changing the signs of all the terms (as the variation is set equal to zero this has no effect on the solution).

Finally, the variational problem can now be summarised as

$$\begin{cases} \delta\Pi(E) = 0 \\ E = -E^{\text{inc}} \quad \text{on } \Gamma_1 \end{cases} \quad (2.3.15)$$

and the solution can now be discretised.

### 2.3.2 Discretisation

The finite element solution proceeds by discretising the finite element domain into smaller elements and defining on each element a set of basis functions with which the field inside that element is approximated. That is, inside an element  $e$  the field  $E^e$  is approximated using  $N^e$  basis functions as

$$E^e = \sum_{i=1}^{N^e} a_i^e \lambda_i^e \quad (2.3.16)$$

where  $a_i^e$  is an unknown weighting coefficient associated with the basis function  $\lambda_i^e$ . Similarly on each edge  $s$  residing on  $\Gamma_2$ , the field is approximated as

$$E^s = \sum_{i=1}^{M^s} a_i^s \lambda_i^s. \quad (2.3.17)$$

Depending on the discretisation used, the evaluation of the basis functions (2.3.16) on an edge of an element may automatically reduce to (2.3.17). In this case the basis functions approximating the field on  $\Gamma_2$  are simply a subset of the basis functions approximating the field in  $\Omega_1$ , since  $\Gamma_2$  consists of the edges of a certain number of elements in  $\Omega_1$ .

Because adjacent elements approximate the field at a shared node an added restriction is placed on the unknown weighting coefficients associated with that node. That is, the coefficients within the different elements and associated with the same node, should have the same value. This restriction is enforced by mapping each node from a local number within an element or edge to a global number and assembling the complete system equation according to the global numbers.

Substituting the expansions of (2.3.16) and (2.3.17) into the functional (2.3.5) and taking the variation with respect to the unknown coefficients  $a_i$  gives

$$\begin{aligned} \frac{\partial \Pi(E)}{\partial a_i} &= \sum_{j=1}^N a_j \iint_{\Omega_1} \frac{\partial \lambda_i}{\partial x} \frac{\partial \lambda_j}{\partial x} + \frac{\partial \lambda_i}{\partial y} \frac{\partial \lambda_j}{\partial y} - k_0^2 \lambda_i \lambda_j \, d\Omega \\ &\quad + \sum_j^M a_j \int_{\Gamma_2} \lambda_i \gamma \lambda_j \, d\Gamma. \end{aligned} \quad (2.3.18)$$

In this discretised functional  $N$  is the number of nodes in the domain  $\Omega_1$  and

$M$  the number of nodes on the boundary  $\Gamma_2$ . Note that the nodes on  $\Gamma_2$  are a subset of the nodes in  $\Omega_1$  which means  $\{a_j | j = 1, 2, \dots, M\} \subset \{a_j | j = 1, 2, \dots, N\}$ . The result is that (2.3.18) implies  $N$  expressions in  $N$  unknown coefficients. Setting the variation equal to zero and writing (2.3.18) in matrix form one obtains the system equation

$$[K] \{a\} = \{0\} \quad (2.3.19)$$

where

$$K_{ij} = \iint_{\Omega_1} \left[ \frac{\partial \lambda_i}{\partial x} \frac{\partial \lambda_j}{\partial x} + \frac{\partial \lambda_i}{\partial y} \frac{\partial \lambda_j}{\partial y} - k_0^2 \lambda_i \lambda_j \right] d\Omega + \int_{\Gamma_2} \lambda_i \gamma \lambda_j d\Gamma. \quad (2.3.20)$$

Note that any basis function not associated with a node on the boundary  $\Gamma_2$  evaluates to zero on this boundary, in which case the contour integral term in (2.3.20) is simply zero. Also, because only basis functions within the same element or adjacent elements are non-zero over a common definition range, there are only local interactions between these basis functions. As a result thereof the system matrix is sparse.

All that remains is to enforce the Dirichlet boundary condition on  $\Gamma_1$ . This is achieved by letting the weighting coefficients  $a_x$  associated with the nodes on  $\Gamma_1$  assert the required values so that  $E = -E^{\text{inc}}$  at each of these nodes. Two ways to incorporate this restriction into the matrix equation (2.3.19) are considered. In either case it is useful to assume that the global numbering scheme is such that the weighting coefficients associated with nodes on  $\Gamma_1$  are grouped together at the low end of the global numbers. The system equation (2.3.19) can then be written as

$$\begin{bmatrix} K_{xx} & K_{xy} \\ K_{yx} & K_{yy} \end{bmatrix} \begin{Bmatrix} a_x \\ a_y \end{Bmatrix} = \begin{Bmatrix} 0 \\ 0 \end{Bmatrix}. \quad (2.3.21)$$

After letting the known coefficients assert the correct values  $a_x = X$  and rearranging the final system equation is obtained

$$[K_{yy}] \{a_y\} = \{-K_{yx}X\}. \quad (2.3.22)$$

An alternative method for enforcing the Dirichlet boundary condition is to

specify the known weighting coefficients indirectly in the right hand side vector of (2.3.21). This is done by multiplying an arbitrary, but very large number  $L$  with all the self terms associated with the coefficients  $a_x$  in the system matrix. Also, the correct values of these weighting coefficients  $X$  are multiplied with the same large number  $L$  and are added to the zero right hand side vector. The final system is then

$$\begin{bmatrix} LK_{xx}I + K_{xx}(U - I) & K_{xy} \\ K_{yx} & K_{yy} \end{bmatrix} \begin{Bmatrix} a_x \\ a_y \end{Bmatrix} = \begin{Bmatrix} LX \\ 0 \end{Bmatrix} \quad (2.3.23)$$

where  $I$  is the identity matrix and  $U$  is a matrix filled with ones except on the diagonal where all entries are zero.

Of the two methods to enforce this boundary condition, the first is more efficient as it reduces the size of the system matrix, while the second is easier to implement. Finally the solution is obtained by solving either (2.3.22) or (2.3.23) using any of the various techniques available to solve linear systems.

The discretised solution is now ready to be implemented.

### 2.3.3 Implementation

An essential component of implementing the finite element solution is choosing the element shapes into which the domain is subdivided and defining appropriate expansion functions for these elements. In literature the finite element method has been implemented for a large variety of element shapes and basis functions of various orders. Triangular elements are used here since they allow curved geometries to be modelled accurately and basis functions are easily defined using simplex coordinates on each element.

First order simplex elements are used which means three linear basis functions are used to approximate the field in each element. That is

$$E^e = \sum_{i=1}^3 a_i^e \lambda_i^e \quad (2.3.24)$$

where

$$\lambda_i^e = A_i^e + B_i^e x + C_i^e y. \quad (2.3.25)$$

The coefficients  $A_i^e$ ,  $B_i^e$  and  $C_i^e$  are obtained using the coordinates  $(x_i^e, y_i^e)$  of

the triangle element vertices and the following relation

$$\begin{bmatrix} A_1^e & B_1^e & C_1^e \\ A_2^e & B_2^e & C_2^e \\ A_3^e & B_3^e & C_3^e \end{bmatrix} = \begin{bmatrix} 1 & 1 & 1 \\ x_1^e & x_2^e & x_3^e \\ y_1^e & y_2^e & y_3^e \end{bmatrix}^{-1}. \quad (2.3.26)$$

Each basis function  $\lambda_i^e$  evaluates to unity at the vertex  $(x_i^e, y_i^e)$  and zero at the other two vertices, which means that each of the basis functions uniquely specifies the field at a single node of the triangle. Also, since the basis functions are linear, the field on an elemental edge is only a weighted sum of the two basis functions associated with the two nodes of that edge. The third basis function will evaluate to zero at either node and is therefore zero on the entire edge. This is especially useful as it implies that the basis functions can also be used to approximate the field on the finite element exterior boundary. If an element  $e$  has an edge  $s$  on the finite element boundary, the field on that edge is then

$$E^s = \sum_{i=1}^2 a_i^s \lambda_i^s \quad (2.3.27)$$

where  $\lambda_i^s$  simply the simplex coordinate along edge  $s$  and  $a_i^s$  is the weighting coefficient associated with a particular node of the element  $e$ . The compatibility of the basis functions over the elemental areas and boundary edges are therefore automatically ensured.

As linear expansion functions are used the evaluation of (2.3.20) is straightforward. The following result for integrating simplex coordinates over the elemental area on which they are defined is used

$$\iint_{A^e} \lambda_1^i \lambda_2^j \lambda_3^k dS = \frac{2!i!j!k!}{(2+i+j+k)!} A^e \quad (2.3.28)$$

where  $A^e$  is the area of the triangular element on which  $\lambda_i$  is defined [7].

Finally, the system equation is assembled and reduced to (2.3.22) to enforce the Dirichlet boundary condition. The solution to the system equation is the set of weighting coefficients associated with each of the basis functions approximating the field across the finite element domain  $\Omega_1$ . Depending on the specific application some post-processing may be required and is the topic of the next section.

### 2.3.4 Post-processing

The obtained solution allows the field  $E$  to be calculated directly anywhere within the finite element domain  $\Omega_1$ . This is very useful when field data within this domain is required. However, often the field has to be determined in the far-field or a secondary result, such as echo width is required. To calculate these quantities some post-processing is needed.

By the surface equivalence theorem it is possible to determine the field at any point within a region if the tangential field is known on the surface enclosing that region [9]. For the case where the field is known within the domain  $\Omega_1$  and more specifically on the boundary  $\Gamma_2$ , the field can be computed at any point in the exterior region  $\Omega_2$  by using an appropriate near-field to far-field transformation. Such a transformation is given by

$$E(\boldsymbol{\rho}) = \int_{\Gamma_2} \left( E(\boldsymbol{\rho}') \frac{\partial G_0(\boldsymbol{\rho}, \boldsymbol{\rho}')}{\partial n'} - G_0(\boldsymbol{\rho}, \boldsymbol{\rho}') \frac{\partial E(\boldsymbol{\rho}')}{\partial n'} \right) d\Gamma' \quad (2.3.29)$$

where  $G_0$  is the two-dimensional free space scalar Green function defined as

$$G_0(\boldsymbol{\rho}, \boldsymbol{\rho}') = \frac{1}{4j} H_0^{(2)}(k_0 |\boldsymbol{\rho} - \boldsymbol{\rho}'|). \quad (2.3.30)$$

In (2.3.29) the primed coordinates  $\boldsymbol{\rho}'$  are used to indicate the point on the enclosing surface (source point) and the unprimed coordinates  $\boldsymbol{\rho}$  indicate the point in the exterior region (observer point). For a complete derivation of this integral equation, refer to Appendix B.1.

The evaluation of (2.3.29) allows the field  $E$  to be calculated at any point  $\boldsymbol{\rho} \in \Omega_2$ . Because the only unknown in (2.3.29) is the field  $E(\boldsymbol{\rho})$  which appears on the left-hand side, the integral on the right-hand side can be evaluated directly. As the integral is evaluated on  $\Gamma_2$ , all elements that have edges on this boundary have to be identified as well as the edges within these elements that form the boundary.

It is useful to define for each of these edges local coordinates in which one principal axis is directed along the boundary edge and the other principal axis directed normally outward from that edge. Figure 2.3 shows the local coordinates for a particular edge. The transformation relating the global coordinates



$(x, y)$  to the local coordinates  $(u, v)$  is given by

$$\begin{Bmatrix} u \\ v \end{Bmatrix} = \begin{bmatrix} -\sin(\alpha) & \cos(\alpha) \\ \cos(\alpha) & \sin(\alpha) \end{bmatrix} \begin{Bmatrix} x \\ y \end{Bmatrix}. \quad (2.3.31)$$

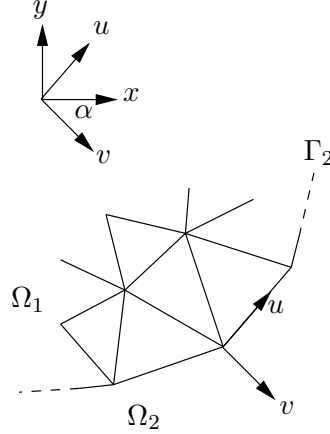


**Figure 2.3:** Coordinate rotation on a boundary edge.

In evaluating the integral in (2.3.29) the electric field  $E(\boldsymbol{\rho}')$  is approximated as constant over a single edge and equal to its value in the middle of that edge. Computing the normal directional derivative of the electric field at an edge is done using

$$\frac{\partial E_z}{\partial n'} = \sum_{i=1}^3 a_i \nabla \lambda_i \cdot \hat{i}_n \quad (2.3.32)$$

where  $\hat{i}_n$  is a unit vector pointed normally outward on the boundary edge. It is noted that since the expansion functions  $\lambda_j$  are linear, the directional derivative of the field is constant over a single element and thus also constant on the boundary edge. The expansion functions can be calculated in the original coordinates  $(x, y)$  and the unit vector is then obtained from (2.3.31)

$$\hat{i}_n = \cos(\alpha)\hat{i}_x + \sin(\alpha)\hat{i}_y. \quad (2.3.33)$$

As for the electric field the Green function and its normal derivative are assumed constant on an edge and is evaluated in the middle of each edge. This approximation is valid since the argument of the Green function is within a

factor equal to the distance  $|\boldsymbol{\rho} - \boldsymbol{\rho}'|$ . If this distance is very large, as is the case when computing far-fields, small variations in the position of the source point  $\boldsymbol{\rho}'$  do not have a significant effect. Calculating the normal derivative of the Green function is done using the local coordinates  $(u, v)$  as it simplifies the task. In local coordinates the Green function is

$$G_0(u, v, u', v') = \frac{1}{j4} H_0^{(2)} \left( k_0 \sqrt{(u - u')^2 + (v - v')^2} \right). \quad (2.3.34)$$

Using the properties of the Hankel function (see Appendix A) the normally outward directional derivative is simply calculated

$$\frac{\partial G_0}{\partial n'} = \frac{\partial G_0}{\partial v'} = \frac{k_0}{j4} \frac{H_1^{(2)} \left( k_0 \sqrt{(u - u')^2 + (v - v')^2} \right)}{\sqrt{(u - u')^2 + (v - v')^2}} (v - v'). \quad (2.3.35)$$

Finally the integral can be evaluated to give the field at  $\boldsymbol{\rho}$ .

If the echo width of the scatterer is required the field has to be evaluated at a sufficiently large distance. In antenna theory an observer is in the far-field when at a distance

$$R = \frac{2D^2}{\lambda} \quad \text{for } D > \lambda \quad (2.3.36)$$

from the scatterer, where  $D$  is the largest dimension of the scatterer [8]. Using the diameter as the largest dimension, the echo width is calculated at a distance larger than  $R$  as

$$\sigma_{2D} = 2\pi\rho \frac{|E^{\text{scat}}|^2}{|E^{\text{inc}}|^2} \Big|_{\rho=10R}. \quad (2.3.37)$$

Finally, if an analytic solution is known it is useful to define an error indicating the accuracy of the obtained solution. To compute an error value for a solution the scattered field is computed at a number of points in the finite element domain using both the obtained solution and the analytic solution. A relative error is then calculated at each point using

$$\varepsilon_r^s = \left\| \frac{E_s^{\text{FEM}} - E_s^{\text{TRUE}}}{E_s^{\text{TRUE}}} \right\| \quad (2.3.38)$$

and the root mean square of the error is then calculated to give a single error

indication

$$\varepsilon_{\text{RMS}} = \sqrt{\sum_{s=1}^M \frac{(\varepsilon_r^s)^2}{M}}. \quad (2.3.39)$$

## 2.4 Conclusion

In this chapter a typical two-dimensional scattering problem has been presented as the unbounded problem to be solved using the finite element method. A finite element method was formulated and the need for a proper mesh termination scheme was motivated. Some implementation and post-processing issues of the finite element solution were also discussed.

Now the issue of proper mesh termination at the outer boundary of the finite element domain can be addressed.

## Chapter 3

# Mesh Termination Schemes in 2D

In the previous chapter a two-dimensional scattering problem was presented and solved via the finite element method. During the formulation of this solution it was stated that the finite element domain has to be terminated properly at the exterior boundary as to model correctly an infinite free space region and it was assumed that this could be achieved by applying a certain boundary condition. The focus of this chapter is to consider various methods how such a proper termination can be achieved for the previously formulated finite element solution.

First a brief overview of early developments concerning this aspect of the finite element method is given. Then different mesh termination schemes are presented, specifically Absorbing Boundary Conditions (ABC), the Finite Element Boundary Integral (FEBI) method and Infinite Elements (IE) are discussed. Finally these methods are compared using different criteria.

### 3.1 Background

One of the earliest applications of the finite element method to unbounded electromagnetic problems appeared in 1971 [10] where the method was hybridised with an integral equation formulation to solve the Laplace equation. The next year marked the first application of the finite element method to solve electromagnetic wave problems in an unbounded domain [1] when a similar hybridised solution was published [11].

Since then various different approaches towards handling the exterior region in unbounded problems followed. Some of these approaches aimed at discretising the exterior region by using infinite elements [12], [13] and [14] or recursive condensation [15]. Other approaches focussed on specifying an appropriate boundary condition on the exterior boundary of the finite element domain, such as absorbing boundary conditions. Some early theoretical work on this include [16] and [17] while one of the first notable applications to electromagnetics is found in [18].

The use of Perfectly Matched Layers (PML) [19] originally developed for finite difference methods and later adopted by the finite element method is also worth mentioning in this respect.

## 3.2 Absorbing Boundary Conditions

One way to terminate the finite element domain as to prevent unphysical reflections from the outer boundary is by enforcing a boundary condition that acts to absorb any fields incident on that boundary. Boundary conditions of this type are simply called absorbing boundary conditions. The formulation assumes a certain asymptotic form of the scattered field and incorporates this approximation by way of a boundary condition of the third kind.

### 3.2.1 Formulation

In the far-field region, scattered fields approach a certain asymptotic form, depending on the geometry of the problem. For the problem in Figure 2.1 the scattered field can be approximated as

$$E(\rho, \phi) \approx A(\phi) \frac{e^{-jk_0\rho}}{\sqrt{\rho}} \quad (3.2.1)$$

where  $\rho$  is the radial variable and  $\phi$  the angular variable in the circular cylindrical coordinate system. The angular function  $A$  is some unknown function dependent on the scatterer. Taking the first derivative of (3.2.1) with respect to  $\rho$  and rearranging gives

$$\frac{\partial E}{\partial \rho} + \left( jk_0 + \frac{1}{2\rho} \right) E = 0 \quad (3.2.2)$$

which is the first order absorbing boundary condition. For a circular boundary the derivative with respect to  $\rho$  is equivalent to a outward normal directional derivative which allows (3.2.2) to be written as

$$\nabla E \cdot \hat{i}_n + \gamma E = 0. \quad (3.2.3)$$

In this form the boundary condition is recognised as the boundary condition of the third kind assumed on  $\Gamma_2$  in the previous chapter, (2.3.3). This means applying the first order boundary condition on  $\Gamma_2$  simply requires substituting

$$\gamma = jk_0 + \frac{1}{2\rho} \quad (3.2.4)$$

in the functional

$$\Pi(E) = \iint_{\Omega_1} \nabla E \cdot \nabla E - k_0^2 E^2 \, d\Omega + \int_{\Gamma_2} E \gamma E \, d\Gamma \quad (3.2.5)$$

and the first order ABC is incorporated into the finite element solution.

Higher order absorbing boundary conditions can be derived by using a higher order expansion to approximate the far-field and proceeding in a similar manner as for the first order absorbing boundary condition. The second order absorbing boundary condition [3] is given by

$$\frac{\partial E}{\partial \rho} + \left( jk_0 + \frac{1}{2\rho} - \frac{1}{8\rho^2(1/\rho + jk_0)} - \frac{1}{2\rho^2(1/\rho + jk_0)} \frac{\partial^2}{\partial \phi^2} \right) E = 0. \quad (3.2.6)$$

As for the first order absorbing boundary condition, this can be rewritten in the form of (3.2.3) with the exception that  $\gamma$  is now a second order differential operator. Fortunately  $\gamma$  is still symmetric under the integral on the boundary  $\Gamma_2$  if this boundary is circular and the functional derived in Section 2.3.1 is still valid. Substituting

$$\gamma = jk_0 + \frac{1}{2\rho} - \frac{1}{8\rho^2(1/\rho + jk_0)} - \frac{1}{2\rho^2(1/\rho + jk_0)} \frac{\partial^2}{\partial \phi^2} \quad (3.2.7)$$

into the contour integral of (3.2.5) gives

$$\Pi(E) = \iint_{\Omega_1} \nabla E \cdot \nabla E - k_0^2 E^2 \, d\Omega + \int_{\Gamma_2} E \left[ \gamma_1 + \gamma_2 \frac{\partial^2}{\partial \phi^2} \right] E \, d\Gamma \quad (3.2.8)$$

where

$$\gamma_1 = jk_0 + \frac{1}{2\rho} - \frac{1}{8\rho^2(1/\rho - jk_0)} \quad (3.2.9)$$

$$\gamma_2 = -\frac{1}{2\rho^2(1/\rho - jk_0)}. \quad (3.2.10)$$

In its current form (3.2.8) requires the field  $E$  to be twice differentiable which requires also the field expansion functions to be twice differentiable, and hence linear basis functions cannot be used. However, noting that for a circular boundary  $\Gamma_2$  the differential  $d\Gamma = \rho d\phi$  and using integration by parts allows one order of differentiation to be shifted to obtain

$$\Pi(E) = \iint_{\Omega_1} \nabla E \cdot \nabla E - k_0^2 E^2 d\Omega + \int_{\Gamma_2} \gamma_1 E^2 + \gamma_2 \left( \frac{\partial E}{\partial \phi} \right)^2 d\Gamma. \quad (3.2.11)$$

Using this form linear basis functions can be used and the second order ABC for a circular boundary is incorporated into the finite element solution.

The above results apply specifically to circular outer boundaries. In many instances a non-circular outer boundary is preferred, for example to reduce the number of mesh elements for problems involving scatterers with a large axial ratio. The following substitutions allow the above results to be used with such a non-circular outer boundary

$$\frac{\partial}{\partial \rho} \rightarrow \frac{\partial}{\partial n}, \quad \frac{1}{\rho} \rightarrow \kappa(s), \quad \frac{1}{\rho^2} \frac{\partial^2}{\partial \phi^2} \rightarrow \frac{\partial^2}{\partial s^2}. \quad (3.2.12)$$

Here  $\kappa(s)$  is the curvature of the outer boundary  $\Gamma_2$  as a function of arc length  $s$  along that boundary. The differential  $\partial n$  is directed normally outward on  $\Gamma_2$ . The above substitutions are exact for a circular boundary but are only approximations for a non-circular boundary. Consequently the use of non-circular boundaries involves a loss in accuracy. In either case, these substitutions are used.

It is clear that the finite element solution obtained in Section 2.3 is easily adapted to incorporate absorbing boundary conditions. The functional is simply substituted with (3.2.5) or (3.2.11) for first or second order absorbing boundary conditions, respectively. It is noted that the sparsity of the resulting linear system is conserved due to the similar form of the solution.

The finite element method incorporating absorbing boundary conditions can now be implemented.

### 3.2.2 Implementation

Since the formulation of the finite element solution including absorbing boundary conditions is very similar to the solution of Section 2.3 it is clear that implementation does not raise many new issues. However, a few comments are in order.

Recall that the curvature  $\kappa(s)$  on the outer boundary  $\Gamma_2$  has to be calculated to evaluate the contour integral in either (3.2.5) or (3.2.11), depending on the order of the absorbing boundary condition. For an arbitrary curve in space the curvature is defined as

$$\kappa(s) = \left\| \frac{\partial^2 \mathbf{v}(s)}{\partial s^2} \right\| \quad (3.2.13)$$

where  $\mathbf{v}(s)$  defines the curve parameterised by its length  $s$ . The curvature of a circle is constant and equal to the inverse of its radius. Assuming that the boundary  $\Gamma_2$  is smooth it can be approximated as circular over a small section and the curvature is then easily calculated for every such small section. This technique is practically implemented as follows.

For each boundary edge ( $s_2$ ) the two edges adjacent to it are identified ( $s_1$  and  $s_3$ ). A normal vector is extended from the midpoint of each of these edges as shown in Figure 3.1. Curvature radii  $r_{12}$  and  $r_{23}$  are defined for the edge pairs ( $s_1, s_2$ ) and ( $s_2, s_3$ ), respectively. The curvature radius at the centre edge is then approximated as the mean of  $r_{12}$  and  $r_{23}$ .

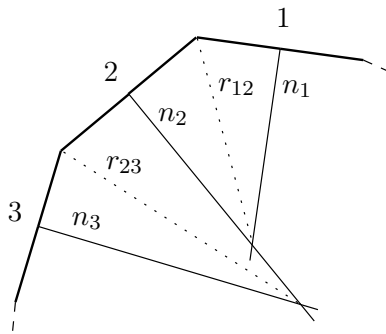


**Figure 3.1:** An approximate curvature radius is calculated locally for an edge.

If a second order absorbing boundary condition is used the derivative of the field with respect to arc length along the outer boundary is also required.



This is equivalent to computing the tangential directional derivative of the expansion functions along the boundary  $\Gamma_2$ . Using a locally defined coordinate system as in Section 2.3.4 to compute the normally directed derivative, the tangentially directed derivative can be computed by

$$\frac{\partial E}{\partial s} = \sum_{i=1}^3 a_i \nabla \lambda_i \cdot \hat{i}_t \quad (3.2.14)$$

where

$$\hat{i}_t = -\sin(\alpha)\hat{i}_x + \cos(\alpha)\hat{i}_y. \quad (3.2.15)$$

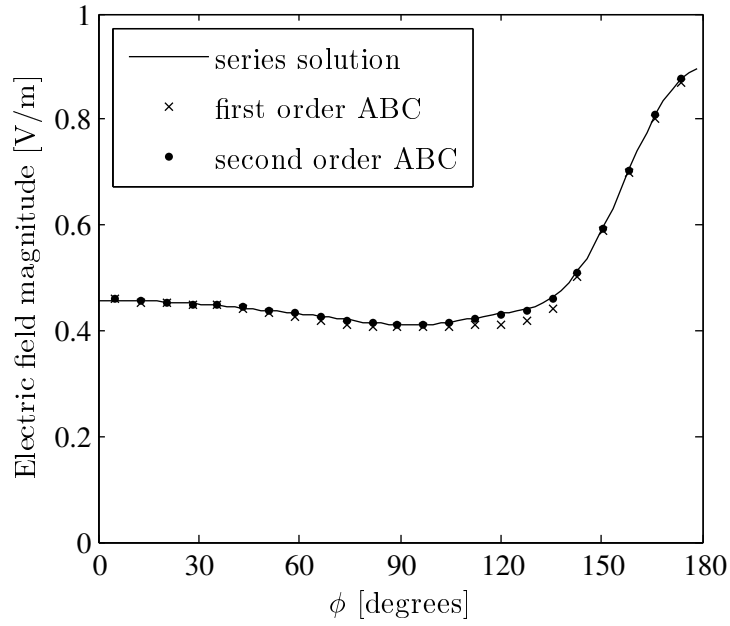
With an appropriate mesh termination implemented at the outer boundary  $\Gamma_2$  the finite element solution can be used to solve the scattering problem of Section 2.2. Numerical results are presented in the next section.

### 3.2.3 Results

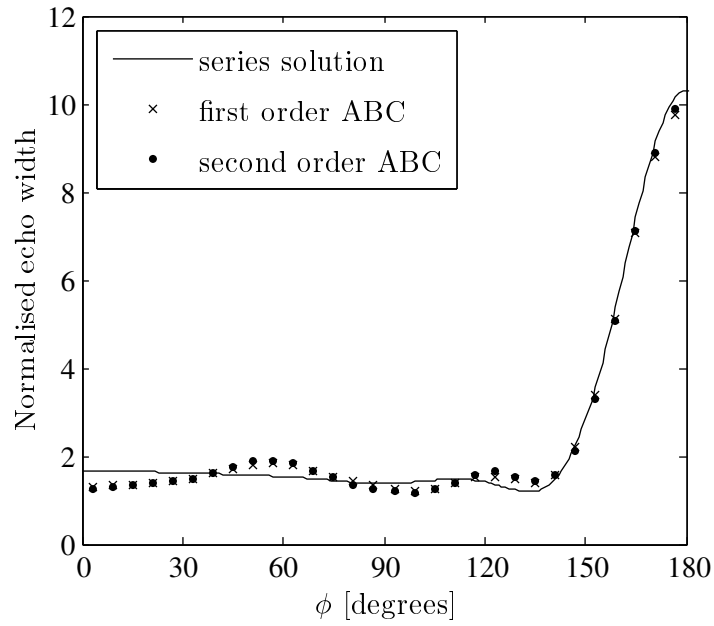
The finite element solution is applied to calculate the scattered near-field as well as the bistatic echo width of a perfectly electrical conducting cylinder which illuminated by a transverse magnetic polarised incident plane wave. The incident electric field strength is 1 V/m and the cylinder has a radius of  $0.5\lambda$ . In the mesh the longest edge length is  $\lambda/15$  and the finite element domain is terminated at a distance  $1.0\lambda$  from the cylinder surface.

Figure 3.2 shows the calculated scattered field along with the analytic solution. The scattered field is computed on the exterior boundary. Although the results of the first and second order absorbing boundary conditions are rather similar, the superior accuracy of the second order ABC is visible for angles around  $\phi \approx 130$  degrees.

In Figure 3.3 the echo width normalised to wavelength is calculated through post-processing of the obtained near-field. Since the accuracy of the echo width is rather poor in comparison to that for the near-field, it is concluded that the post-processing introduces a considerable loss in accuracy.



**Figure 3.2:** Scattered electric near-field computed using absorbing boundary conditions.



**Figure 3.3:** Echo width of perfectly electrical conducting cylinder computed using absorbing boundary conditions.

### 3.3 Finite Element Boundary Integral Method

Another way to terminate the finite element domain is by completely specifying the field and its normal derivative on the outer boundary of the domain. This is the gist of the finite element boundary integral method. The formulation of this method [3] is discussed in the next section, followed by a few comments concerning implementation, and finally numerical results are presented.

#### 3.3.1 Formulation

Instead of using the asymptotic form (3.2.1) to obtain the normal derivative of the field on the exterior boundary, as was done for the absorbing boundary conditions, this derivative of the field is introduced as another unknown quantity in the system. That is, on the exterior boundary the normal derivative of the field is specified as

$$\nabla E \cdot \hat{i}_n = -H \quad \text{on} \quad \Gamma_2 \quad (3.3.1)$$

where  $H$  represents another unknown to be solved. By noting the similarity between this boundary condition and (2.3.3) the functional of (2.3.5) becomes

$$\Pi(E) = \iint_{\Omega_1} \nabla E \cdot \nabla E - k_0^2 E^2 \, d\Omega + 2 \int_{\Gamma_2} EH \, d\Gamma. \quad (3.3.2)$$

Note that a factor 2 appears in front of the integral over  $\Gamma_2$ . To show how this functional is obtained, consider the expression for  $\Pi(E)$  in (2.3.13), repeated here

$$\begin{aligned} \Pi(E) = & \iint_{\Omega_1} -\nabla E \cdot \nabla E + k_0^2 E^2 \, d\Omega + \oint_{\Gamma_1+\Gamma_2} E(\nabla E \cdot \hat{i}_n) \, d\Gamma \\ & + \oint_{\Gamma_1+\Gamma_2} E(\nabla E_1 \cdot \hat{i}_n) - E_1(\nabla E \cdot \hat{i}_n) \, d\Gamma. \end{aligned} \quad (3.3.3)$$

Recall that both  $E$  and  $E_1$  satisfy the inhomogeneous Dirichlet boundary condition on  $\Gamma_1$ , that is  $E, E_1 = -E^{\text{inc}}$ . From (3.3.1) we also have  $\nabla E \cdot \hat{i}_n = -H$  and  $\nabla E_1 \cdot \hat{i}_n = -H$  on  $\Gamma_2$ . Enforcing these boundary conditions in (3.3.3)

gives

$$\begin{aligned}
\Pi(E) &= \iint_{\Omega_1} -\nabla E \cdot \nabla E + k_0^2 E^2 \, d\Omega - \int_{\Gamma_1} E^{\text{inc}}(\nabla E \cdot \hat{i}_n) \, d\Gamma - \int_{\Gamma_2} EH \, d\Gamma \\
&\quad + \int_{\Gamma_1} E^{\text{inc}}(\nabla E \cdot \hat{i}_n) - E^{\text{inc}}(\nabla E_1 \cdot \hat{i}_n) \, d\Gamma \\
&\quad - \int_{\Gamma_2} EH - E_1 H \, d\Gamma. \tag{3.3.4}
\end{aligned}$$

In the above expression the terms not containing  $E$  are discarded and the integrals over  $\Gamma_1$  then cancel as before. By grouping the integrals over  $\Gamma_2$  and again changing the signs of all the terms finally gives the result (3.3.2).

The finite element solution requires taking the first variation in the functional with respect to the unknown  $E$  and setting this variation equal to zero. However, both  $E$  and  $H$  are unknown in (3.3.2) which means that an added restriction is required to obtain a solvable system. Recall from Section 2.3.4 that a near-field to far-field transformation was used to relate the field  $E$  at any point in the region  $\Omega_2$  to the field and its normal derivative on  $\Gamma_2$ . This transformation was in the form of an integral equation

$$E(\boldsymbol{\rho}) = \int_{\Gamma_2} \left( E(\boldsymbol{\rho}') \frac{\partial G_0(\boldsymbol{\rho}, \boldsymbol{\rho}')}{\partial n'} - G_0(\boldsymbol{\rho}, \boldsymbol{\rho}') \frac{\partial E(\boldsymbol{\rho}')}{\partial n'} \right) d\Gamma'. \tag{3.3.5}$$

Since both regions  $\Omega_1$  and  $\Omega_2$  represent free space the continuity conditions of  $E$  across the interface  $\Gamma_2$  are

$$E|_{\Gamma_2^+} = E|_{\Gamma_2^-} \quad \text{and} \quad \frac{\partial E}{\partial n}|_{\Gamma_2^+} = \frac{\partial E}{\partial n}|_{\Gamma_2^-}. \tag{3.3.6}$$

Now letting  $\boldsymbol{\rho} \rightarrow \Gamma_2$  and enforcing the boundary condition (3.3.1) gives

$$E(\boldsymbol{\rho}) = \int_{\Gamma_2} \left( E_z(\boldsymbol{\rho}') \frac{\partial G_0(\boldsymbol{\rho}, \boldsymbol{\rho}')}{\partial n'} + G_0(\boldsymbol{\rho}, \boldsymbol{\rho}') H(\boldsymbol{\rho}') \right) d\Gamma' \tag{3.3.7}$$

where both  $\boldsymbol{\rho}'$  and  $\boldsymbol{\rho}$  are now on  $\Gamma_2$ .

The Green function and its derivative both have a singularity at zero, that is where  $\boldsymbol{\rho} = \boldsymbol{\rho}'$ . For this reason the evaluation of the integral over  $\Gamma_2$  has to be done very carefully. Fortunately integration over the singularity of the Green function results in a finite value and the second term inside the integral of (3.3.7) poses no problems (see Appendix B.2). Working around the singularity of the normal derivative of the Green function is a bit more

complicated.

First the contour  $\Gamma_2$  on which the integral is evaluated is divided into two parts

$$\Gamma_2 = \lim_{r \rightarrow 0} [\Gamma_{2-} + C_r] \quad (3.3.8)$$

where  $C_r$  is a semi-circular path with radius  $r$  and centred about the point on  $\Gamma_2$  where the singularity occurs. In the limit  $\Gamma_{2-}$  simply becomes  $\Gamma_2$  excluding the singular point. It can be shown that integrating the first term in (3.3.7) over  $C_r$  in the limit as  $r$  approaches zero evaluates to  $\frac{1}{2}E(\boldsymbol{\rho})$  (see Appendix B.3). This means that the integral equation reduces to

$$\frac{1}{2}E(\boldsymbol{\rho}) = \int_{\Gamma_{2-}} E(\boldsymbol{\rho}') \frac{\partial G_0(\boldsymbol{\rho}, \boldsymbol{\rho}')}{\partial n'} d\Gamma' + \int_{\Gamma_2} G_0(\boldsymbol{\rho}, \boldsymbol{\rho}') H(\boldsymbol{\rho}') d\Gamma' \quad (3.3.9)$$

which is the desired restriction on  $E$  and  $H$  to render the system solvable.

### 3.3.2 Discretisation

Proceeding as usual for the finite element solution, the problem domain is discretised and the field expansions within each element are defined. As before  $E$  is approximated within each element and on the domain boundary using a weighted set of basis functions. Now another unknown  $H$  has to be discretised in order to evaluate (3.3.2) and (3.3.9).

On the boundary  $\Gamma_2$  the unknown  $H$  is discretised in similar fashion to  $E$  using

$$H^s = \sum_{i=1}^{M^s} b_i^s \lambda_i^s. \quad (3.3.10)$$

Substituting the expansions for  $E$  and  $H$  into (3.3.2) and taking the variation with respect to the unknown coefficient  $a_i$  associated with  $E$ , gives

$$\begin{aligned} \frac{\partial \Pi(E)}{\partial a_i} &= \sum_{j=1}^N a_j \iint_{\Omega_1} \frac{\partial \lambda_i}{\partial x} \frac{\partial \lambda_j}{\partial x} + \frac{\partial \lambda_i}{\partial y} \frac{\partial \lambda_j}{\partial y} - k_0^2 \lambda_i \lambda_j d\Omega \\ &\quad + \sum_{j=1}^M b_j \int_{\Gamma_2} \lambda_i \lambda_j d\Gamma. \end{aligned} \quad (3.3.11)$$

As before  $N$  is the number of nodes in  $\Omega_1$  and  $M$  is the number of nodes on  $\Gamma_2$ . Because each  $a_j$  is associated with the expansion of  $E$  and each  $b_j$  is associated with the expansion of  $H$ ,  $\{a_j | j = 1, 2, \dots, N\} \cap \{b_j | j = 1, 2, \dots, M\} = \emptyset$ .

This means that the discretised functional (3.3.11) implies  $N$  expressions in  $N + M$  unknowns. Again setting the variation equal to zero and writing in matrix form gives

$$\begin{bmatrix} K & C \end{bmatrix} \begin{Bmatrix} a \\ b \end{Bmatrix} = \begin{Bmatrix} 0 \\ 0 \end{Bmatrix} \quad (3.3.12)$$

where

$$K_{ij} = \iint_{\Omega_1} \left[ \frac{\partial \lambda_i}{\partial x} \frac{\partial \lambda_j}{\partial x} + \frac{\partial \lambda_i}{\partial y} \frac{\partial \lambda_j}{\partial y} - k_0^2 \lambda_i \lambda_j \right] d\Omega \quad (3.3.13)$$

$$C_{ij} = \int_{\Gamma_2} \lambda_i \lambda_j d\Gamma. \quad (3.3.14)$$

Discretising the boundary integral equation starts with substituting the expansions for  $E$  and  $H$  on  $\Gamma_2$  in (3.3.9). For  $\boldsymbol{\rho}$  on edge  $s$  this equation becomes

$$\frac{1}{2}E(\boldsymbol{\rho}) = \sum_{\substack{j=1 \\ j \neq s}}^M a_j \int_{\Gamma_2^j} \lambda_j \frac{\partial G_0(\boldsymbol{\rho}, \boldsymbol{\rho}')}{\partial n'} d\Gamma' + \sum_{j=1}^M b_j \int_{\Gamma_2^j} \lambda_j G_0(\boldsymbol{\rho}, \boldsymbol{\rho}') d\Gamma' \quad (3.3.15)$$

where the  $\Gamma_2^j$  denotes the  $j$ th segment on the boundary  $\Gamma_2$  and the singularity occurs on segment  $\Gamma_2^s$ . That is, somewhere on the  $s$ th segment  $\boldsymbol{\rho} = \boldsymbol{\rho}'$ . A Galerkin method is applied by multiplying (3.3.15) with the  $M$  basis functions used to approximate  $E$  and  $H$ , and again integrating over  $\Gamma_2$ . The result is

$$\begin{aligned} \frac{1}{2}a_s \int_{\Gamma_2^i} \lambda_i \lambda_s d\Gamma &= \int_{\Gamma_2^i} \lambda_i \sum_{\substack{j=1 \\ j \neq s}}^M a_j \int_{\Gamma_2^j} \lambda_j \frac{\partial G_0(\boldsymbol{\rho}, \boldsymbol{\rho}')}{\partial n'} d\Gamma' d\Gamma \\ &+ \int_{\Gamma_2^i} \lambda_i \sum_{j=1}^M b_j \int_{\Gamma_2^j} \lambda_j G_0(\boldsymbol{\rho}, \boldsymbol{\rho}') d\Gamma' d\Gamma. \end{aligned} \quad (3.3.16)$$

Rewriting the above equation in matrix form gives

$$\begin{bmatrix} P' & Q \end{bmatrix} \begin{Bmatrix} a \\ b \end{Bmatrix} = \begin{Bmatrix} 0 \\ 0 \end{Bmatrix} \quad (3.3.17)$$

where

$$P_{ij} = \begin{cases} \int_{\Gamma_2^i} \lambda^i \int_{\Gamma_2^j} \lambda^j \frac{\partial G_0}{\partial n'} d\Gamma' d\Gamma & i \neq j \\ 0 & i = j \end{cases} \quad (3.3.18)$$

$$Q_{ij} = \int_{\Gamma_2^i} \lambda^i \int_{\Gamma_2^j} \lambda^j G_0 d\Gamma' d\Gamma \quad (3.3.19)$$

and  $P' = P - \frac{1}{2}C$ ,  $C$  having the same definition as in (3.3.14). This system provides an additional set of  $M$  equations in  $M + N$  unknowns and combining it with (3.3.12) yields a solvable system

$$\begin{bmatrix} K & C \\ P' & Q \end{bmatrix} \begin{Bmatrix} a \\ b \end{Bmatrix} = \begin{Bmatrix} 0 \\ 0 \end{Bmatrix}. \quad (3.3.20)$$

A few comments concerning the dimensions and assembly of the matrices in the above equation are in order. As there are  $N$  nodes associated with  $E$  in the finite element domain we have  $K_{N \times N}$ . This matrix represents the mutual interaction between basis functions approximating  $E$  and since finite element interactions are only local this matrix is sparse. The matrix  $C$  represents the interaction between basis functions associated with  $E$  and the basis functions associated with  $H$  which means it is  $C_{N \times M}$ . Again due to the local interaction characteristic of the finite element solution this matrix is also sparse. In fact, entire rows of this matrix are zero for rows associated with nodes that do not reside on  $\Gamma_2$ . Similarly we have  $P'_{M \times N}$  which also represents interaction between the basis functions associated with  $E$  and the basis functions associated with  $H$ , but from (3.3.16) this interaction is global. The result is a partially full matrix, where the columns associated with nodes not on  $\Gamma_2$  are zero. Since  $Q$  contains only global mutual interaction between the basis functions associated with  $H$  this matrix is full and has dimensions  $Q_{M \times M}$ . The complete system matrix is therefore partially full, partially sparse and not symmetric.

As for the finite element solution in Section 2.3.1 the inhomogeneous Dirichlet boundary condition is applied writing the complete system as

$$\begin{bmatrix} K_{xx} & K_{xy} & C_x \\ K_{yx} & K_{yy} & C_y \\ P'_x & P'_y & Q \end{bmatrix} \begin{Bmatrix} a_x \\ a_y \\ b \end{Bmatrix} = \begin{Bmatrix} 0 \\ 0 \\ 0 \end{Bmatrix}. \quad (3.3.21)$$

and specifying the known coefficients directly  $a_x = X$  to obtain

$$\begin{bmatrix} K_{yy} & C_y \\ P'_y & Q \end{bmatrix} \begin{Bmatrix} a_y \\ b \end{Bmatrix} = \begin{Bmatrix} -K_{yx}X \\ -P'_xX \end{Bmatrix} \quad (3.3.22)$$

which is the final system to be solved. Note that  $P'_x$  is usually an empty matrix since there are typically no interaction between the basis functions associated with nodes on  $\Gamma_1$  and the basis functions associated with the nodes on  $\Gamma_2$ . Also, since the system matrix is partly sparse and partly full, it can be subdivided into separate submatrices in order to take advantage of the sparsity property [3]. This means that the system equation (3.3.22) can be solved indirectly which is computationally more efficient than a direct solution.

### 3.3.3 Implementation

The implementation of the finite element part of the above formulated solution remains mainly unchanged, whereas the implementation of the boundary integral part raises a few issues. Here this implementation is discussed in detail.

As for the approximation of  $E$  in the finite element solution linear basis functions are used to approximate  $H$  on  $\Gamma_2$

$$H^s = \sum_{i=1}^2 b_i^s \lambda_i^s. \quad (3.3.23)$$

Substituting this expansion along with the expansion for  $E$  into (3.3.13) and (3.3.14) and evaluating, one obtains the finite element matrices for the solution as before. Evaluating the boundary integral matrix entries is not as simple.

Recalling the definition of the Green function (2.3.30) which contains the Hankel function, it is clear that the integrals in (3.3.18) and (3.3.19) cannot be evaluated analytically and a numerical integration technique has to be employed. Note that in the following the discussion is specifically centered on evaluation of the integral containing the product of  $H$  and the Green function, but the same applies for the term containing  $E$  and the derivative of the Green function.

A simple way to evaluate these integrals numerically is to approximate the Green function as constant when the integration is performed on a segment. In this case integration reduces to multiplying the constant value of the  $G_0$  on



a segment by the integral of the basis function over that segment. Since the argument of  $G_0$  is proportional to the distance between the source coordinate  $\boldsymbol{\rho}'$  and observer coordinate  $\boldsymbol{\rho}$  this approximation is fair if the source and observer segments are relatively far apart. However, due to the singular nature of  $G_0$  it varies rapidly for small arguments, which means the approximation is no longer valid if the source and observer segments are in close proximity. Such a case calls for a more accurate approach. A method which retains the simplicity of the above described integration technique but is more accurate at the cost of relatively little overhead is therefore employed [3].

Each segment on  $\Gamma_2$  is subdivided into a number of smaller subsegments. On each of these subsegments  $G_0$  is again approximated as constant, meaning that the variation of  $G_0$  along the entire segment is now approximated as piecewise constant. To evaluate the integral on a subsegment, the assumed constant value of  $G_0$  is multiplied by the integral of the basis function for  $H$  over that subsegment. Obtaining the integration along the entire segment then means summing the integrations over all the subsegments for that edge. The subdivision scheme for two segments is illustrated in Figure 3.4.

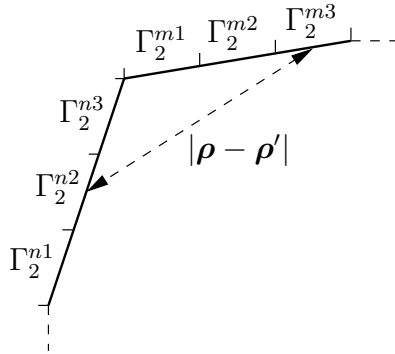


**Figure 3.4:** Subdivision of segments to integrate the Green function more accurately.

For a source segment  $\Gamma_2^i$  and observer segment  $\Gamma_2^j$ , each subdivided into  $L$  subsegments, the matrix entry  $Q_{ij}$  then becomes

$$Q_{ij} = \sum_{m=1}^L \int_{\Gamma_2^{im}} \lambda^i \sum_{n=1}^L \int_{\Gamma_2^{jn}} \lambda^j G_0^{mn} d\Gamma' d\Gamma, \quad \Gamma_2^{im} \neq \Gamma_2^{jn} \quad (3.3.24)$$

where  $\Gamma_2^{im}$  is the  $m$ th subsegment of the observer segment and  $\Gamma_2^{jn}$  is the  $n$ th subsegment of the source segment. Here  $G_0^{mn}$  is a constant equal to the Green

function evaluated for the source coordinate  $\boldsymbol{\rho}'$  at the centre of  $\Gamma_2^{jn}$  and the observer coordinate  $\boldsymbol{\rho}$  at the centre of  $\Gamma_2^{im}$ .

When the source and observer segments and subsegments coincide the above described technique fails as the Green function becomes singular and  $G_0^{mn}$  cannot be evaluated. For these subsegments the basis functions are assumed constant and the following approximation is used to integrate over the singularity of the Green function

$$\int_{-\delta/2}^{\delta/2} \int_{-\delta/2}^{\delta/2} G_0(k_0|x-x'|) dx' dx = \frac{\delta^2}{j^4} \left[ 1 - \frac{j^2}{\pi} \ln(0.0.1987k_0\delta) \right]. \quad (3.3.25)$$

As mentioned earlier, the above technique is also used to evaluate the integral containing  $E$  and the derivative of the Green function. Note however that (3.3.16) already excludes coinciding segments.

With the boundary integral termination of the finite element mesh implemented the finite element boundary integral method can be applied to solve the scattering problem of Section 2.2. The results are presented next.

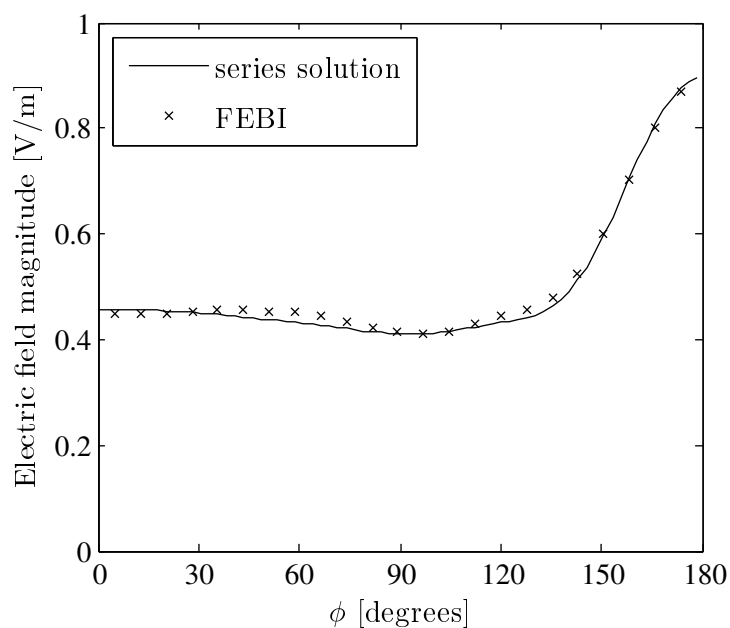
### 3.3.4 Results

The same problem solved with the use of absorbing boundary conditions in Section 3.2.3 is solved here using the finite element boundary integral method. The cylinder has a radius of  $0.5\lambda$ , the finite element domain is terminated at a distance of  $1.0\lambda$  from the cylinder surface and the maximum edge length in the mesh is  $\lambda/15$ .

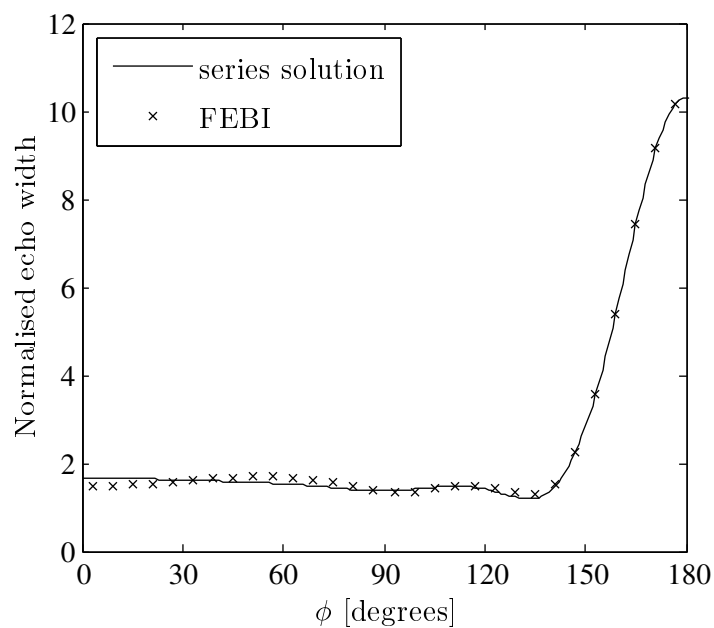
Figure 3.5 shows the scattered field computed on the exterior boundary along with the analytic solution. The results are fairly accurate and comparable to the accuracy of the first order absorbing boundary condition.

Figure 3.6 shows the calculated bistatic echo width of the cylinder. It is interesting to note that although the near-field results seem less accurate for the boundary integral termination than for the absorbing boundary condition termination, the converse seems true for the echo width.

Recall from Section 2.3.4 on the post-processing of the finite element solution that an integral transformation is used to calculate the far-field and thus the echo width. The derivative of  $E$  is required in this transformation and needs to be calculated from the obtained solution of the weighting coefficients and the basis functions for the ABC termination. Taking the derivative then



**Figure 3.5:** Scattered electric near-field computed using the finite element boundary integral method.



**Figure 3.6:** Echo width of perfectly conducting electrical cylinder computed using the finite element boundary integral method.

results in a zeroth order approximation, since the basis functions are linear. Contrary to this the FEBI yields this derivative as part of the solution meaning that a first order approximation is obtained. Consequently the post-processing is done more accurately resulting in a more accurate result for the echo width.

### 3.3.5 Interior Resonances

At this point it is worth discussing a problem that has been observed with the use of the finite element boundary integral method. That is, the occurrence of interior resonances at certain frequencies for a particular mesh [20]. First a discussion of the source of the problem is given, followed by an alternative formulation of the FEBI method and finally some results concerning the resonance problem are presented.

#### 3.3.5.1 Source of Interior Resonances

Consider first the problem of determining the waveguide modes for a cylinder of arbitrary cross-section numerically. Using a boundary integral on the surface of the cylinder to determine the field anywhere within the cylinder, an equation can be set up to determine these frequencies. Specifically if the transverse magnetic modes are to be computed, the total electric field has to be solved and an appropriate integral equation for this purpose is

$$E(\boldsymbol{\rho}) = \oint_{\Gamma_2} \left( G_0(\boldsymbol{\rho}, \boldsymbol{\rho}') \frac{\partial E(\boldsymbol{\rho}')}{\partial n'} - E(\boldsymbol{\rho}') \frac{\partial G_0(\boldsymbol{\rho}, \boldsymbol{\rho}')}{\partial n'} \right) d\Gamma' \quad (3.3.26)$$

which is simply the negative of (3.3.5) since the field is now determined on the inside of  $\Gamma_2$ . The perimeter of the cylinder is  $\Gamma_2$  and the integral is along a closed contour since the entire region interior to  $\Gamma_2$  is included in the problem domain. Noting that  $E(\boldsymbol{\rho}') = 0$  on the surface of a perfectly electrical conducting cylinder (since  $E$  now represents the total field) the above equation is reduced to

$$E(\boldsymbol{\rho}) = \oint_{\Gamma_2} G_0(\boldsymbol{\rho}, \boldsymbol{\rho}') \frac{\partial E(\boldsymbol{\rho}')}{\partial n'} d\Gamma'. \quad (3.3.27)$$

The integral operator in the above equation becomes singular for certain frequencies, specifically these are the TM mode cut-off frequencies for a waveguide with a cross-section perimeter  $\Gamma_2$ . Now an important point is emphasised. Since the integral operator in (3.3.27) becomes singular at these cut-off frequencies for the waveguide problem, the same operator in (3.3.26) would also

become singular at these frequencies whether or not the boundary condition for a conducting surface is enforced on  $E$ . That is, the singular nature of the integral operator in (3.3.27) also affects the solution to (3.3.26) irrespective of the properties of the boundary represented by  $\Gamma_2$ . This means that also for the boundary integral termination of the finite element mesh, where the  $\Gamma_2$  is only a fictitious boundary separating two free space regions, the solution is affected near these resonant frequencies.

Various methods have been proposed to eliminate the occurrence of these interior resonances, such as combined field formulations and combined source formulations [21]. However, incorporating these methods into the finite element boundary integral solution formulated here is rather difficult. A simple method to prevent the interior resonances from corrupting the solution is by introducing a small loss into the boundary integral equation [3]. This is equivalent to adding a small imaginary part to the wavenumber in equation (3.3.5). That is

$$k_0 \rightarrow k_0(1 + j\alpha), \quad \alpha \ll 1. \quad (3.3.28)$$

Although this is effective in eliminating the interior resonance problem, it also affects the final solution obtained for the FEBI method and the lossy solution deviates from the lossless solution. More specifically, if the FEBI method is formulated for the total field the solution is very sensitive to the introduced loss and more than one solution is required so that extrapolation techniques can be used to obtain the lossless solution free of interior resonances. Fortunately for the scattered field formulation of the FEBI, as is used here, the solution is relatively insensitive to the introduction of loss and extrapolation to a lossless solution is unnecessary.

In what follows results affected by interior resonances are presented for both the scattered field and the total field formulation. As the scattered field formulation has already been discussed, a brief overview of the total field formulation is warranted.

### 3.3.5.2 Total Field Solution

An overview of the total field formulation for the finite element boundary integral solution to the 2D scattering problem as in [3] is presented here.

The finite element part of the total field formulation is very much similar to that for the scattered field formulation and the functional to be rendered

stationary is unchanged

$$\Pi(E) = \iint_{\Omega_1} \nabla E \cdot \nabla E - k_0^2 E^2 \, d\Omega + 2 \int_{\Gamma_2} EH \, d\Gamma \quad (3.3.29)$$

where  $E$  now denotes the total electric field and  $H$  is defined in terms of the normal derivative of  $E$  on the boundary  $\Gamma_2$

$$\nabla E \cdot \hat{i}_n = -H \quad \text{on } \Gamma_2. \quad (3.3.30)$$

Notice that the boundary condition on the perfectly electrical conducting surface of the scatterer is now a homogeneous Dirichlet boundary condition

$$E = 0 \quad \text{on } \Gamma_1. \quad (3.3.31)$$

Obviously this boundary condition cannot be used to drive the system as before since it does not include the incident electric field. For the total field formulation the incident field is shifted to the integral equation

$$E(\boldsymbol{\rho}) = E^{\text{inc}}(\boldsymbol{\rho}) + \int_{\Gamma_2} \left( E(\boldsymbol{\rho}') \frac{\partial G_0(\boldsymbol{\rho}, \boldsymbol{\rho}')}{\partial n'} - G_0(\boldsymbol{\rho}, \boldsymbol{\rho}') \frac{\partial E(\boldsymbol{\rho}')}{\partial n'} \right) d\Gamma'. \quad (3.3.32)$$

The derivation of this integral equation assumes a current source in the free space exterior region  $\Omega_2$  to produce the incident field, see Appendix B.1. Enforcing the boundary condition (3.3.30) on  $\Gamma_2$  and adopting the same procedure as for the scattered field formulation to remove the singularity of the derivative of the Green function the integral equation becomes

$$\frac{1}{2} E(\boldsymbol{\rho}) = E^{\text{inc}}(\boldsymbol{\rho}) + \int_{\Gamma_{2-}} E(\boldsymbol{\rho}') \frac{\partial G_0(\boldsymbol{\rho}, \boldsymbol{\rho}')}{\partial n'} d\Gamma' + \int_{\Gamma_2} G_0(\boldsymbol{\rho}, \boldsymbol{\rho}') H(\boldsymbol{\rho}') d\Gamma'. \quad (3.3.33)$$

The functional (3.3.29) and integral equation (3.3.33) are discretised and combined into a single system similar as for the scattered field solution to obtain a linear system. Solution of the system finally yields the total electric field.

In order to validate the total field solution the scattering problem is solved and the results compared to the analytic solution. The electric near-field around a cylinder with radius  $0.5\lambda$  is calculated using a mesh in which the maximum edge length is  $\lambda/15$  and the exterior boundary is at a distance of  $1.0\lambda$  from the cylinder surface. Figure 3.7 shows the calculated total field and

the analytic solution. Clearly the solution is rather accurate and the accuracy of the total field formulation seems comparable to that of the scattered field formulation.

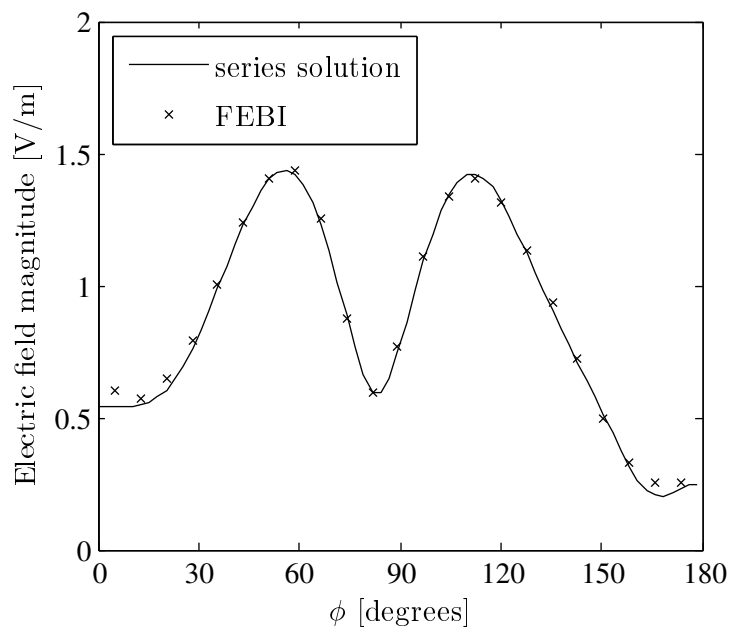


**Figure 3.7:** Total electric near-field computed using the total field formulation of the finite element boundary integral method.

### 3.3.5.3 Effect of Interior Resonances on Solution Accuracy

Some results concerning the interior resonance problem are now presented. Results obtained using the scattered field formulation as well as the total field formulation are presented and compared.

It has already been mentioned that the interior resonances occur near the waveguide cut-off frequencies associated with a conducting enclosure of which the surface coincides with the finite element domain exterior boundary. If this boundary is circular with a radius  $a$  then the TM mode cut-off frequencies [8] are

$$(f_c^{\text{TM}})_{mn} = \frac{\chi_{mn}}{2\pi a \sqrt{\mu\epsilon}} \quad (3.3.34)$$

where  $\chi_{mn}$  is the  $n$ th zero of the  $m$ th order Bessel function of the first kind,  $J_m(\chi_{mn}) = 0$ .

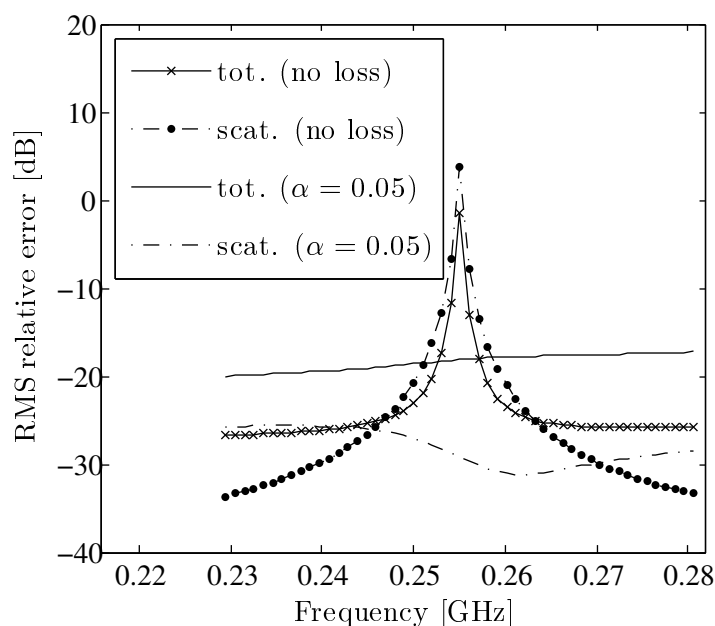


**Figure 3.8:** Susceptibility of the finite element boundary integral method to interior resonances.

Figure 3.8 shows the error in the field as computed using the FEBI method near the  $TM_{01}$  cut-off frequency associated with the circular boundary  $\Gamma_2$ . Results show the error for the total and scattered field formulations, both without loss and with a loss of  $\alpha = 0.05$ . The boundary radius is 0.45 m which means the cut-off frequency is 0.2551 GHz.

Clearly the interior resonance has a significant effect on the solution and by adding loss to the system the resonance is eliminated. Also note that the lossy solution obtained with the scattered field solution is more accurate than that for the total field solution at the frequency where the resonance occurs.

At higher frequencies the resonance problem is even worse, since the waveguide cut-off frequencies are more closely spaced. Figure 3.9 shows the solution errors for the same problem, but at a higher frequency.

The resonances visible are associated with the cut-off frequencies of the following modes, in order of increasing frequency,  $TM_{32}$  and  $TM_{13}$ . Results are shown only for the scattered field solution with different amounts of loss. Notice that by adding a sufficient amount of loss the solution error seems to level out so the accuracy obtained at the resonant frequencies are about the same as for frequencies where the resonances do not occur. This means that



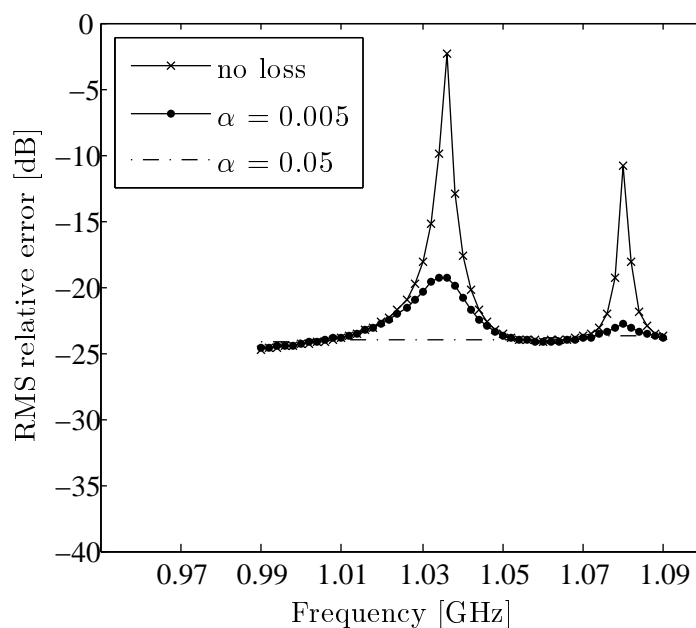


**Figure 3.9:** Interior resonances at higher frequencies.

the error caused by the resonance is decreased below the error caused by other factors, such as mesh fineness and distance from the scatterer to the mesh termination boundary.

Finally, at the cut-off frequency 1.0363 GHz of the  $\text{TM}_{32}$  mode the total and scattered field solutions are obtained with different loss factors in the range  $\alpha \in [10^{-5}; 10^{-1}]$ . The effect on the solution accuracy is shown in Figure 3.10. A steep improvement in accuracy is observed for small values of the loss factor. Notice that as the loss is increased beyond a certain point the accuracy of the total field solution again degrades, while for the scattered field solution the accuracy remains more or less constant. For the total field solution this means that although the error induced by the resonance is eliminated, further calculations are required to calculate the lossless solution through extrapolation, as mentioned earlier. However, for the scattered field solution the result is comforting as it implies that a relatively large loss can be chosen to ensure that the resonance is eliminated.

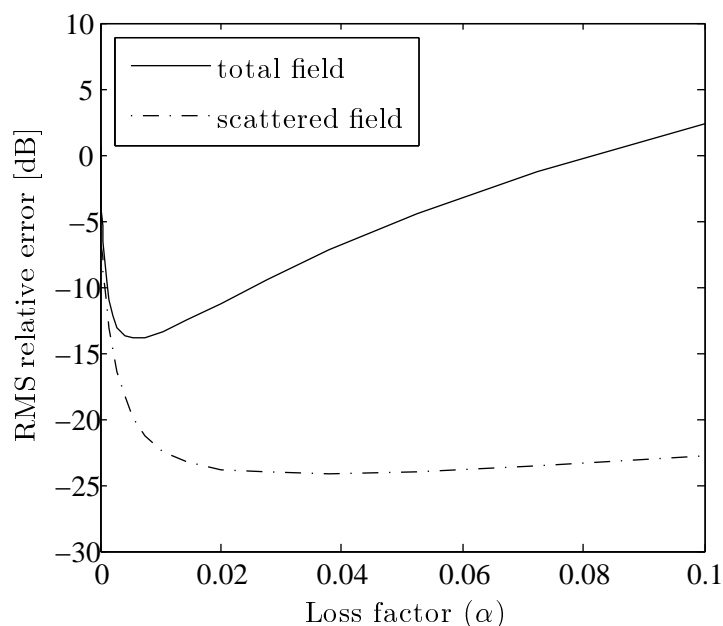


**Figure 3.10:** Effect of loss on the solution accuracy for the finite element boundary integral method near an interior resonance.

## 3.4 Infinite Elements

Both the boundary integral and absorbing boundary condition schemes terminate the finite element mesh by enforcing certain restrictions on the field at the exterior boundary of the finite element domain. Contrary to this, the infinite element scheme actually shifts the exterior boundary of the solution domain to infinity where the Sommerfeld radiation condition is applied. This is accomplished by attaching a special kind of element which has infinite size (hence the name) to the exterior of the finite element domain. The formulation of the infinite element method is now presented.

### 3.4.1 Formulation

As before the aim is to solve the Helmholtz differential equation, however now a solution is sought in the domain  $\Omega_\infty = \Omega_1 + \Omega_2$ , see Figure 3.11. Notice that the boundary  $\Gamma_2$  becomes redundant (however it again becomes important when discretisation is discussed) and the problem domain is terminated by  $\Gamma_\infty$  which is at an infinite distance. Because the exterior boundary of the infinite element domain is at infinity the unbounded nature of the scattering problem

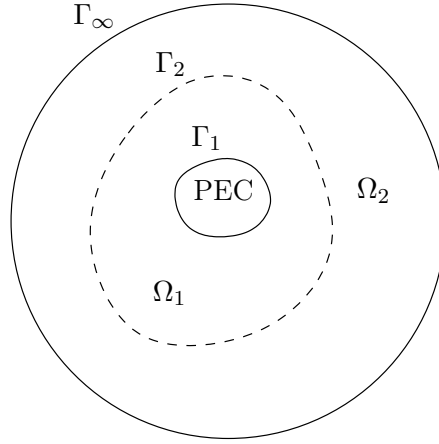


**Figure 3.11:** The infinite element domain for the scattering problem in two dimensions.

is now accurately modelled.

Obtaining a unique solution to the Helmholtz equation again requires adequate specification of the boundary conditions. Consider the boundary condition that is to be enforced at  $\Gamma_\infty$ . Clearly the field should vanish at this boundary. However, requiring only that the field vanishes is insufficient to yield a unique solution [22] and a more stringent condition has to be enforced. Such a condition is the so-called Sommerfeld radiation condition which has the following general form

$$\lim_{x \rightarrow \infty} \left[ x^h \left( \frac{\partial E}{\partial |x|} + jk_0 E_z \right) \right] = 0 \quad \text{and} \quad (3.4.1)$$

$$\lim_{x \rightarrow \infty} [E] = \mathcal{O} \left( \frac{1}{x^h} \right) \quad (3.4.2)$$

where  $h = \frac{n-1}{2}$  and  $n$  is the number of spatial dimensions. For circular cylindrical coordinates this becomes

$$\lim_{\rho \rightarrow \infty} \left[ \sqrt{\rho} \left( \frac{\partial E}{\partial \rho} + jk_0 E \right) \right] = 0 \quad \text{and} \quad (3.4.3)$$

$$\lim_{\rho \rightarrow \infty} [E] = \mathcal{O} \left( \frac{1}{\sqrt{\rho}} \right). \quad (3.4.4)$$

Notice that (3.4.3) can be enforced by

$$\nabla E \cdot \hat{i}_n + jk_0 E = 0 \quad \text{on} \quad \Gamma_\infty \quad (3.4.5)$$

for a circular  $\Gamma_\infty$ . The restriction on  $E$  specified by (3.4.4) will be enforced later by an appropriate form of the expansion functions used in  $\Omega_\infty$ . As before the inhomogeneous Dirichlet boundary condition still applies on  $\Gamma_1$ . Thus the boundary value problem to be solved is now

$$\begin{aligned} \nabla^2 E + k_0^2 E &= 0 & \text{in } \Omega_\infty \\ E &= -E^{\text{inc}} & \text{on } \Gamma_1 \\ \nabla E \cdot \hat{i}_n + jk_0 E &= 0 & \text{on } \Gamma_\infty. \end{aligned} \quad (3.4.6)$$

Noting the similarity between (3.4.6) and (2.3.4) the boundary value problem can be solved by rendering the following functional stationary

$$\Pi(E) = \iint_{\Omega_\infty} \nabla E \cdot \nabla E - k_0^2 E^2 \, d\Omega + \int_{\Gamma_\infty} jk_0 E^2 \, d\Gamma. \quad (3.4.7)$$

Note that the second integral in the above expression does not vanish as a result of the radiation condition (3.4.4). In the discussion that follows it is also useful to divide the integral over  $\Omega_\infty$  into an integral over the finite element domain  $\Omega_1$  and the infinite element domain  $\Omega_2$ . The functional is then written in the following form

$$\begin{aligned} \Pi(E) &= \iint_{\Omega_1} \nabla E \cdot \nabla E - k_0^2 E^2 \, d\Omega \\ &+ \iint_{\Omega_2} \nabla E \cdot \nabla E - k_0^2 E^2 \, d\Omega + \int_{\Gamma_\infty} jk_0 E^2 \, d\Gamma. \end{aligned} \quad (3.4.8)$$

Discretisation of the infinite element solution can now proceed.

### 3.4.2 Discretisation

The formulation of the infinite element solution treats both regions  $\Omega_1$  and  $\Omega_2$  similarly meaning that the boundary  $\Gamma_2$  becomes redundant. However, here it is useful to reintroduce this boundary as the separation between the finite element region  $\Omega_1$  and the infinite element region  $\Omega_2$ . With this separation and noting that the results thus far obtained for the finite element region are similar to those in Chapter 2, it is concluded that the discretisation of the finite element part of the solution remains the same as before. Attention can now be turned to discretising the infinite element part of the solution.

With  $\Omega_1$  subdivided into smaller elements the boundary  $\Gamma_2$  is automatically

subdivided into segments. The same applies to the subdivision of  $\Omega_2$  into infinite elements and in order to enforce the continuity of  $E$  across  $\Gamma_2$ , the discretisation in  $\Omega_2$  should be compatible with that in  $\Omega_1$ . Simply stated, a segment on  $\Gamma_2$  which is an edge of a finite element in  $\Omega_1$  should also be an edge of an infinite element in  $\Omega_2$ .

Enforcing the edge of a finite element on the boundary to be exactly the edge of the attached infinite element can be cumbersome, nonetheless this has been achieved in literature using various approaches. In [13] the infinite element is mapped to a standard finite element and in [14] an infinite element is developed to be compatible with arbitrary finite element shapes. However, an elegant approach is presented in [23] where infinite elements are designed to fit an elliptical boundary  $\Gamma_2$ . Although  $\Gamma_2$  is discretised by a set of segments, the approximation is valid if the segments are short and if the curvature of the boundary is very small. Here this approach is used to implement the infinite element scheme, although a circular boundary is assumed instead of an elliptical boundary.

Again in order to be compatible with the field expansions within finite elements having an edge on  $\Gamma_2$ , the basis functions within the infinite elements have to be chosen carefully. The field expansion should also adhere to (3.4.4) of the Sommerfeld radiation condition since the infinite elements approximate the field in an unbounded region. Since both  $\Gamma_2$  and  $\Gamma_\infty$  are circular these restrictions on the basis functions can be satisfied by two independent functions. Traversing a segment on  $\Gamma_2$  is equivalent to a variation in the angular variable  $\phi$  and the compatibility restriction can be satisfied with an angular function  $A(\phi)$ . The radial decay restriction on the basis function can obviously only be satisfied by a certain radial function  $R(\rho)$ . Let the basis functions approximating  $E$  inside an infinite element therefore be defined as

$$\lambda_{ij} = A_i(\phi)R_j(\rho). \quad (3.4.9)$$

This separation also allows the infinite element to be made compatible with higher order finite elements by increasing the order of  $A_i$ , while a better approximation of the field in the far-zone is obtained by increasing the order of  $R_j$ . If the order of the angular function is  $N_A$  and that of the radial function

is  $N_R$ , then the field within the  $e$ th infinite element is expressed as

$$E^e = \sum_{k=1}^{N_R \times N_A^e} c_k^e \lambda_k^e \quad (3.4.10)$$

where the mapping  $(ij) \rightarrow k$  is used to map each pair of angular and radial functions to a unique basis function.

Substituting the expansions for the infinite elements into (3.4.8) and taking the derivative with respect to the unknown coefficient  $c_i$  gives

$$\begin{aligned} \frac{\partial \Pi_2}{\partial c_i} &= \sum_{j=1}^{N_2} c_j \iint_{\Omega_2} \frac{\partial \lambda_i}{\partial \rho} \frac{\partial \lambda_j}{\partial \rho} + \frac{1}{\rho^2} \frac{\partial \lambda_i}{\partial \phi} \frac{\partial \lambda_j}{\partial \phi} - k_0^2 \lambda_i \lambda_j \, d\Omega \\ &\quad + \sum_{j=1}^{N_2} c_j \int_{\Gamma_\infty} j k_0 \lambda_i \lambda_j \, d\Gamma \end{aligned} \quad (3.4.11)$$

where there are  $N_2$  nodes in the infinite element region. Equating the derivative to zero and writing in matrix form gives

$$[K_2]\{c\} = \{0\} \quad (3.4.12)$$

where

$$\begin{aligned} K_{2ij} &= \iint_{\Omega_2} \frac{\partial \lambda_i}{\partial \rho} \frac{\partial \lambda_j}{\partial \rho} + \frac{1}{\rho^2} \frac{\partial \lambda_i}{\partial \phi} \frac{\partial \lambda_j}{\partial \phi} - k_0^2 \lambda_i \lambda_j \, d\Omega \\ &\quad + \int_{\Gamma_\infty} j k_0 \lambda_i \lambda_j \, d\Gamma. \end{aligned} \quad (3.4.13)$$

The expansions for the finite elements are also substituted into (3.4.8) to obtain after differentiating with respect to the unknown coefficient  $a_i$  the result

$$\frac{\partial \Pi_1(E)}{\partial a_i} = \sum_{j=1}^{N_1} a_j \iint_{\Omega_1} \frac{\partial \lambda_i}{\partial x} \frac{\partial \lambda_j}{\partial x} + \frac{\partial \lambda_i}{\partial y} \frac{\partial \lambda_j}{\partial y} - k_0^2 \lambda_i \lambda_j \, d\Omega \quad (3.4.14)$$

where there are  $N_1$  nodes in the finite element region. Different from before no contour integral appears in this expression. Letting the derivative equal zero and writing in matrix form gives

$$[K_1]\{a\} = \{0\} \quad (3.4.15)$$

where

$$K_{1ij} = \iint_{\Omega_1} \frac{\partial \lambda_i}{\partial x} \frac{\partial \lambda_j}{\partial x} + \frac{\partial \lambda_i}{\partial y} \frac{\partial \lambda_j}{\partial y} - k_0^2 \lambda_i \lambda_j \, d\Omega. \quad (3.4.16)$$

Since each node on  $\Gamma_2$  belongs to a finite and an infinite element we have  $\{a_j \mid j = 1, 2, \dots, N_1\} \cap \{c_j \mid j = 1, 2, \dots, N_2\} \neq \emptyset$ . This means that the total number of unknowns in the system is  $N < N_1 + N_2$  and that the systems in (3.4.12) and (3.4.15) should be assembled into a single system. The result is

$$\begin{bmatrix} K'_1 & K'_{11} & 0 \\ K'_{11}T & K_{12} & K'_{22} \\ 0 & K'_{22}T & K'_2 \end{bmatrix} \begin{Bmatrix} a' \\ b \\ c' \end{Bmatrix} = \begin{Bmatrix} 0 \\ 0 \\ 0 \end{Bmatrix} \quad (3.4.17)$$

where  $b$  are the coefficients associated with nodes on  $\Gamma_2$  and where  $a'$  and  $c'$  are the coefficients associated with nodes in the finite and infinite element regions, respectively, but not on  $\Gamma_2$ .

The subdivision of the main system matrix is as follows. The mutual interaction between unknowns in  $\Omega_1$  and not on  $\Gamma_2$  is represented by  $K'_1$ , while the mutual interaction between unknowns in  $\Omega_2$  and not on  $\Gamma_2$  are represented by  $K'_2$ . Interaction between the unknowns on  $\Gamma_2$  and unknowns in  $\Omega_1$  but not on  $\Gamma_2$  is represented by  $K'_{11}$  and similarly for unknowns in  $\Omega_2$  and the matrix  $K'_{22}$ . Finally the mutual interaction between unknowns on  $\Gamma_2$  is contained in  $K_{12}$ .

As before the Dirichlet boundary condition on  $\Gamma_1$  can be enforced by directly specifying the values of the coefficients associated with the nodes on  $\Gamma_1$ . Notice also that the system matrix is sparse since the interaction between the basis functions in the infinite element region is also only local.

Finally, note that the definition (3.4.9) of the basis functions for the infinite elements can be exploited to simplify the expression for the infinite element matrix. That is

$$K_{2ij} = I_{ij}^{R1} I_{ij}^{A1} + I_{ij}^{R2} I_{ij}^{A2} - k_0^2 I_{ij}^{R3} I_{ij}^{A1} + j k_0 I_{ij}^{R4} I_{ij}^{A1} \quad (3.4.18)$$

where after substituting the differentials  $d\Omega$  and  $d\Gamma$  with  $d\rho$  and  $\rho d\phi$  in the

circular cylindrical coordinate system

$$I_{ij}^{R1} = \lim_{\tilde{\rho} \rightarrow \infty} \int_{\rho_2}^{\tilde{\rho}} \frac{dR_i}{d\rho} \frac{dR_j}{d\rho} \rho d\rho \quad (3.4.19)$$

$$I_{ij}^{R2} = \lim_{\tilde{\rho} \rightarrow \infty} \int_{\rho_2}^{\tilde{\rho}} R_i R_j \frac{1}{\rho} d\rho \quad (3.4.20)$$

$$I_{ij}^{R3} = \lim_{\tilde{\rho} \rightarrow \infty} \int_{\rho_2}^{\tilde{\rho}} R_i R_j \rho d\rho \quad (3.4.21)$$

$$I_{ij}^{R4} = \lim_{\tilde{\rho} \rightarrow \infty} [R_i R_j \tilde{\rho}] \quad (3.4.22)$$

$$I_{ij}^{A1} = \int_{\phi_1}^{\phi_2} A_i A_j d\phi \quad (3.4.23)$$

$$I_{ij}^{A2} = \int_{\phi_1}^{\phi_2} \frac{dA_i}{d\phi} \frac{dA_j}{d\phi} d\phi. \quad (3.4.24)$$

In the above  $\rho_2$  is the radius of the circular boundary  $\Gamma_2$ . The finite element solution using an infinite element mesh termination scheme can now be implemented.

### 3.4.3 Implementation

As usual the finite element domain is subdivided into triangular elements on which simplex basis functions approximate the field. It is now necessary to define the shape and basis functions for the infinite elements and to show that they are compatible with the finite elements on  $\Gamma_2$ .

Earlier it was noted that the evaluation of a simplex basis function defined for a triangle is exactly zero on the edge opposite the vertex with which it is associated. This means that on a triangle edge the field is approximated as the weighted sum of only two linear functions and each of these functions varies from unity at the node with which it is associated to zero at the other node. For an edge on  $\Gamma_2$  which is circular, the two nodes are at the same radial coordinate and only their angular coordinates are different. However, along the edge the radial coordinate decreases to a minimum at the centre of the edge. If this edge is very short in comparison to the radius of  $\Gamma_2$  this variation in radius is very small and the edge can be approximated as lying entirely on  $\Gamma_2$ , see Figure 3.12.

Now the basis functions on the edge associated with the finite element can



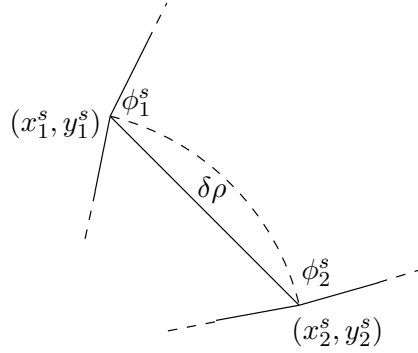


**Figure 3.12:** Compatibility between finite and infinite elements.

be defined as an angular function

$$A_m^s(\phi) = \frac{\phi - \phi_n^s}{\phi_m^s - \phi_n^s} \quad (3.4.25)$$

where  $\phi_i^s$  is the angular coordinate of node  $i$  on segment  $s$ . Using this as the angular function in (3.4.9) then implies that compatibility between the finite element and infinite element basis functions can be ensured by requiring that the radial function evaluates to unity on  $\Gamma_2$ .

The radial dependency of the basis functions are chosen to satisfy (3.4.4) and to include the phase variation of the field. A general high order function as in [23] is used so an arbitrary order radial expansion is available. In order to define such an expansion, the required number of nodes are placed on the radial edges of the infinite element as shown in Figure 3.13 for a third order element. For a  $N_R$ th order expansion  $N_R + 1$  nodes are placed on each radial edge, where one of the nodes is at infinity. The spacing of these nodes is arbitrary and it was found that a linear spacing in multiples of the radius of  $\Gamma_2$  gives good results.

Now the radial function is defined

$$R_m^e(\rho) = e^{-jk_0(\rho - \rho_m^e)} \sum_{n=1}^{N_R} h_{mn}^e \rho^{\frac{1}{2} - n} \quad (3.4.26)$$

where  $N_R$  is the order of radial expansion. The phase term  $e^{jk_0\rho_m^e}$  and coefficients  $h_{mn}^e$  are used to normalize the basis function  $R_m^e$  to unity at a radius of  $\rho_i^e$  so field continuity can be enforced easily. The coefficients  $h_{mn}^e$  can be

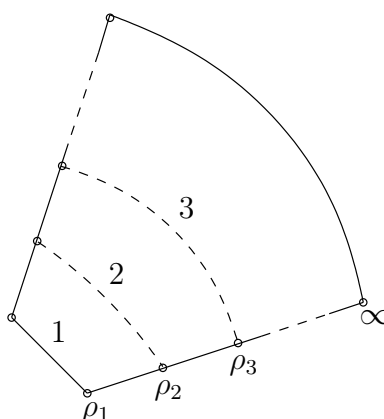


**Figure 3.13:** Placement of radial nodes for higher order infinite elements.

calculated from

$$[H][S] = [I] \quad (3.4.27)$$

where  $S_{mn} = \rho_n^{\frac{1}{2}-m}$  for  $m = 1, 2, \dots, N_R$  and  $I$  is the identity matrix. Notice that (3.4.27) implies that each radial function evaluates to unity at the radius of the node with which it is associated and to zero at the other node radii.

The basis functions for the infinite element are then simply the product of (3.4.25) and (3.4.26). Substituting these basis functions into the expressions (3.4.19) through (3.4.22) results in rather lengthy expressions and are not given here, for a detailed evaluation see Appendix C.1. However, a few comments concerning the evaluation of these integrals are worth mentioning.

Firstly, due to the exponential factor present in the radial function, not all of the integrals can be evaluated analytically. Specifically some of the integrals reduce to the  $E_n$ -function

$$E_n(x) = \int_1^\infty \frac{e^{-xt}}{t^n} dt \quad (3.4.28)$$

which has to be approximated by a finite sum, see Appendix A.2. Secondly, some of the integrals are evaluated to obtain the following undefined oscillatory term

$$\lim_{\bar{\rho} \rightarrow \infty} \left[ e^{-jk_0 \bar{\rho}} \right]. \quad (3.4.29)$$

Fortunately, adding these terms according to (3.4.18) cancels these terms and the sum is well defined. Finally, note that if the spacing of the radial nodes is the same for every element, then the integrals (3.4.19) through (3.4.22) are

the same for all the infinite elements. Therefore these integrals need only be calculated once during a single solution.

Some results obtained using the infinite element scheme are presented in the following section.

### 3.4.4 Results

As for the other mesh termination schemes, the infinite element method is used to calculate the scattered electric field around a perfectly conducting cylinder with a radius  $0.5\lambda$ . The same mesh used with the other schemes are used here. The boundary separating the finite element and infinite element regions is at a distance  $1.0\lambda$  from the cylinder surface and the maximum edge length in the finite element mesh is  $\lambda/15$ .

Figure 3.14 shows the scattered field computed on the boundary  $\Gamma_2$  for various orders of the radial expansion (3.4.26), along with the analytic solution. Already for first order elements the results seem rather accurate and there seems to be little difference in the accuracy gained by using higher order elements. Such a rapid convergence in the accuracy of infinite elements of different orders were also observed in [23] for meshes where the boundary

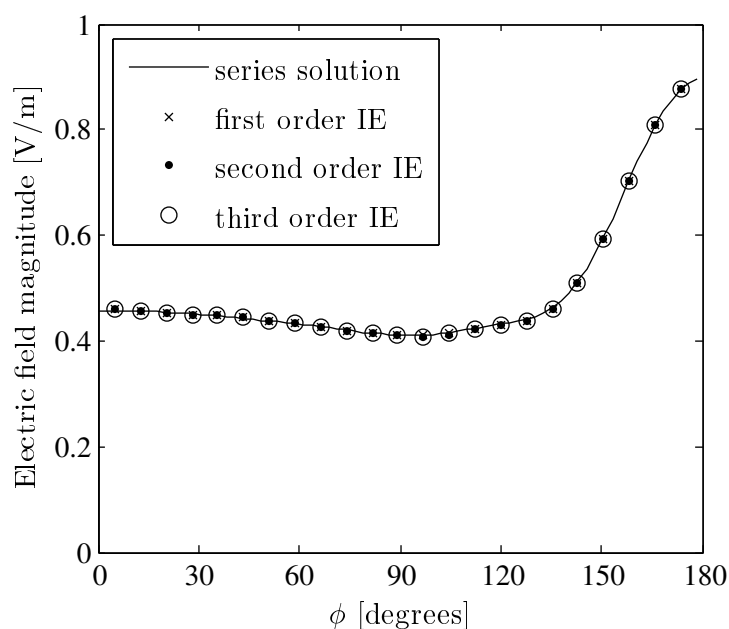


**Figure 3.14:** Scattered electric near-field computed using infinite elements with various orders of radial expansions.

separating the finite element and infinite element domains is sufficiently far from the scatterer.

Figure 3.15 shows the bistatic echo width of the cylinder as calculated using the near-field to far-field transformation. Again the results are not as accurate as the scattered field and as for the absorbing boundary conditions, this is attributed to the low degree of accuracy with which the derivative of the field is approximated within the finite element region.

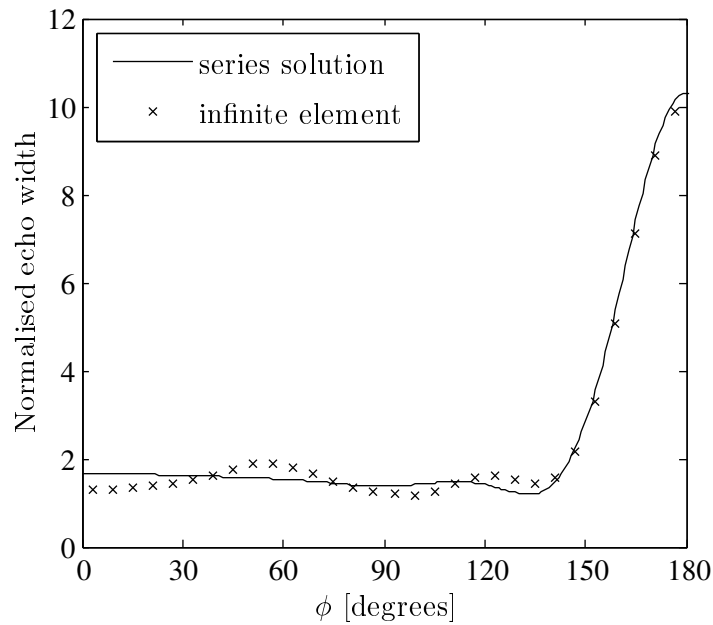


**Figure 3.15:** Echo width of perfectly electrical conducting cylinder computed using infinite elements with a third order radial expansion.

#### 3.4.4.1 Galerkin Weighted and Complex Conjugate Weighted Infinite Elements

It is well-known that the variational formulation of the finite element method results in exactly the system obtained with using the Galerkin weighted residual formulation. That is, the solution thus far presented is equivalently a Galerkin weighted residual solution. Considering again the radial function used in the infinite element expansion function, it is found that the exponential factor is responsible for the complexity of the integrals arising from evaluating the elemental matrix entries. In [14] and [24] a proposed method

to simplify these integrals is to use a complex conjugate weighted residual formulation. Here such a solution is implemented and the results compared to those obtained with the Galerkin weighted infinite elements.

With a complex conjugate weighting function the matrix entries for each infinite element (3.4.12) becomes

$$K_{2ij} = \iint_{\Omega_2} \frac{\partial \lambda_i}{\partial \rho} \frac{\partial \bar{\lambda}_j}{\partial \rho} + \frac{1}{\rho^2} \frac{\partial \lambda_i}{\partial \phi} \frac{\partial \bar{\lambda}_j}{\partial \phi} - k_0^2 \lambda_i \bar{\lambda}_j \, d\Omega + \int_{\Gamma_\infty} j k_0 \lambda_i \bar{\lambda}_j \, d\Gamma \quad (3.4.30)$$

where  $\bar{z}$  represents the complex conjugate of  $z$ . Since real-valued basis functions are used in the finite element region, the results for the finite element matrix equation are retained. For the infinite element matrices this means that the integrals in (3.4.19) through (3.4.22) contain only negative order polynomial functions in  $\rho$  that are easily evaluated analytically (see Appendix C.2).

The same scattering problem as before is solved here using the complex conjugate weighted infinite element solution. Figure 3.16 shows the calculated scattered field and the analytic solution. The results are rather poor for the

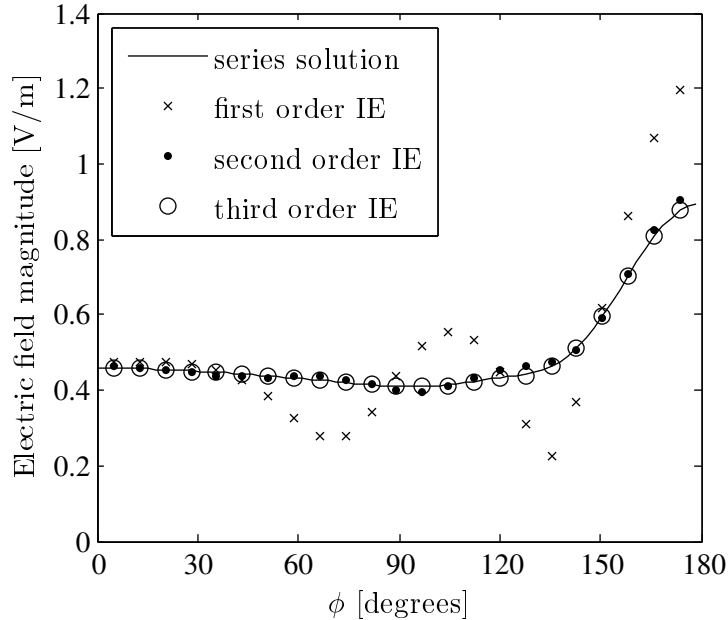


**Figure 3.16:** Scattered electric near-field computed using complex conjugate weighted infinite elements.

first order infinite elements, but for second order and higher order expansions the results compare well with the Galerkin infinite element results.

## 3.5 Comparison of Mesh Termination Schemes

The motivation for an appropriate mesh termination scheme when using a finite element method to solve unbounded problems has already been stated. Three such schemes were formulated, implemented and used to solve a typical unbounded problem, yielding relatively accurate results. Here these methods are compared [25] on the grounds of accuracy, computational efficiency and implementation complexity.

### 3.5.1 Solution Accuracy

One of the most important considerations when deciding on a mesh termination scheme is the desired level of accuracy. In order to compare the accuracy of the various schemes directly, each is used to solve the same scattering problem encountered before and an error is calculated according to (2.3.38) and (2.3.39) for each solution.

One of the factors affecting the accuracy of any finite element solution is the mesh fineness. In general, the solution error decreases with an increase in mesh fineness, which is a decrease in the average edge length in the mesh. Here the different mesh termination schemes are applied to solve the scattered field around a cylinder with a radius  $0.5\lambda$  and for  $\Gamma_2$  at a distance of  $1.0\lambda$  from the cylinder surface. The maximum edge length in the mesh is varied from  $\lambda/10$  to  $\lambda/30$ .

Figure 3.17 shows the performance of the various methods for an increasing mesh fineness. As expected the first order absorbing boundary condition results in a larger error than does the second order. It is interesting to note that the first order infinite element is nearly exactly as accurate as the second order ABC. For a coarser mesh the different schemes give more or less the same accuracy since the error due to the coarseness of the mesh becomes dominant. All the methods show a steady decrease in error with an increase in mesh fineness as expected.

Another factor affecting specifically the accuracy of a finite element solution of unbounded problems is the distance at which the finite element domain is terminated. Since the formulation of various mesh termination schemes

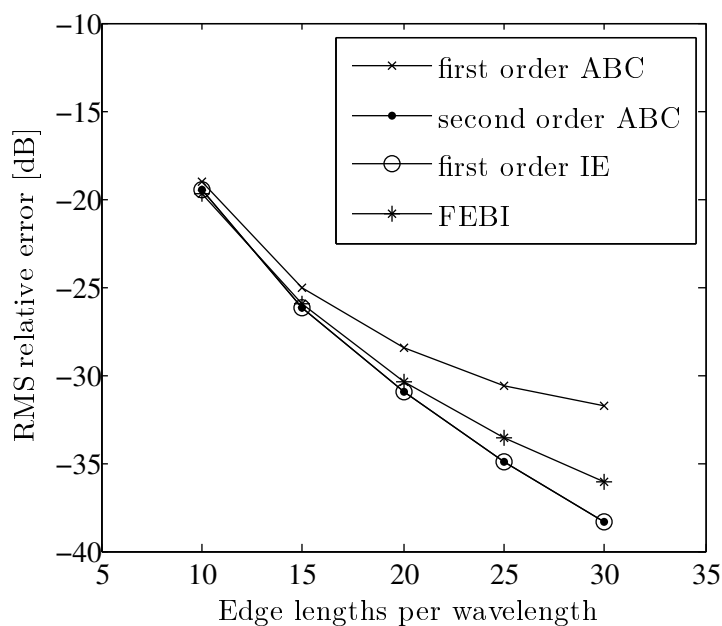


**Figure 3.17:** Effect of mesh fineness on the error for different mesh termination schemes.

(specifically the absorbing boundary conditions) depend on the termination being at a sufficiently far distance it is expected that the solution accuracy should generally improve as the distance to the termination is increased. Here the different schemes are used to calculate again the scattered field around the cylinder, but with the maximum edge length in the finite element mesh constant at  $\lambda/25$  and with  $\Gamma_2$  varying between  $1.0\lambda$  to  $2.0\lambda$  from the cylinder surface.

Figure 3.18 shows the performance of the various schemes. What is interesting is the fact that the accuracy of the first order ABC and the FEBI method generally improves as the boundary is shifted outward, while the converse seems true for the accuracy of the second order ABC and the infinite element scheme. The loss in accuracy as the boundary is shifted outward is attributed to numerical dispersion in the mesh [26]. As the electrical size of a mesh is increased the accumulated error increases and a loss in accuracy results.

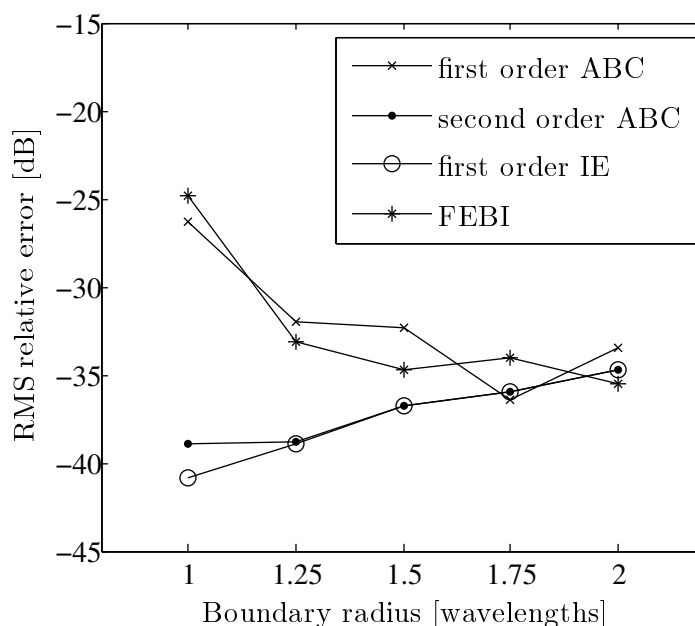


**Figure 3.18:** Effect of outer boundary radius on the error for different mesh termination schemes.

## 3.5.2 Computational Efficiency

One of the key advantages of the finite element method as a numerical solution is that the system matrix is usually sparse and as a result memory requirements are relatively low. In addition to the memory efficiency, many fast solution algorithms are specially suited for sparse matrices and the required solution time is also decreased. Obviously the employed mesh termination scheme also affects the computational efficiency of the finite element method and these effects are considered here, first using qualitative arguments and then with the aid of some calculated results.

### 3.5.2.1 Memory Requirements

First consider the impact of the termination schemes on the resulting system matrix. Since the absorbing boundary conditions are implemented by simply specifying a boundary condition on the exterior boundary, no new unknowns are introduced and the sparsity of the matrix is unaltered. For this scheme the memory requirements remain the same.

Using infinite elements more unknowns are introduced only if the radial expansions are of order second or higher. Since the interactions for infinite



elements are still only local the system matrix remains sparse for low order infinite elements, but with an increase in order of the radial expansions used, the infinite element part of the matrix becomes increasingly dense. For infinite elements then, more memory may be required depending on the order of the infinite elements, but the added demand on memory is expected to remain relatively low.

Employing the finite element boundary integral method, a number of unknowns are added to the system. In addition to the finite element matrix, three more matrices comprise the total system matrix to include the interactions concerning these added unknowns. One of these matrices represents local interactions between the added unknowns and the finite element system and is therefore sparse. The other two matrices represent global interactions implying full matrices. Consequently the added demand on memory is relatively high for this scheme.

### 3.5.2.2 Solution Time

Consider now the impact of the different schemes on the time required to solve a typical problem. This time may be divided into two parts, one part being the time required to compute the system matrices and the other the time needed to solve the resulting system equation.

Since the solution time is dependent on the number of unknowns in the system and the properties of the matrix, it can be concluded from the above that the solution time is expected to be more or less the same for an ABC termination and a low order infinite element scheme. For higher order infinite elements the solution time is expected to increase slightly and the FEBI method should be the most expensive in this respect.

Filling the system matrix for the finite element method requires running through the total number of elements in the mesh and adding the relevant entries for that element in the system matrix. The required time for this operation is therefore in the order of the number of elements in the mesh. Using an ABC requires similarly running through the number of segments on the exterior boundary and adding the entries for each segment into the system matrix and the impact on the matrix fill-in time is not significant.

For infinite elements the impact on the matrix fill-in time is similar to that for an ABC since the number of infinite elements is the same as the number of segments on the exterior boundary. However, the number of entries per

infinite element is proportional to the square of the order of that element and for high order elements this effect can be observed. Still, the matrix fill-in time remains relatively low even for higher order elements.

Matrix fill-in for the FEBI method entails filling three matrices in addition to the finite element matrix. For the added matrix representing local interactions, the fill-in time is again proportional to the number of segments on the exterior boundary. Filling the matrices representing global interaction, however is proportional to the square of the number of these segments. Consequently the fill-in time for the FEBI is expected to be rather expensive.

### 3.5.2.3 Some Results

Some results can now be presented to support the above arguments. The finite element method is used to solve the scattering problem first using a second order ABC, then using first and third order infinite elements and finally using the FEBI method. All solutions are obtained for the same mesh in which the exterior boundary is  $1.0\lambda$  from the cylinder surface and in which the longest edge length is  $\lambda/25$ .

Table 3.1 shows the computational costs incurred for the various methods. The second and third columns list the total number of unknowns in the system and the number of non-zero elements in the system matrix, respectively. Columns four and five list the fill-in and solution times in milliseconds of processor time as for an AMD Athlon™ 64 Dual Core 4400+ processor.

Method	Unknowns	Non-zero	Fill-in [ms]	Solution [ms]
ABC	3 910	26 740	1 906	141
IE (1st)	3 910	26 740	1 891	141
IE (3rd)	4 380	32 380	2 547	125
FEBI	4 145	137 895	27 391	484

**Table 3.1:** Computational costs for different mesh termination schemes.

The number of unknowns are the same for the ABC and the first order infinite elements, while the FEBI method and third order infinite element scheme adds more unknowns to the system. For the ABC and infinite element schemes the number of non-zero elements in the system matrix remain relatively low, but a drastic increase is observed for the FEBI method. Similar behaviour

is observed for the required fill-in time of the various methods. Finally, it is noted that the FEBI method also results in the longest solution time.

### 3.5.3 Other Considerations

The various mesh termination schemes for the finite element method have been compared on the grounds of accuracy and computational efficiency. In addition to these criteria, other considerations also apply when choosing an appropriate mesh termination scheme. Here a few of these considerations are briefly discussed.

Of the methods considered, the absorbing boundary condition is surely the simplest to implement. Very few additional data structures are required and even for a second order ABC the added required calculations are rather simple. However, when a higher order ABC is required the formulation becomes rather complicated. In this respect the infinite element scheme is superior since the implementation allows an arbitrary order of approximation of the field. The price paid for this ability is an increased number of unknowns in the system and a few added data structures, complicating the implementation somewhat.

For the FEBI method the greatest difficulty lies in integrating the Green function accurately, especially near the singularity. Some added data structures are required to account for the extra unknowns and matrices and when solving the final system in parts as suggested at the end of Section (3.3.22) the implementation becomes more complicated.

It was noted earlier that since the ABC are specially developed for a circular exterior boundary a loss in accuracy results from using a boundary that is not circular. In many instances the use of such a boundary is preferred, for example using an elliptic boundary for a scatterer with a large axial ratio is advantageous since it implies fewer elements are required in the mesh to ensure that the outer boundary is sufficiently far from the scatterer. The infinite element scheme presented in [23] is especially well-suited for such applications as the formulation is done in an elliptic cylindrical coordinate system. A non-circular boundary does not pose any problems for FEBI method, in fact the boundary does not even need to be convex. With some adjustments the method can even be applied to boundaries that are not entirely smooth [3].

Finally, it is noted that the decision on an appropriate mesh termination has to be done with the specific application in mind. The use of existing

structures and routines within a working finite element solution holds many advantages, especially from a software engineering point of view.

### 3.6 Conclusion

Various methods exist by which a finite element domain can be terminated when solving unbounded problems. Three such methods were considered here and are absorbing boundary conditions of first and second order, the finite element boundary integral method and infinite elements of various orders.

The formulation, discretisation and implementation of each of these methods were discussed in turn. Each method was also applied to solve a typical scattering problem and the results presented. For the finite element boundary integral method attention was also given to the interior resonance problem. The use of Galerkin weighted infinite elements were also compared to the use of complex conjugate weighted infinite elements and the former were found to be superior.

Finally, the different mesh termination schemes were compared directly using various criteria, most prominently solution accuracy and computational efficiency, while some comparisons concerning implementation and application were also made.

## Chapter 4

# A Finite Element Solution in 3D

As before a finite element solution is presented here by way of solving a typical unbounded problem. Although many of the same principles apply for the three-dimensional case as in two dimensions, the implementation of such a solution is typically much more complicated. Also owing to the nature of the problems solved, in many instances the need exists for a vector finite element solution.

First some background on the development of the vector finite element method in three dimensions is presented. Then typical three-dimensional problems are given along with analytic solutions, after which the finite element solution is formulated. Again the finite element solution assumes that the domain is terminated properly by a simple boundary condition and a mesh termination scheme is only presented in the next chapter.

Since the focus here is on incorporating this termination scheme into an existing finite element code, the implementation of the finite element solution is briefly discussed and reference is only made to issues affecting the application of the termination scheme.

### 4.1 Background

Extension of the finite element method to three dimensions for scalar fields naturally followed from the method in two dimensions. However, some important advances in connection with vector fields are worth mentioning.

Traditionally, as for the finite element method in structural mechanics, vector fields in electromagnetic finite element methods were incorporated by simply representing each vector component as a scalar quantity [1], leading to

nodal finite elements. Later another approach to representing a vector field was suggested, that is the use of vector basis functions.

Use of mixed-order vector finite elements was suggested for triangular elements in [27] and extended to tetrahedral and rectangular elements in three dimensions in [28]. Some of the earliest applications of edge elements to electrical engineering are found in [29] and later in [30] where edge elements are specifically applied to high-frequency electromagnetics. A valuable overview of the earlier work on edge elements in computational electromagnetics is found in [31].

Higher order elements gained attention as computation power increased and the need for more accurate solutions arose. Some of the first work on higher order edge elements appeared in [32]. More recent work on higher order finite elements include [33] which is considered a standard reference on the subject.

## 4.2 Unbounded Problems in 3D

Two unbounded three-dimensional problems are considered here. The first is the scattering from a perfectly electrical conducting sphere. Since the far-field approximation is only valid at a relatively far distance from the sphere, a very accurate finite element solution would require immense processing power unless a very accurate mesh termination scheme is employed. For this reason a second problem is also considered, that is determining the field radiated by a short current filament. The far-field approximation for this problem is accurate at a much smaller distance. A description of these problems and analytic solutions follow.

### 4.2.1 Scattering from a Conducting Sphere

The scattering problem is shown in Figure 4.1. A conducting sphere with radius  $r_a$  is illuminated by a plane wave and the scattered electric field is calculated.

Due to the relative simplicity of the problem, an analytical solution can be obtained as derived in [8]. Basically this is done by expanding the incident plane wave and the scattered field into infinite series of Riccati-Bessel functions and matching the coefficients on the surface of the scatterer so the total

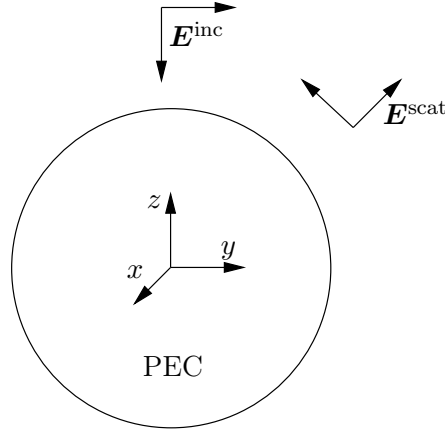


**Figure 4.1:** Description of the three-dimensional scattering problem.

tangential field becomes zero. For an incident electric field

$$\mathbf{E}^{\text{inc}} = E_0 e^{-jk_0 \cos(\theta) \hat{i}_x} \quad (4.2.1)$$

the scattered electric field components are

$$\begin{aligned} E_r^{\text{scat}} &= -jE_0 \cos(\phi) \sum_{n=1}^{\infty} b_n \left[ \hat{H}_n^{(2)''}(k_0 r) \right. \\ &\quad \left. + \hat{H}_n^{(2)}(k_0 r) \right] P_n^1(\cos(\theta)) \end{aligned} \quad (4.2.2)$$

$$\begin{aligned} E_\theta^{\text{scat}} &= \frac{E_0}{k_0 r} \cos(\phi) \sum_{n=1}^{\infty} \left[ j b_n \hat{H}_n^{(2)'}(k_0 r) \sin(\theta) P_n^{1'}(\cos(\theta)) \right. \\ &\quad \left. - c_n \hat{H}_n^{(2)}(k_0 r) \frac{P_n^1(\cos(\theta))}{\sin(\theta)} \right] \end{aligned} \quad (4.2.3)$$

$$\begin{aligned} E_\phi^{\text{scat}} &= \frac{E_0}{k_0 r} \sin(\phi) \sum_{n=1}^{\infty} \left[ j b_n \hat{H}_n^{(2)'}(k_0 r) \frac{P_n^1(\cos(\theta))}{\sin(\theta)} \right. \\ &\quad \left. - c_n \hat{H}_n^{(2)}(k_0 r) \sin(\theta) P_n^{1'}(\cos(\theta)) \right] \end{aligned} \quad (4.2.4)$$

where the coefficients  $b_n$  and  $c_n$  are

$$b_n = -j^{-n} \frac{(2n+1)}{n(n+1)} \frac{\hat{J}_n'(k_0 a)}{\hat{H}_n^{(2)'}(k_0 a)} \quad (4.2.5)$$

$$c_n = -j^{-n} \frac{(2n+1)}{n(n+1)} \frac{\hat{J}_n(k_0 a)}{\hat{H}_n^{(2)}(k_0 a)}. \quad (4.2.6)$$

In the above the single prime and double prime are used to indicate the first and second derivatives with respect to the full argument of the functions.  $\hat{H}_n^{(2)}$  is the Riccati-Hankel function of the second kind,  $\hat{J}_n$  is the Riccati-Bessel function of the first kind and  $P_n^1$  is an associated Legendre polynomial, see Appendix A. Thus the scattering problem is solved.

### 4.2.2 Radiation by a Current Filament

The radiating current filament problem<sup>1</sup> is shown in Figure 4.2. A time-harmonic current of constant magnitude  $I_0$  flows along a short segment  $L$  at the origin and orientated along the  $z$ -axis.

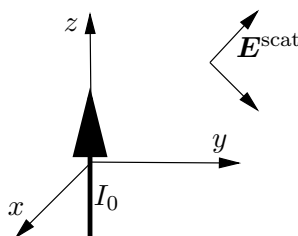


**Figure 4.2:** Description of the radiating current filament problem.

From [9] the vector potential  $\mathbf{A}(\mathbf{r})$  is related to a point current source density through the free space Green function in three dimensions

$$G_0(\mathbf{r}, \mathbf{r}') = \frac{e^{-jk_0|\mathbf{r}-\mathbf{r}'|}}{4\pi|\mathbf{r}-\mathbf{r}'|}. \quad (4.2.7)$$

The same relation exists between the scalar potential  $\Phi(\mathbf{r})$  and a point charge. By integrating over the volume of the current source and its associated charge density the vector and scalar potentials can be obtained and the electric field can be computed using

$$\mathbf{E}(\mathbf{r}) = -\nabla\Phi(\mathbf{r}) - j\omega\mathbf{A}(\mathbf{r}). \quad (4.2.8)$$

## 4.3 A Finite Element Solution

The problem to be solved with the finite element method is dynamic in nature. Furthermore, the unknown field is a vector quantity and the equation that

<sup>1</sup>Thanks to M.M. Botha for a working *Matlab* implementation of this solution.



needs to be solved is the vector wave equation

$$\nabla \times \nabla \times \mathbf{E} - k_0^2 \mathbf{E} = -jk_0 Z_0 \mathbf{J} \quad (4.3.1)$$

where  $Z_0$  is the free space impedance and  $\mathbf{J}$  represents a current density in the volume of interest. Solving the scattering problem of Section 4.2.1 the current density is simply zero and the system is driven with an incident electric field. For the problem of Section 4.2.2 the system is driven by the current filament at the origin which is represented by the current density. Separate formulations for these problems are presented.

### 4.3.1 FEM Solution to the Scattering Problem

For the scattering problem the homogeneous vector wave equation is solved for the scattered field, denoted by  $\mathbf{E}$ , in the free space region around the scatterer. The finite element domain  $\Omega_1$  is bounded by the surface of the scatterer and some exterior boundary at a finite distance outside the scatterer surface. As before the tangential component of the total field is zero on the conducting surface which means the scattered field satisfies the following condition on the surface of the conducting sphere

$$\hat{i}_n \times \mathbf{E} = -\hat{i}_n \times \mathbf{E}^{\text{inc}}. \quad (4.3.2)$$

It is assumed that a homogeneous boundary condition of the third kind applies at the exterior boundary

$$\hat{i}_n \times (\nabla \times \mathbf{E}) + \gamma \hat{i}_n \times (\hat{i}_n \times \mathbf{E}) = 0. \quad (4.3.3)$$

With  $\Gamma_1$  denoting the surface of the scatterer and  $\Gamma_2$  the exterior boundary, the boundary-value problem can now be stated as

$$\begin{aligned} \nabla \times \nabla \times \mathbf{E} - k_0^2 \mathbf{E} &= 0 & \text{in } \Omega_1 \\ \hat{i}_n \times \mathbf{E} &= -\hat{i}_n \times \mathbf{E}^{\text{inc}} & \text{on } \Gamma_1 \\ \hat{i}_n \times (\nabla \times \mathbf{E}) + \gamma \hat{i}_n \times (\hat{i}_n \times \mathbf{E}) &= 0 & \text{on } \Gamma_2. \end{aligned} \quad (4.3.4)$$

Following a procedure similar to that presented in Section 2.3.1 for handling the inhomogeneous boundary condition a functional for the problem can be

obtained using

$$\Pi(\mathbf{E}) = \langle \mathcal{L}\mathbf{E}, \mathbf{E} \rangle - \langle \mathcal{L}\mathbf{E}, \mathbf{E}_1 \rangle + \langle \mathcal{L}\mathbf{E}_1, \mathbf{E} \rangle \quad (4.3.5)$$

where  $\mathbf{E}_1$  is some solution to the boundary value problem (4.3.4). The operator is

$$\mathcal{L}(\cdot) = \nabla \times \nabla \times (\cdot) - k_0^2(\cdot) \quad (4.3.6)$$

and the inner product is defined by

$$\langle \mathbf{A}, \mathbf{B} \rangle = \iiint_{\Omega_1} \mathbf{A} \cdot \mathbf{B} \, d\Omega. \quad (4.3.7)$$

Expanding (4.3.5) using the definition of the inner product gives

$$\begin{aligned} \Pi(\mathbf{E}) &= \iiint_{\Omega_1} \mathbf{E} \cdot (\nabla \times \nabla \times \mathbf{E} - k_0^2 \mathbf{E}) \, d\Omega \\ &\quad + \iiint_{\Omega_1} \mathbf{E} \cdot (\nabla \times \nabla \times \mathbf{E}_1) - \mathbf{E}_1 \cdot (\nabla \times \nabla \times \mathbf{E}) \, d\Omega. \end{aligned} \quad (4.3.8)$$

Using the first and second Green vector theorems on the first and second integrals, respectively, the expression becomes

$$\begin{aligned} \Pi(\mathbf{E}) &= \iiint_{\Omega} (\nabla \times \mathbf{E}) \cdot (\nabla \times \mathbf{E}) - k_0^2 \mathbf{E} \cdot \mathbf{E} \, d\Omega \\ &\quad + \oint_{\Gamma_1 + \Gamma_2} [\mathbf{E} \times (\nabla \times \mathbf{E}_1)] \cdot \hat{i}_n - [\mathbf{E}_1 \times (\nabla \times \mathbf{E})] \cdot \hat{i}_n \, d\Gamma \\ &\quad + \oint_{\Gamma_1 + \Gamma_2} [\mathbf{E} \times (\nabla \times \mathbf{E})] \cdot \hat{i}_n \, d\Gamma. \end{aligned} \quad (4.3.9)$$

The vector triple product identity  $(\mathbf{A} \times \mathbf{B}) \cdot \mathbf{C} = (\mathbf{C} \times \mathbf{A}) \cdot \mathbf{B}$  allows the terms inside surface integrals to be manipulated to a form to which the applicable boundary conditions can be applied. After applying the boundary conditions and discarding terms not containing  $\mathbf{E}$  the desired result is obtained

$$\begin{aligned} \Pi(\mathbf{E}) &= \iiint_{\Omega} (\nabla \times \mathbf{E}) \cdot (\nabla \times \mathbf{E}) - k_0^2 \mathbf{E} \cdot \mathbf{E} \, d\Omega \\ &\quad + \iint_{\Gamma_2} \gamma(\hat{i}_n \times \mathbf{E}) \cdot (\hat{i}_n \times \mathbf{E}) \, d\Gamma. \end{aligned} \quad (4.3.10)$$

### 4.3.2 FEM Solution to the Radiation Problem

The finite element solution for the radiating current source differs from that for the scattering problem in three respects. First, since there is a current source within the finite element domain, the inhomogeneous vector wave equation is solved. Second, the finite element domain  $\Omega_1$  is entirely enclosed by the exterior boundary  $\Gamma_2$ . Finally, the solution is formulated in terms of the total field, which is here also denoted by  $\mathbf{E}$ . Since there is no incident field for this problem, the total field is exactly the field radiated by the current source.

Again assuming a homogeneous boundary condition of the third kind on the exterior boundary, the boundary-value problem is stated as follows

$$\begin{aligned}\nabla \times \nabla \times \mathbf{E} - k_0^2 \mathbf{E} &= -jk_0 Z_0 \mathbf{J} \quad \text{in } \Omega_1 \\ \nabla \times \mathbf{E} + \gamma(\hat{i}_n \times \mathbf{E}) &= 0 \quad \text{on } \Gamma_2.\end{aligned}\quad (4.3.11)$$

Using the same definition of the operator and inner product as for the previous section, and noting that the operator is now symmetric due to the homogeneous boundary conditions, a valid functional can be defined using (2.3.9) repeated here

$$\Pi(\mathbf{E}) = \langle \mathcal{L}\mathbf{E}, \mathbf{E} \rangle - 2\langle \mathbf{E}, g \rangle \quad (4.3.12)$$

where  $g = -jk_0 Z_0 \mathbf{J}$ . Expanding the expression gives

$$\Pi(\mathbf{E}) = \iiint_{\Omega_1} \mathbf{E} \cdot (\nabla \times \nabla \times \mathbf{E} - k_0^2 \mathbf{E}) \, d\Omega - 2 \iiint_{\Omega_1} -jk_0 Z_0 \mathbf{J} \cdot \mathbf{E} \, d\Omega \quad (4.3.13)$$

where the second vector Green theorem is applied on the first term to obtain

$$\begin{aligned}\Pi(\mathbf{E}) &= \iiint_{\Omega_1} (\nabla \times \mathbf{E}) \cdot (\nabla \times \mathbf{E}) - k_0^2 \mathbf{E} \cdot \mathbf{E} \, d\Omega + j2k_0 Z_0 \iiint_{\Omega_1} \mathbf{J} \cdot \mathbf{E} \, d\Omega \\ &\quad + \iint_{\Gamma_2} [\mathbf{E} \times (\nabla \times \mathbf{E})] \cdot \hat{i}_n \, d\Gamma.\end{aligned}\quad (4.3.14)$$

Again using the triple vector product identity and applying the boundary condition on  $\Gamma_2$  gives the desired result

$$\begin{aligned}\Pi(\mathbf{E}) &= \iiint_{\Omega_1} (\nabla \times \mathbf{E}) \cdot (\nabla \times \mathbf{E}) - k_0^2 \mathbf{E} \cdot \mathbf{E} \, d\Omega + j2k_0 Z_0 \iiint_{\Omega_1} \mathbf{J} \cdot \mathbf{E} \, d\Omega \\ &\quad + \iint_{\Gamma_2} \gamma(\hat{i}_n \times \mathbf{E}) \cdot (\hat{i}_n \times \mathbf{E}) \, d\Gamma.\end{aligned}\quad (4.3.15)$$

### 4.3.3 Discretisation

The finite element domain is again subdivided into smaller elements and within each element basis functions are defined which approximate the unknown quantity. Different from before, the elements are now volumetric and the basis functions are vector functions.

The electric field is approximated within each element as

$$\mathbf{E}^e = \sum_{i=1}^{N^e} a_i^e \mathbf{N}_i^e \quad (4.3.16)$$

and on the surfaces of the elements that form the boundary of the finite element domain the field is

$$\mathbf{E}^s = \sum_{i=1}^{M^e} a_i^e \mathbf{N}_i^e. \quad (4.3.17)$$

For the scalar finite element solution field continuity was enforced on the nodes of the area elements. There only the vector component of the field that is perpendicular to the plane of the finite element domain was solved and the continuity therefore implies tangential continuity of the field. Enforcing tangential continuity here is somewhat more complicated. Low order basis functions are typically associated with edges of the finite elements and possess special properties along their associated edges. For example constant tangential linear normal (CT/LN) elements have a constant tangential component on its associated edge and a linear normal component on all other edges of the element. The tangential field on an elemental edge is then uniquely defined by a single basis function. Enforcing tangential continuity of the field then simply requires that the unknowns of different elements associated with the same shared edge are set equal during assembly of the system (assuming that shared edges have the same direction locally within different elements).

Substituting the expansions for the field in the functional for the scattering problem and differentiating with respect to the unknown coefficients  $a_i$  gives

$$\begin{aligned} \frac{\partial \Pi(\mathbf{E})}{\partial a_i} &= \sum_{j=1}^N a_j \iiint_{\Omega_1} (\nabla \times \mathbf{N}_i) \cdot (\nabla \times \mathbf{N}_j) - k_0^2 \mathbf{N}_i \cdot \mathbf{N}_j \, d\Omega \\ &\quad + \sum_{j=1}^M a_j \iint_{\Gamma_2} \gamma (\hat{i}_n \times \mathbf{N}_i) \cdot (\hat{i}_n \times \mathbf{N}_j) \, d\Gamma. \end{aligned} \quad (4.3.18)$$

Similar arguments apply regarding the assembly of the surface integral term as for the two-dimensional case, since each node on the surface is exactly a node in the finite element domain. Setting the variation equal to zero one obtains again a matrix system for which the Dirichlet boundary condition on  $\Gamma_1$  can be enforced by specifying the known coefficients  $a_x = X$  as for the two-dimensional solution. The system is then

$$[K_{yy}]\{a\} = \{-K_{yx}X\} \quad (4.3.19)$$

where the matrix entries  $K_{ij}$  are computed as

$$\begin{aligned} K_{ij} = & \iiint_{\Omega_1} (\nabla \times \mathbf{N}_i) \cdot (\nabla \times \mathbf{N}_j) - k_0^2 \mathbf{N}_i \cdot \mathbf{N}_j \, d\Omega \\ & + \iint_{\Gamma_2} \gamma (\hat{i}_n \times \mathbf{N}_i) \cdot (\hat{i}_n \times \mathbf{N}_j) \, d\Gamma. \end{aligned} \quad (4.3.20)$$

When the functional for the radiating current problem is discretised the result is somewhat different

$$\begin{aligned} \frac{\partial \Pi(\mathbf{E})}{\partial a_i} = & \sum_{j=1}^N a_j \iiint_{\Omega_1} (\nabla \times \mathbf{N}_i) \cdot (\nabla \times \mathbf{N}_j) - k_0^2 \mathbf{N}_i \cdot \mathbf{N}_j \, d\Omega \\ & + \sum_{j=1}^M a_j \iint_{\Gamma_2} \gamma (\hat{i}_n \times \mathbf{N}_i) \cdot (\hat{i}_n \times \mathbf{N}_j) \, d\Gamma \\ & + jk_0 Z_0 \sum_{i=1}^N \iiint_{\Omega_1} \mathbf{J} \cdot \mathbf{N}_i \, d\Omega. \end{aligned} \quad (4.3.21)$$

The last term in the above does not contain any unknown coefficients and is the driving vector for the system. Setting the above variation to zero gives

$$[K]\{a\} = \{g\} \quad (4.3.22)$$

where  $K_{ij}$  is as defined in (4.3.20) and

$$g_i = j2k_0 Z_0 \iiint_{\Omega_1} \mathbf{J} \cdot \mathbf{N}_i \, d\Omega. \quad (4.3.23)$$

### 4.3.4 Implementation

A few implementation issues that affect the incorporation of a mesh termination scheme are addressed here. The issues are mainly concerned with the type of element and the basis functions used.

The first consideration is the element shape used to subdivide the finite element domain. Here tetrahedral elements are used as they allow more accurate geometrical modelling of curved surfaces than for example brick elements. The use of tetrahedral elements implies that the exterior boundary of the finite element domain is approximated as a number of triangular surfaces. As the curvature of the boundary becomes smaller and the edge lengths of the triangular surfaces become shorter, the approximation becomes more accurate.

Higher order basis functions are available in the existing FEM solver, however here only the first order Whitney basis functions are used. These basis functions are defined in terms of the simplex coordinates for a tetrahedral element as

$$\mathbf{N}_i^e = \lambda_{i1}^e \nabla \lambda_{i2}^e - \lambda_{i2}^e \nabla \lambda_{i1}^e \quad (4.3.24)$$

where edge  $\mathbf{N}_i^e$  is associated with the edge  $i$  connecting nodes  $i1$  and  $i2$  in element  $e$ . The simplex coordinates associated with each vertex  $(x_i, y_i, z_i)$  of the element [7] is

$$\lambda_i^e = A_i^e + B_i^e x + C_i^e y + D_i^e z \quad (4.3.25)$$

where

$$\begin{bmatrix} A_1^e & B_1^e & C_1^e & D_1^e \\ A_2^e & B_2^e & C_2^e & D_2^e \\ A_3^e & B_3^e & C_3^e & D_3^e \\ A_4^e & B_4^e & C_4^e & D_4^e \end{bmatrix} = \begin{bmatrix} 1 & 1 & 1 & 1 \\ x_1^e & x_2^e & x_3^e & x_4^e \\ y_1^e & y_2^e & y_3^e & y_4^e \\ z_1^e & z_2^e & z_3^e & z_4^e \end{bmatrix}^{-1}. \quad (4.3.26)$$

It can be verified that the basis function  $\mathbf{N}_i^e$  in (4.3.24) is exactly normal on all edges of the element  $e$  except for the  $i$ th edge. On this edge the basis function has also a tangential component which is constant and equal to the inverse of the length of that edge. The local numbering scheme employed to number the edges of the tetrahedral is given in Table 4.1.

Finally the evaluation of the Whitney basis functions on a face of the tetrahedral is considered. Since each basis function is linear and exactly normal on all the edges except the edge with which it is associated, it is easily verified

Edge	Node $i$	Node $j$
1	1	2
2	1	3
3	1	4
4	2	3
5	2	4
6	3	4

**Table 4.1:** Local edge numbers for a tetrahedral element.

that each basis function has only tangential components on the two faces containing that edge of the tetrahedral. On each of these faces the basis functions reduce to the two-dimensional Whitney basis functions

$$\mathbf{W}_i^s(x', y') = \lambda_{i1}^s \nabla \lambda_{i2}^s - \lambda_{i2}^s \nabla \lambda_{i1}^s \quad (4.3.27)$$

where simplex coordinates  $\lambda_i^s$  are defined using local coordinates in the plane of the tetrahedral face. That is, in (2.3.25) the global coordinates  $(x, y)$  are simply substituted with the coordinates  $(x', y')$  that define a plane containing the triangular face of the tetrahedral. Similar to the three-dimensional form, each of these functions has a non-zero tangential component only on the edge with which it is associated. Employing the numbering scheme in Table 4.1 and numbering the vertices of the triangle in increasing order of the numbers within the tetrahedral automatically numbers the edges for a triangular element according to Table 4.2.

Edge	Node $i$	Node $j$
1	1	2
2	1	3
3	2	3

**Table 4.2:** Local edge numbers for a triangular face.

## 4.4 Conclusion

In this chapter typical three-dimensional unbounded problems were presented after which a vector finite element solution was formulated. Some issues regarding the implementation of the solution that affect the development of a mesh termination scheme were also addressed.

Now an appropriate mesh termination scheme for this finite element solution can be presented.



## Chapter 5

# Infinite Elements in 3D

As for the finite element method in two dimensions, when solving an unbounded problem in three dimensions the finite element domain has to be terminated properly. There are many such methods derived for three dimensions, in fact each of the methods discussed for two dimensions has a three-dimensional equivalent. However, in three dimensions the methods become increasingly more complicated. This is especially true for finite element methods formulated for vector quantities.

Here such a termination in the form of infinite elements is presented. First some background on mesh termination in three dimensions is given. Then the finite element solutions formulated for the unbounded problems in three dimensions are adapted to include the infinite elements. The infinite element itself is then developed and incorporated into the finite element solution. Finally some concluding comments are made.

### 5.1 Background

Mesh termination of the finite element domain has been a subject of research for years and many different techniques have been proposed, developed and implemented successfully for three-dimensional vector finite elements. Included are absorbing boundary conditions [34], the use of perfectly matched layers [35] and the finite element boundary integral method [36]. Infinite elements have also been applied to three-dimensional problems, although it is not as widely used by the electromagnetic community as are some of the other methods.

Some developments on three-dimensional infinite elements found in litera-

ture include [37] which uses infinite elements to solve scattering problems for bodies of revolution and [38] where the Laplace and Helmholtz equations are solved in three dimensions. A formulation of the infinite element method compatible with edge elements can be found in [39]. However, the infinite element presented there is designed for a finite element mesh in which the elements are spherically conformal hexahedrals. This type of infinite element is not directly compatible with tetrahedral elements which are widely used in finite element implementations. Here a new type of infinite element is developed specifically with this compatibility in mind, and comprises a novel contribution [40].

## 5.2 Infinite Element Solution Formulation

The infinite element solution in three dimensions aims at finding a solution in an infinite domain. As in the two-dimensional case this implies that the boundary  $\Gamma_2$  is discarded and a boundary at infinity  $\Gamma_\infty$  is introduced. The solution domain then becomes  $\Omega_\infty = \Omega_1 + \Omega_2$  which is enclosed by  $\Gamma_\infty$  for the radiating current source problem, and by the boundaries  $\Gamma_\infty$  and  $\Gamma_1$  for the scattering problem, the latter boundary coinciding with the surface of the scatterer.

With  $\Gamma_2$  replaced by  $\Gamma_\infty$  the boundary-value problems (4.3.4) and (4.3.11) are simply adapted by replacing the boundary condition of the third kind applied at  $\Gamma_2$  with a radiation condition at  $\Gamma_\infty$ . Since the field is now a vector quantity the form of the Sommerfeld radiation condition in (3.4.2) cannot be directly applied. Here this radiation condition [41] asserts the following form

$$\lim_{r \rightarrow \infty} \left[ r \left( \nabla \times \mathbf{E} + jk_0(\hat{i}_r \times \mathbf{E}) \right) \right] = 0 \quad \text{and} \quad (5.2.1)$$

$$\lim_{r \rightarrow \infty} [\mathbf{E}] = \mathcal{O} \left( \frac{1}{r} \right). \quad (5.2.2)$$

Condition (5.2.1) can be enforced by

$$\nabla \times \mathbf{E} + jk_0(\hat{i}_n \times \mathbf{E}) = 0 \quad \text{on} \quad \Gamma_\infty \quad (5.2.3)$$

if the boundary at infinity is spherical, while the condition (5.2.2) can be met by a proper choice of basis functions. Noting that by simply letting  $\gamma \rightarrow jk_0$  and  $\Gamma_2 \rightarrow \Gamma_\infty$  the functionals (4.3.10) and (4.3.15) can be used to solve the boundary value problems of the previous chapter in an infinite domain. The

result is

$$\begin{aligned} \Pi(\mathbf{E}) = & \iiint_{\Omega_\infty} (\nabla \times \mathbf{E}) \cdot (\nabla \times \mathbf{E}) - k_0^2 \mathbf{E} \cdot \mathbf{E} \, d\Omega \\ & + jk_0 \iint_{\Gamma_\infty} (\hat{i}_n \times \mathbf{E}) \cdot (\hat{i}_n \times \mathbf{E}) \, d\Gamma \end{aligned} \quad (5.2.4)$$

for the scattering problem and

$$\begin{aligned} \Pi(\mathbf{E}) = & \iiint_{\Omega_\infty} (\nabla \times \mathbf{E}) \cdot (\nabla \times \mathbf{E}) - k_0^2 \mathbf{E} \cdot \mathbf{E} \, d\Omega + j2k_0 Z_0 \iiint_{\Omega_1} \mathbf{J} \cdot \mathbf{E} \, d\Omega \\ & + jk_0 \iint_{\Gamma_\infty} (\hat{i}_n \times \mathbf{E}) \cdot (\hat{i}_n \times \mathbf{E}) \, d\Gamma \end{aligned} \quad (5.2.5)$$

for the radiating current source problem. Note that the functional for the radiating current problem assumes that all current sources are within the finite element domain.

Finally it is noted that, analogous to the infinite element formulation in two-dimensions, each of the volume integrals over  $\Omega_\infty$  in the above functionals can be split into an integral over the finite element domain  $\Omega_1$  and an integral over the infinite element domain  $\Omega_2$ .

### 5.3 Discretisation

The discretisation of the finite element region has already been discussed. Here the discretisation of the infinite element region is discussed with compatibility with the finite element region in mind.

Here the boundary  $\Gamma_2$  is again reintroduced as the interface between the finite and infinite element regions. Compatibility between the finite elements and infinite elements connected to this interface means two requirements have to be met. One is that elements on either side of the interface leave the same footprint on this surface. The other is that the basis function within the finite and infinite elements have the same tangential component along the edges defining these footprints, so tangential field continuity can be enforced easily.

Again it is useful to specify the basis functions inside an infinite element as the product of a function in the radial variable and a function in the angular variables for a spherical coordinate system. However, since the basis functions

are now vectors three such products have to be specified per basis function

$$\mathbf{N}_{ij} = R_i^r A_j^r \hat{i}_r + R_i^\theta A_j^\theta \hat{i}_\theta + R_i^\phi A_j^\phi \hat{i}_\phi. \quad (5.3.1)$$

As before this form allows the compatibility between the finite and infinite elements to be enforced by an appropriate choice of angular functions, while condition (5.2.2) of the Sommerfeld radiation condition can be met by appropriate choice of radial functions. In addition, the order of the basis functions can be controlled separately in the angular and radial directions. Mapping each pair  $(ij) \rightarrow k$  the field within each infinite element is approximated as

$$\mathbf{E}^e = \sum_{k=1}^{N_R^e \times N_A^e} c_k^e \mathbf{N}_k^e. \quad (5.3.2)$$

The field expansions defined for the finite elements and for the infinite elements can now be substituted into the functional (5.2.4). Differentiating with respect to the unknown coefficients and equating the result to zero yields the system

$$\begin{bmatrix} K'_{1yy} & K'_{11} & 0 \\ K'_{11} & K'_{12} & K'_{22} \\ 0 & K'_{22} & K'_2 \end{bmatrix} \begin{Bmatrix} a' \\ b \\ c' \end{Bmatrix} = \begin{Bmatrix} -K'_{1yx} X \\ 0 \\ 0 \end{Bmatrix} \quad (5.3.3)$$

for the scattering problem, where the Dirichlet boundary condition is already enforced. The subdivision of the matrices and unknown coefficient vector is similar to that in Section 3.4.2 for the two-dimensional infinite elements. Only now, the finite element matrix  $K_1$  and infinite element matrix  $K_2$  are

$$K_{1ij} = \iiint_{\Omega_1} (\nabla \times \mathbf{N}_i) \cdot (\nabla \times \mathbf{N}_j) - k_0^2 \mathbf{N}_i \cdot \mathbf{N}_j \, d\Omega \quad (5.3.4)$$

$$\begin{aligned} K_{2ij} &= \iiint_{\Omega_1} (\nabla \times \mathbf{N}_i) \cdot (\nabla \times \mathbf{N}_j) - k_0^2 \mathbf{N}_i \cdot \mathbf{N}_j \, d\Omega \\ &+ jk_0 \oiint_{\Gamma_\infty} (\hat{i}_r \times \mathbf{N}_i) \cdot (\hat{i}_r \times \mathbf{N}_j) \, d\Gamma. \end{aligned} \quad (5.3.5)$$

For the radiating current problem the resulting system equation is

$$\begin{bmatrix} K'_1 & K'_{11} & 0 \\ K'_{11} & K_{12} & K'_{22} \\ 0 & K'_{22} & K'_2 \end{bmatrix} \begin{Bmatrix} a' \\ b \\ c' \end{Bmatrix} = \begin{Bmatrix} g \\ 0 \\ 0 \end{Bmatrix} \quad (5.3.6)$$

where  $g$  again represents the driving current source and has the same definition as in (4.3.23). The finite element matrix  $K_{1ij}$  and infinite element matrix  $K_{2ij}$  have the same definition as for the scattering problem.

Finally, note that the specification of the infinite element basis functions as the product of an angular and a radial function allows the integrals over the volume of the infinite element to be divided into an integral over the solid angle subtended by the infinite element and an integral in the radial direction.

## 5.4 The 3D Infinite Element

A new three-dimensional infinite element is developed here. First the shape of the element is considered and then the basis functions are defined on that element.

### 5.4.1 Infinite Element Shape

Using tetrahedral elements to discretise the finite element domain, the boundary  $\Gamma_2$  is approximated by a surface comprised of a number of triangular elements. The vertices of these triangular elements lie exactly on  $\Gamma_2$  and for a spherical boundary, these vertices can be connected on  $\Gamma_2$  by spherically conformal triangular surfaces. As already noted, the smaller the curvature of  $\Gamma_2$  (in this case implying a larger spherical radius), the better the boundary is approximated by the finite element triangular surfaces. This means that in the limit the spherically conformed triangular surfaces on  $\Gamma_2$  will approach the finite element triangular surfaces. Each of these spherically conformed triangular surfaces are now used as the base of the infinite element. The infinite element is then formed by a radial sweep of this surface toward infinity in the radial direction. Figure 5.1 shows such an element along with the finite element triangular surface to which it is attached.

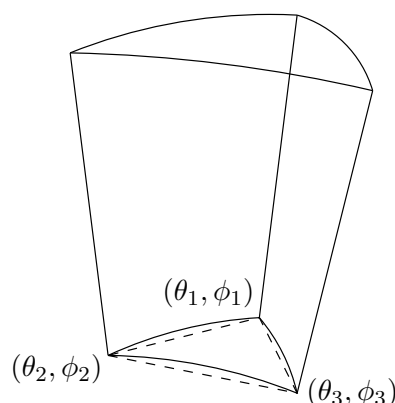


**Figure 5.1:** The shape of the three-dimensional infinite element.

## 5.4.2 Infinite Element Basis Functions

Basis functions can now be defined for the infinite element with which the field is approximated. Clearly each element has nine edges, three along angular paths on  $\Gamma_2$ , three along angular paths on  $\Gamma_\infty$  and three in the radial direction. Since the field vanishes at infinity, no basis functions are associated with the edges on  $\Gamma_\infty$  and six basis functions are defined per element.

### 5.4.2.1 Radial Edge Basis Functions

The basis functions associated with the radial edges can only represent the radial component of the field, meaning (5.3.1) becomes

$$\mathbf{N}_{ij} = R_i^r A_j^r \hat{i}_r. \quad (5.4.1)$$

Since this component of the field is non-radiating,  $R_i^r$  should decay at a faster rate than  $r^{-1}$ . An exponential factor is also required to account for phase variation of the field. Finally a normalisation factor is introduced so the basis function will evaluate to unity on the boundary  $\Gamma_2$  where the  $r = r_a$ . The radial function is then

$$R^r(r) = \left(\frac{r_a}{r}\right)^2 e^{-jk_0(r-r_a)} \quad (5.4.2)$$

where the subscript  $i$  from (5.4.1) has been dropped, since the radial function is the same for all radial edge basis functions.

These basis functions are automatically normal on the angular edges, since

they only have a radial vector component. To ensure that each radial basis function has a non-zero tangential component on only one radial edge, a linear interpolation function  $A_j^r$  is used. Noting that a similar linear interpolation function was used for the nodal finite elements in Section 2.3.3, the angular function can now be defined

$$A_j^r(\theta, \phi) = A_j + B_j\theta + C_j\phi \quad (5.4.3)$$

where the coefficients  $A_j, B_j$  and  $C_j$  are related to the angular coordinates of the spherically conformal triangular base of the infinite element by

$$\begin{bmatrix} A_1^e & B_1^e & C_1^e \\ A_2^e & B_2^e & C_2^e \\ A_3^e & B_3^e & C_3^e \end{bmatrix} = \begin{bmatrix} 1 & 1 & 1 \\ \theta_1^e & \theta_2^e & \theta_3^e \\ \phi_1^e & \phi_2^e & \phi_3^e \end{bmatrix}^{-1}. \quad (5.4.4)$$

These basis functions may be interpreted as the simplex coordinates on the spherically conformal triangular base surface of the infinite element.

Finally, note that as a result of the normalisation in (5.4.2) the basis functions evaluate to unity at the nodes on the base surface of the infinite element. Therefore it also makes sense to associate these basis functions with the nodes of the element. This notion is also particularly useful for the extension to higher order infinite elements which is discussed later.

#### 5.4.2.2 Angular Edge Basis Functions

Since the edges of the infinite element on  $\Gamma_2$  are in the angular direction, only the angular components of the field are represented and the basis function becomes

$$N_{ij} = R_i^\theta A_j^{\theta\hat{i}} + R_i^\phi A_j^{\phi\hat{i}}. \quad (5.4.5)$$

In the far-zone the angular components of the field are radiating, meaning that these components should comply with (5.2.2) of the Sommerfeld radiation condition. That is, the order of decay for these components should be in the order of  $r^{-1}$ . Again adding an exponential factor and a normalisation factor, and realising that  $R_i^\theta$  and  $R_i^\phi$  should be the same, the radial function becomes

$$R^\theta = R^\phi = R^A = \left(\frac{r_a}{r}\right) e^{-jk_0(r-r_a)} \quad (5.4.6)$$

where the subscript  $i$  from (5.4.5) has been dropped since the radial function is the same for all angular edge basis functions.

Equivalent to the radially directed basis functions and angular edges, the angular basis functions are automatically normal on the radial edges. An angular function is therefore required to ensure that each angular edge basis function has a non-zero tangential component on only one edge. Recall from Section 4.3.4 that the Whitney basis functions defined in terms of the simplex coordinates for a triangular surface exhibited such a property. Now substituting the simplex coordinates in (4.3.27) with the functions (5.4.3) the Whitney vector functions become

$$\mathbf{W}_j^A(\theta, \phi) = A_{j1}^r \nabla A_{j2}^r - A_{j2}^r \nabla A_{j1}^r = (s_j + t_i \phi) \hat{i}_\theta + (u_i + v_i \theta) \hat{i}_\phi. \quad (5.4.7)$$

It is important to note that in performing the surface gradient operation in the above, the angular spherical coordinates are treated as rectilinear. The surface gradient operator is then

$$\nabla = \frac{\partial}{\partial \theta} \hat{i}_\theta + \frac{\partial}{\partial \phi} \hat{i}_\phi. \quad (5.4.8)$$

With this definition of the gradient operator the functions defined in (5.4.7) are exactly equivalent to the Whitney functions on a triangular surface due to the similarity between (5.4.3) and the simplex coordinates on triangle.

Since the angular edges are shared between finite elements and infinite elements, the basis functions associated with these edges should be compatible. As mentioned in Section 4.3.4, when the Whitney basis functions in a tetrahedral are evaluated on the face of the tetrahedral, the Whitney basis functions on a triangle element are obtained. This means that by using the angular function of (5.4.7) and due to the normalisation of the radial function in (5.4.6), the compatibility between the infinite element and finite element basis functions are ensured within a scaling factor. Therefore all that remains to ensure compatibility is to compensate for this scaling factor.

Notice that the tangential component of the Whitney function on its associated edge is equal to the inverse of the length of that edge. For the finite element tetrahedrals, where the vertices are defined in Cartesian coordinates, this length is simply

$$\ell_j^{xyz} = \sqrt{(x_{j1} - x_{j2})^2 + (y_{j1} - y_{j2})^2 + (z_{j1} - z_{j2})^2} \quad (5.4.9)$$



and the tangential component of the Whitney function along its associated edge is

$$\mathbf{W}_j \cdot \hat{i}_t = \frac{1}{\ell_j^{xyz}}. \quad (5.4.10)$$

Equivalently for the functions defined in (5.4.7) on the infinite elements, where the vertices are defined in spherical coordinates, the length is

$$\ell_j^{\theta\phi} = \sqrt{(\theta_{j1} - \theta_{j2})^2 + (\phi_{j1} - \phi_{j2})^2} \quad (5.4.11)$$

and the tangential component of such a function along its associated edge is

$$\mathbf{W}_j^A \cdot \hat{i}_t = \frac{1}{\ell_j^{\theta\phi}}. \quad (5.4.12)$$

By letting  $\ell_j = \ell_j^{\theta\phi} / \ell_j^{xyz}$  the final form of the angular functions for the angular edges are defined

$$A_j^{\theta} \hat{i}_\theta + A_j^{\phi} \hat{i}_\phi = \ell_j (s_j + t_j \phi) \hat{i}_\theta + \ell_j (u_j + v_j \theta) \hat{i}_\phi \quad (5.4.13)$$

to ensure compatibility between the finite element and infinite element basis functions. In other words, the angular edge functions of the infinite element are scaled by the angular length (5.4.11) of the edge as well as the inverse of the Cartesian length (5.4.9) for that edge. This ensures that the tangential component of an infinite element basis function on its associated edge is equal to the tangential component of a finite element basis function associated with that same edge.

### 5.4.3 Higher Order Elements

With the angular and radial dependency of the basis functions separately defined, the transition to higher order elements in either the angular or radial functions is relatively simple. Higher order angular functions are desired when the finite element discretisation uses higher order elements, which is not the case here and only basis functions with higher order radial functions are developed.

Increasing the order of the infinite element can be understood as adding more angular edges at different radii in the infinite element. This automatically adds nodes on the radial edges at the same radii, analogous to the higher

order two-dimensional infinite elements and higher order radial functions are obtained in a similar way as before.

Ensuring that the highest power of the radial variable is  $r^{-1}$  in the expansion for the angular field, the radial function  $R^A$  of (5.4.6) can be defined as

$$R_m^A(r) = e^{-jk_0(r-r_m)} \sum_{n=1}^{N_R} h_{mn}^{(1)} r^{-n} \quad (5.4.14)$$

where the added angular edges are at radii  $r_m$  for  $m = 1, 2, \dots, N_R$  and  $N_R$  is the order of the radial expansion. The subscript  $m$  is introduced and used here to distinguish between radial functions associated with edges at different radii. By forcing the function to be exactly zero at all radii  $r_k, k \neq m$  and to evaluate to unity at  $r_k, k = m$ , the coefficients  $h_{mn}^{(1)}$  can be obtained from

$$[H^{(1)}][S^{(1)}] = [I] \quad (5.4.15)$$

where  $I$  is the identity matrix and  $s_{mn}^{(1)} = r_n^{-m}$ . Similarly a higher order expansion for the radial function  $R^r$  of (5.4.2) for the radially directed field can be defined

$$R_m^r(r) = e^{-jk_0(r-r_m)} \sum_{n=1}^{N_R} h_{mn}^{(2)} r^{-1-n} \quad (5.4.16)$$

where the highest power of the radial variable is  $r^{-2}$ . The coefficients  $h_{mn}^{(2)}$  are obtained from

$$[H^{(2)}][S^{(2)}] = [I] \quad (5.4.17)$$

where  $s_{mn}^{(2)} = r_n^{-1-m}$ .

Thus the infinite element can be implemented up to an arbitrary order of radial expansion.

#### 5.4.4 Local Numbering

With the basis functions defined it is useful to summarise the above results and to mention the numbering scheme employed within an infinite element.

Each of the basis functions is associated either with an angular edge or with a node on a radial edge. These associations can be defined using an index  $i = 1, 2, \dots, 6$ , where  $i \leq 3$  indicates an angular edge basis function and  $i \geq 4$  indicates a radial node basis function. In addition, each basis function can also be associated with a particular order radius when higher order radial functions

are used. This association can be indicated by an index  $n = 1, 2, \dots, N_R$ . Now the basis functions are

$$\mathbf{N}_{in} = \begin{cases} e^{-jk_0(r-r_n)} \sum_{m=1}^{N_R} h_{nm}^{(1)} r^{-m} \left( (s_i + t_i \phi) \hat{i}_\theta + (u_i + v_i \theta) \hat{i}_\phi \right) \ell_i & i = 1, 2, 3 \\ e^{-jk_0(r-r_n)} \sum_{m=1}^{N_R} h_{nm}^{(2)} r^{-1-m} (A_i + B_i \theta + C_i \phi) \hat{i}_r & i = 4, 5, 6. \end{cases} \quad (5.4.18)$$

Mapping each index pair to a unique number within the infinite element  $(in) \rightarrow k$  the field inside the element becomes

$$\mathbf{E}^e = \sum_{k=1}^{6N_R} c_k^e \mathbf{N}_k^e \quad (5.4.19)$$

and six basis functions are added with each increase in the radial order of the element.

The numbering scheme for an infinite element has to be compatible with the tetrahedral to which it is attached. First the nodes are numbered from which edge and basis function numbers can be derived. The nodes shared between the infinite element and the tetrahedral are numbered first in increasing order of the local numbers within the tetrahedral. This is done so that the orientation of the angular edges within the infinite element is the same as in the tetrahedral element. Thereafter the nodes introduced by using higher order infinite elements are numbered in the same order for each successive radii. Figure 5.2 shows the node numbers for a single third order infinite element.

The six basis functions of the first order infinite element are numbered as follows. Basis functions 1, 2 and 3 are associated with angular edges shared by the infinite element and the attached tetrahedral, and are numbered according to the same convention used in Table 4.2. Basis functions 4, 5 and 6 are associated with the nodes shared by the infinite element and the attached tetrahedral, and are numbered in increasing node order. This scheme is summarised in Table 5.1 where the connection between the basis function number and the nodes of the infinite element is given.

Basis functions within a higher order element are similarly numbered in increasing order as the associated node radii increase.

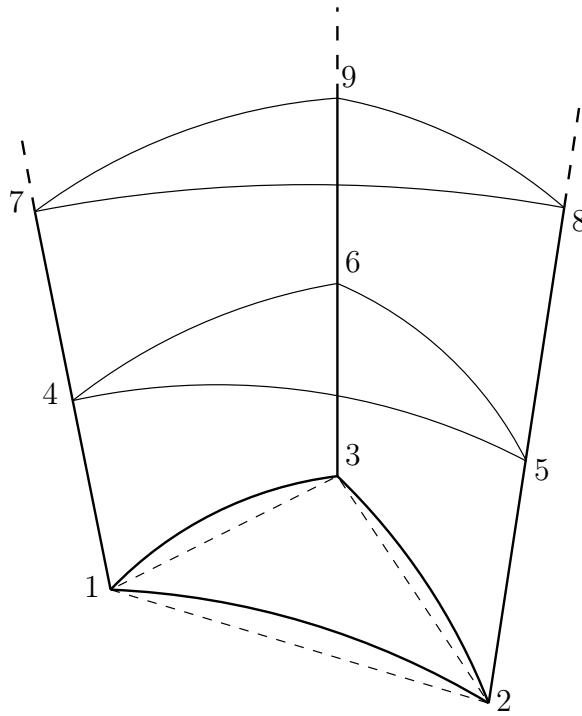


**Figure 5.2:** Node numbers for a higher order infinite element.

Basis function	Node $i$	Node $j$
1	1	2
2	1	3
3	2	3
4	1	-
5	2	-
6	3	-

**Table 5.1:** First order basis function numbers and associated nodes.

#### 5.4.5 Evaluating Elemental Matrices

Finally the elemental matrices for the infinite elements can be calculated by substituting the basis function definitions into (5.3.5). This entails some lengthy mathematical manipulation and the process is presented in detail in Appendix D. Here a few important comments are made regarding this.

As for the two-dimensional infinite elements, substituting the basis functions and integrating over the infinite volume of the elements result in terms

containing the the following undefined oscillatory form

$$\lim_{\tilde{r} \rightarrow \infty} \left[ e^{-jk_0 \tilde{r}} \right]. \quad (5.4.20)$$

Fortunately the summation over all the integrals cancels the terms containing this factor and each of the elemental matrix entries are well-defined.

It can be verified from Appendix D.1 that not all of the integrals appearing in the definition of the matrix entries can be evaluated analytically. Due to the exponential factor present in the basis functions the  $E_n(x)$  function is again encountered and computed as for the two-dimensional infinite element solution.

In addition, computing the curl of the basis functions in spherical coordinates produces fractions containing a  $\sin(\theta)$  term in the denominator and some mixed polynomial and trigonometric functions in the numerator. At first glance, this seems to be problematic since the integrand becomes singular for  $\theta = 0, \pi$ . However, if the mesh that is used contains nodes exactly at these two points, it can be shown that the singularity is easily removed, see Appendix D.3. Also, in general these fraction functions cannot be integrated analytically and a five-point Gauss-Legendre quadrature method is employed. For details on the implementation of this method, refer to Appendix D.2.

Finally, in computing the coefficients for the basis functions using (5.4.4), the range of the angular variable  $\phi$  has to be considered carefully. Across the  $y = 0$  boundary the mapping from Cartesian coordinates to spherical coordinates is discontinuous in  $\phi$  for  $x > 0$  if the convention  $\phi \in [0; 2\pi)$  is used and discontinuous for  $x < 0$  if the convention  $\phi \in (-\pi; \pi]$  is used. Such a discontinuity is not allowed and for each infinite element having nodes on either side of  $y = 0$  the appropriate convention has to be used. A similar problem occurs for the angular variable  $\theta$ , but again by using a mesh in which there are nodes at  $\theta = 0, \pi$  the problem is eliminated.

## 5.5 Results

The infinite element mesh termination scheme is implemented for the existing finite element electromagnetic solver. Absorbing boundary conditions have already been implemented for this code [42] and are used here as a comparison to the infinite element solution. The scattering and radiating current source

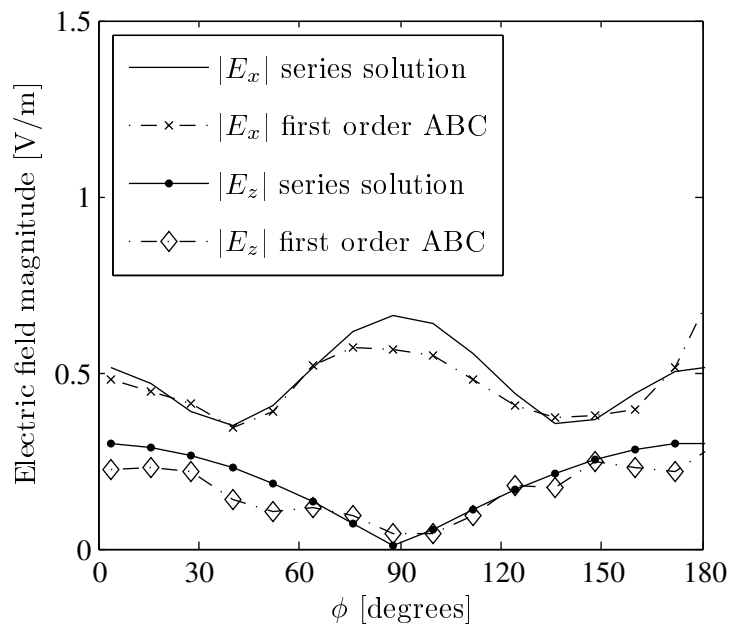
problems defined in Section 4.2 are solved numerically and the results are compared here to the analytic solutions.

### 5.5.1 Scattering Problem

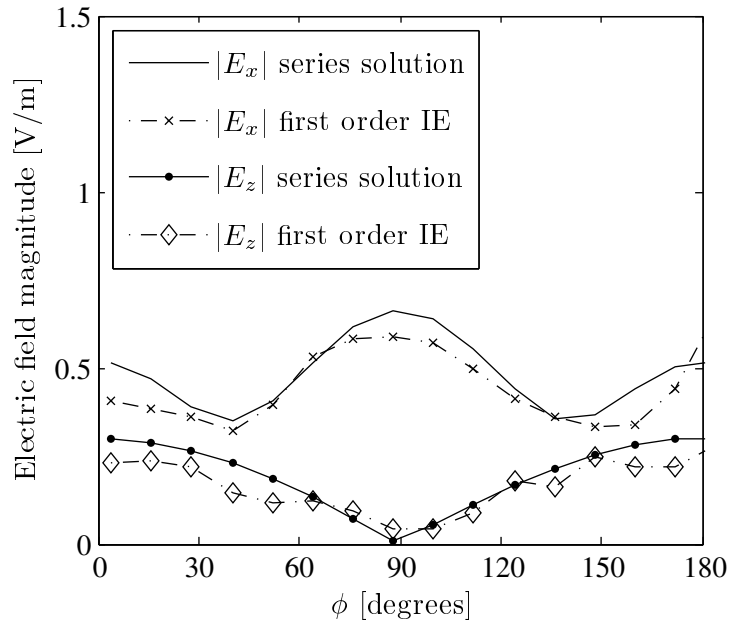
A conducting sphere with a radius of  $0.25\lambda$  is illuminated by an incident  $x$ -polarised plane wave incident along the positive  $z$ -axis. The scattered field is computed at a radius of  $0.33\lambda$  using a mesh in which the maximum edge length is  $\lambda/15$  and the termination boundary is at  $0.5\lambda$ . Using both a first order absorbing boundary condition and a first order infinite element, the scattered field is computed. The results are presented below.

Figure 5.3 shows the  $E_x$  and  $E_z$  components of the scattered field as computed using a first order ABC and Figure 5.4 shows the same field components computed using a first order infinite element. The results are more or less the same for either method and the relative accuracy of each is not immediately visible.

Higher order infinite elements are also used to solve the same problem and to compare the accuracy of the different orders of infinite element to that of the first order ABC, a root mean square relative error is computed as in Sec-



**Figure 5.3:** Scattered field computed using a first order absorbing boundary condition.



**Figure 5.4:** Scattered field computed using a first order infinite element.

tion 2.3.4, here for the dominant  $E_x$  field component. The results are shown in Table 5.2. Also displayed in this table is the number of unknowns for the entire solution. Due to the large error in both the solution with the ABC and the solution with the infinite elements, it is difficult to compare the methods fairly according to solution accuracy. It is noted that for this particular problem the use of a third order infinite element increases the number of unknowns in the system by roughly 50%. Also, unlike the infinite elements in two dimensions, unknowns are added even with a first order radial expansion. This is due to the added basis functions representing the radially directed field.

Method	Percentage error	Unknowns
ABC	19.10	12 315
IE (1st)	21.22	12 994
IE (2nd)	22.81	15 704
IE (3rd)	20.26	18 414

**Table 5.2:** Comparison of accuracy and computational costs of the first order absorbing boundary condition and different orders of infinite elements.

### 5.5.2 Radiation Problem

A radiating current filament with a length of 0.1 m and a source frequency of 1 GHz is placed at the origin, orientated along the  $z$ -axis and the radiated field is computed using a first order ABC and a first order infinite element. The dominant field component in the  $xz$ -plane is  $E_z$ . Figure 5.5 shows this field component as computed at a constant radius in the  $xy$ -plane using the ABC and infinite element solutions. The maximum edge length in the mesh is  $\lambda/15$  and the termination boundary is at  $0.5\lambda$ . Again the two methods seem to result in more or less the same level of accuracy.

By refining the mesh for this current source problem the error behaviour of the two methods can be compared. Figure 5.6 shows how the solution error is affected by refining the mesh from a maximum edge length of  $\lambda/10$  to  $\lambda/20$ . As expected an initial refining of the mesh produces a definite reduction in the error of the solution. The first order infinite element solution does not seem to improve as the mesh is refined beyond  $\lambda/15$ , while the accuracy of the second order infinite element seems to saturate. The third order infinite element could not be used with the finest mesh, due to limited computational resources.

The effect of outer boundary radius on the accuracy of the solution is also

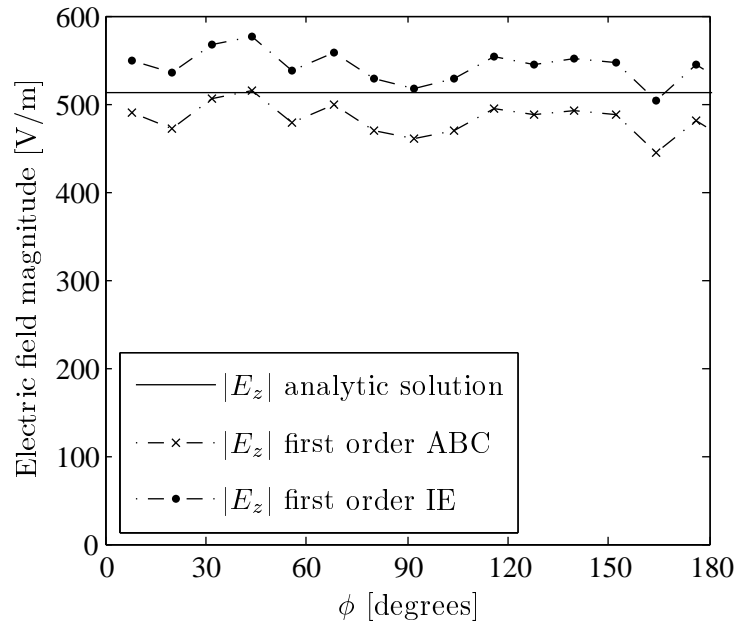


**Figure 5.5:** Radiated field computed using a first order absorbing boundary condition and first order infinite element.



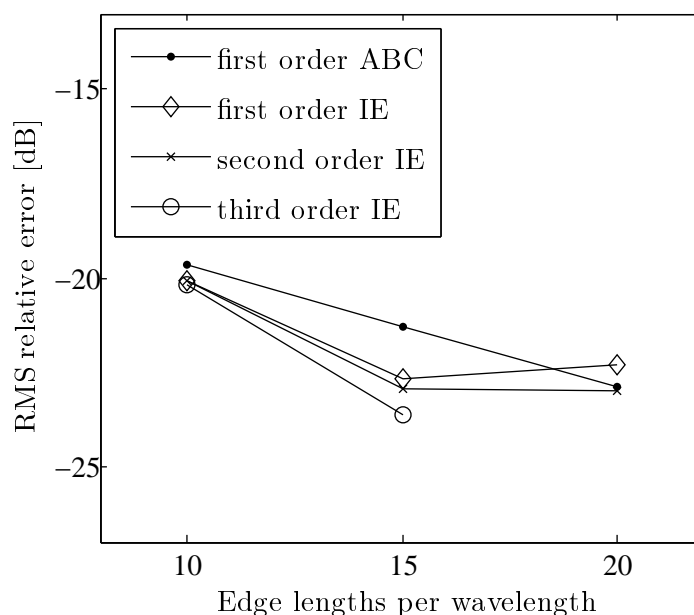


**Figure 5.6:** Effect of mesh fineness on accuracy of absorbing boundary condition and infinite element solutions.

investigated. With the maximum edge length in the mesh equal to  $\lambda/10$  the outer boundary radius is increased from  $0.25\lambda$  to  $1.25\lambda$ . Figure 5.7 shows how the solution error is affected by shifting the boundary  $\Gamma_2$  outward when using a first order ABC and also different orders of infinite elements. Due to limited computational resources, infinite element solutions could not be obtained for the largest boundary radius.

For a relatively close boundary the first order infinite element yields a very large error, while the third order element is slightly more accurate than the first order ABC and second order infinite element. As the boundary is shifted outward the ABC becomes more accurate up to a certain point beyond which other factors inducing error, such as mesh fineness and numerical dispersion, seem to dominate. The infinite elements of different orders result in more or less the same level of accuracy as the boundary is shifted outward and the error is somewhat larger than for the ABC solution.

Again the effect of increasing boundary radius is investigated, but this time at half the source frequency 500 MHz. In terms of electrical length this means the mesh is refined, while the outer boundary radius is effectively halved. Figure 5.8 shows the accuracies of the ABC solution and infinite

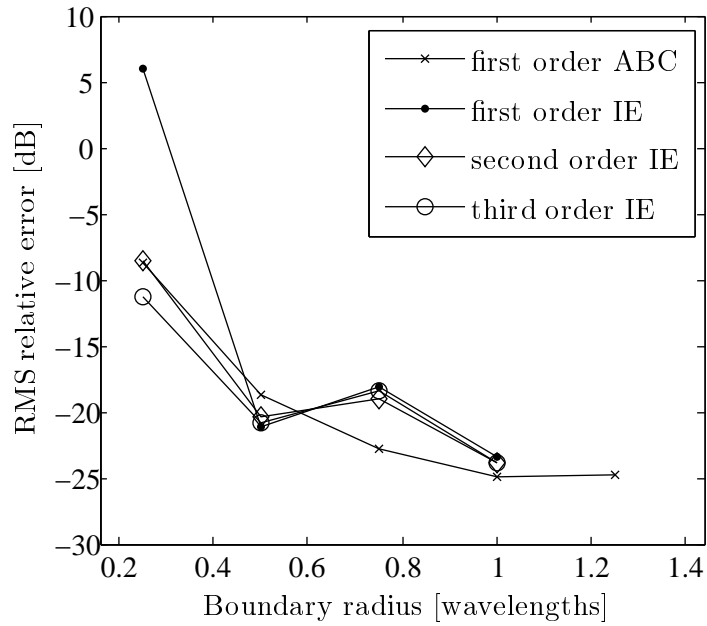


**Figure 5.7:** Effect of boundary radius on accuracy of absorbing boundary condition and infinite element solutions for a coarse mesh.

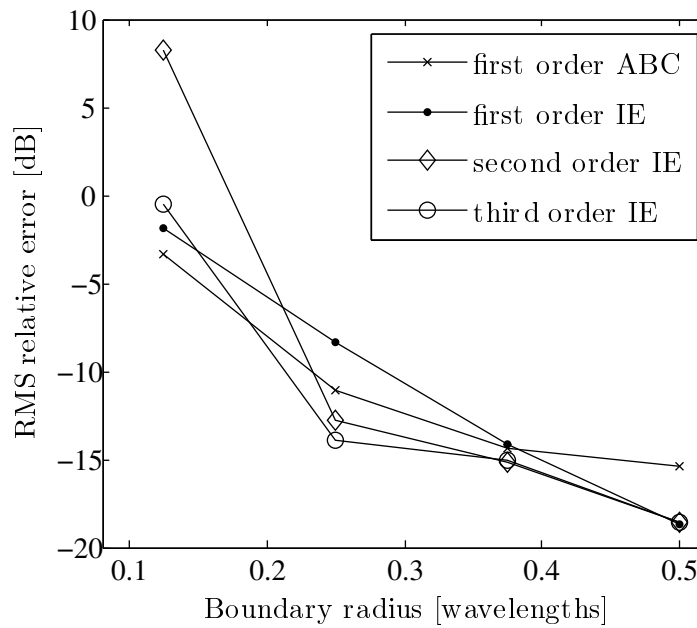


**Figure 5.8:** Effect of boundary radius on accuracy of absorbing boundary condition and infinite element solutions for a fine mesh.

element solutions as the boundary radius is increased from  $0.125\lambda$  to  $0.5\lambda$  for a mesh with a maximum edge length of  $\lambda/20$ . For a very close exterior boundary all solutions result in poor accuracy and a steady decrease in error is observed for an increasing boundary radius. As the boundary radius becomes larger, the first order infinite element yields the largest error, the ABC the second largest error, and the second and third order infinite elements result in more or less the same accuracy. However, with the boundary shifted sufficiently far outward the infinite element solutions seem to be more accurate than the ABC solution.

### 5.5.3 Improving the accuracy of the infinite element scheme

The results show that the infinite element scheme is not significantly more accurate than the ABC termination. One factor that affects the accuracy of the infinite element presented here is the assumption that the curved surfaces of the infinite elements and the flat surfaces of the tetrahedral elements to which they are attached are sufficiently close. In effect when performing the necessary integrations to construct the elemental matrices there is a small volume between each infinite and finite element over which integration is not performed. Also, the tangential field continuity between the infinite and finite element is not enforced exactly, since the field on the finite element and the field on the infinite element are not at the same point in space. Alleviating these problems would require using curvilinear finite elements to form the exterior boundary such that the faces of the finite and infinite elements match exactly. Alternatively, the shape of the infinite element can be modified to have a flat triangular surface. However, this would require redefining the basis functions and generally result in rather complicated expressions.

Another source of error for the infinite element scheme is that scaling in the azimuthal direction due to variation in the zenith angle is not taken into account. The scaling contains a  $\frac{1}{\sin(\theta)}$  term and becomes important near the poles, i.e. where  $\sin(\theta) \approx 0$ . This problem is easily overcome by simply rotating each infinite element away from the poles ( $\theta \approx 0, \pi$ ) and toward the equator ( $\theta \approx \frac{\pi}{2}$ ) before defining the basis functions and performing integration. Note that rotation is done in Cartesian coordinates in order to prevent distortion of the element. This rotation scheme is implemented and results similar to those in Figure 5.8 are produced, as shown in Figure 5.9. A small decrease in error

is observed due to the implemented rotation scheme, but the improvement is not significant.

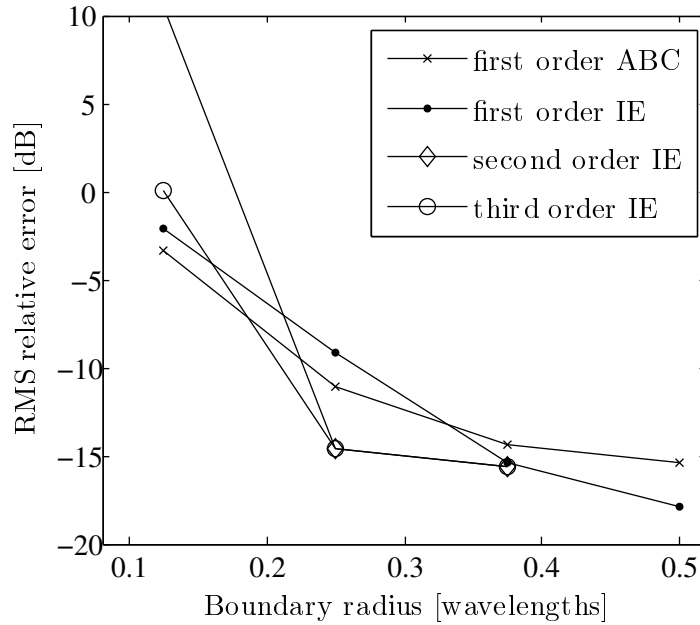


**Figure 5.9:** Effect of boundary radius on accuracy of absorbing boundary condition and infinite element solutions for a fine mesh. The infinite element scheme rotates each infinite element toward the equator.

## 5.6 Conclusion

A new type of three-dimensional infinite element has been developed and implemented as part of an existing vector finite element solver. The performance of the infinite element was compared to that of the first order absorbing boundary condition and it was found that the accuracy of the two termination schemes are more or less equal. A method for improving the accuracy of the infinite element was also suggested.

## Chapter 6

# General Conclusion

The focus of this project has been to compare different mesh termination schemes used to terminate the finite element domain properly when using the finite element method to solve unbounded electromagnetic problems.

First a typical two-dimensional unbounded problem in electromagnetics was presented. A finite element solution was then formulated and the need for a proper mesh termination scheme was motivated. Following this, different mesh termination schemes were formulated and implemented as part of the finite element solution.

Specifically, absorbing boundary conditions, the finite element boundary integral method and higher order infinite elements were considered in turn, with a detailed description of how each method is incorporated into the finite element solution. For the finite element boundary integral method attention was also given to the problem of interior resonances and its elimination by introducing a loss to the system. Galerkin weighted infinite elements were compared to complex conjugate weighted infinite elements, where it was found that the former were more accurate for lower order elements.

A direct comparison of the different two-dimensional mesh termination schemes was carried out under different criteria, specifically solution accuracy, computational efficiency and implementation complexity.

Typical three-dimensional unbounded problems were also presented, after which a vector finite element solution was formulated. A new type of infinite element was developed to be compatible with tetrahedral vector finite elements and incorporated into an existing finite element solver where its performance was compared to that of the first order absorbing boundary condition.

## 6.1 Recommendations

Considering what has been done, there are still numerous topics that warrant further investigation. A few suggestions are made here.

In comparing the different mesh termination schemes in two dimensions a relatively simple scattering problem was considered. Scattering analysis can be performed on more complex bodies with various material properties and different deformations of the exterior boundary may also be considered. Concerning the two-dimensional infinite element, a direct comparison of various infinite element schemes in literature can be performed.

In three dimensions the comparative study can be extended to include more mesh termination schemes, such as the perfectly matched layer and the finite element boundary integral method. Use of the infinite element in conjunction with higher order finite elements and even curvilinear elements to better approximate the exterior boundary can also be investigated.

# Appendices

# Appendix A

## Special Functions

Definitions and properties of some of the special functions encountered are presented here. Specifically attention is given to Bessel and related functions and also the  $En$ -function.

### A.1 Bessel and Related Functions

The Bessel functions [43] are the solutions to the following differential equation

$$x^2 \frac{d^2 y}{dx^2} + x \frac{dy}{dx} + (x^2 - n^2)y = 0. \quad (\text{A.1.1})$$

Two independent solutions to this equation are the Bessel function of the first  $J_n(x)$  and the Bessel function of the second kind  $Y_n(x)$ .

The following recursion formulae are useful for determining the derivatives of these functions

$$\frac{dJ_n(x)}{dx} = \frac{1}{2}(J_{n-1}(x) - J_{n+1}(x)). \quad (\text{A.1.2})$$

A symmetry relation that is also often used is

$$J_{-n}(x) = (-1)^n J_n(x). \quad (\text{A.1.3})$$

Combining (A.1.2) and (A.1.3) the derivatives of the zeroth order Bessel functions are

$$\frac{dJ_0(x)}{dx} = -J_1(x). \quad (\text{A.1.4})$$



Although the above is stated in terms of  $J_n(x)$ , the results also apply exactly to  $Y_n(x)$ .

Some useful asymptotic forms for the Bessel functions are

$$J_n(x) \approx \frac{1}{\Gamma(n+1)} \left(\frac{x}{2}\right)^n \quad x \ll 1, \forall n \quad (\text{A.1.5})$$

$$Y_n(x) \approx \begin{cases} \frac{2}{\pi} \left[ \ln\left(\frac{x}{2}\right) + \gamma \right] & x \ll 1, n = 0 \\ -\frac{\Gamma(n)}{\pi} \left(\frac{2}{x}\right) & x \ll 1, n \neq 0 \end{cases} \quad (\text{A.1.6})$$

where  $\gamma \approx 0.5772156649$  is the Euler-Mascheroni constant and  $\Gamma(x)$  is the Gamma-function.

### A.1.1 Hankel Functions

Hankel functions [44] are special linear combinations of the Bessel functions of the first and second kind. The Hankel function of the first kind  $H_n^{(1)}(x)$  and the Hankel function of the second kind  $H_n^{(2)}(x)$  are defined as

$$\begin{aligned} H_n^{(1)}(x) &= J_n(x) + jY_n(x) \\ H_n^{(2)}(x) &= J_n(x) - jY_n(x). \end{aligned} \quad (\text{A.1.7})$$

Using the derivative properties of the Bessel functions (A.1.4) give an expression for the derivative of the zeroth order Hankel function

$$\frac{dH_0^{(k)}}{dx} = -H_1^{(k)}(x). \quad (\text{A.1.8})$$

Applying the asymptotic forms for the Bessel functions (A.1.5) and (A.1.6) the following results are obtained for the Hankel function of the second kind

$$H_0^{(2)}(x) \approx 1 - j\frac{2}{\pi} \left[ \ln\left(\frac{1}{2}x\right) + \gamma \right] \quad x \ll 1, n = 0 \quad (\text{A.1.9})$$

$$H_1^{(2)}(x) \approx \frac{x}{2} + j\frac{2}{\pi x} \quad x \ll 1, n \neq 0. \quad (\text{A.1.10})$$

### A.1.2 Riccati-Bessel Functions

The Riccati-Bessel functions [45] of the first kind ( $\hat{J}_n$ ) and second kind ( $\hat{Y}_n$ ) are related to the ordinary Bessel functions of the first kind and second kind

by

$$\hat{J}_n(x) = \sqrt{\frac{\pi x}{2}} J_{n+\frac{1}{2}}(x) \quad (\text{A.1.11})$$

$$\hat{Y}_n(x) = -\sqrt{\frac{\pi x}{2}} Y_{n+\frac{1}{2}}(x) \quad (\text{A.1.12})$$

and the Riccati-Hankel function of the second kind is defined as

$$\hat{H}_n^{(2)}(x) = \hat{J}_n(x) - j\hat{Y}_n(x). \quad (\text{A.1.13})$$

The derivatives of Riccati-Bessel functions are obtained using the product rule of differentiation and (A.1.2) to give

$$\frac{d\hat{J}_n(x)}{dx} = \frac{1}{2} \left[ \hat{J}_{n-1}(x) - \frac{1}{x} \hat{J}_n(x) - \hat{J}_{n+1}(x) \right] \quad (\text{A.1.14})$$

$$\begin{aligned} \frac{d^2\hat{J}_n(x)}{dx^2} &= \frac{1}{4} \left[ \hat{J}_{n-2}(x) - \frac{2}{x} \hat{J}_{n-1}(x) + \left( \frac{3}{x^2} - 2 \right) \hat{J}_n(x) \right. \\ &\quad \left. + \frac{2}{x} \hat{J}_{n+1}(x) + \hat{J}_{n+2}(x) \right] \end{aligned} \quad (\text{A.1.15})$$

where the same results also apply to  $\hat{Y}_n(x)$  and  $\hat{H}_n^{(k)}(x)$ .

## A.2 $En$ -Function

The exponential integral [46] denoted  $E_i(x)$  is defined as

$$E_i(x) = -\int_{-x}^{\infty} \frac{e^{-u}}{u} du \quad (\text{A.2.1})$$

from which the  $E_1(x)$ -function is derived

$$E_1(x) = -E_i(-x) = \int_x^{\infty} \frac{e^{-u}}{u} du = \int_1^{\infty} \frac{e^{-xt}}{t} dt \quad (\text{A.2.2})$$

using the substitution  $u = xt$ . Now the  $E_n$ -function is defined

$$E_n(x) = \int_1^{\infty} \frac{e^{-xt}}{t^n} dt. \quad (\text{A.2.3})$$

Using integration by parts a recurrence relation can be obtained to relate  $E_{n+1}$  to  $E_n$

$$\begin{aligned}
 E_{n+1}(x) &= \int_1^\infty \frac{e^{-xt}}{t^{n+1}} dt \\
 &= -\frac{1}{n} \frac{e^{-tx}}{t^n} \Big|_1^\infty - \int_1^\infty \frac{x}{t^n} \frac{e^{-tx}}{t^n} dt \\
 &= \frac{1}{n} [e^{-x} - xE_n(x)]. \tag{A.2.4}
 \end{aligned}$$

Repeatedly expanding the recurrence relation until  $E_1(x)$  is reached gives

$$\begin{aligned}
 E_n(x) &= \frac{[e^{-x} - xE_{n-1}(x)]}{n-1} \\
 &= \frac{e^{-x}}{n-1} - \frac{x[e^{-x} - xE_{n-2}(x)]}{(n-1)(n-2)} \\
 &= \frac{e^{-x}}{n-1} - \frac{xe^{-x}}{(n-1)(n-2)} + \frac{x^2[e^{-x} - xE_{n-3}(x)]}{(n-1)(n-2)(n-3)} \\
 &= \frac{1}{(n-1)!} \left[ (-x)^0 e^{-x} (n-1-1)! + (-x)^1 e^{-x} (n-1-2)! \right. \\
 &\quad \left. + (-x)^2 e^{-x} (n-1-3)! + \dots + (-x)^{n-1} E_1(x) \right] \\
 &= \frac{(-x)^{n-1} E_1(x)}{(n-1)!} + e^{-x} \sum_{m=0}^{n-2} \frac{(-x)^m (n-2-m)!}{(n-1)!}. \tag{A.2.5}
 \end{aligned}$$

The function  $E_1(x)$  can be computed using the series

$$E_1(x) = -\gamma - \ln(x) - \sum_{n=1}^{\infty} \frac{(-x)^n}{n(n!)} \tag{A.2.6}$$

where  $\gamma \approx 0.5772156649$  is the Euler-Mascheroni constant. Often integrals similar to (A.2.3) are encountered where the lower limit is not equal to one. In such a case the integral can be reduced to a form containing  $E_n$  as follows

$$\begin{aligned}
 \int_a^\infty \frac{e^{-xt}}{t^n} dt &= \int_1^\infty \frac{e^{-xau}}{(au)^n} a du \\
 &= \frac{1}{a^{n-1}} \int_1^\infty \frac{e^{-axu}}{u^n} du \\
 &= \frac{1}{a^{n-1}} E_n(ax) \tag{A.2.7}
 \end{aligned}$$

using the substitution  $t = au$ .

### A.3 Legendre Polynomials

The Legendre polynomials [47] are defined as the solutions to the Legendre differential equation

$$(1 - x^2) \frac{d^2 y}{dx^2} - 2x \frac{dy}{dx} + l(l + 1)y = 0. \quad (\text{A.3.1})$$

A Legendre polynomial  $P_l(x)$  of arbitrary order can be calculated using the recurrence relation

$$P_l(x) = \frac{(2l - 1)xP_{l-1}(x)}{l} - \frac{(l - 1)P_{l-2}(x)}{l} \quad (\text{A.3.2})$$

where  $P_0(x) = 1$  and  $P_1(x) = x$ .

The associated Legendre polynomial  $P_l^m(x)$  is defined as

$$P_l^m(x) = (-1)^m (1 - x^2)^{m/2} \frac{d^m}{dx^m} P_l(x). \quad (\text{A.3.3})$$

A useful recurrence relation for the associated Legendre polynomial is

$$(l - m)P_l^m(x) = x(2l - 1)P_{l-1}^m(x) - (l + m - 1)P_{l-2}^m(x) \quad (\text{A.3.4})$$

and the derivative is given by

$$\frac{dP_l^m(x)}{dx} = \frac{lxP_l^m(x) - (l + m)P_{l-1}^m(x)}{1 - x^2} \quad (\text{A.3.5})$$

except at  $x = 0$  where the following expression is used

$$\left. \frac{dP_l^m(x)}{dx} \right|_{x=0} = \frac{2^{m+1} \sin\left(\frac{1}{2}\pi(l + m)\right) \Gamma\left(\frac{1}{2}l + \frac{1}{2}m + 1\right)}{\sqrt{\pi} \Gamma\left(\frac{1}{2}l - \frac{1}{2}m + \frac{1}{2}\right)}. \quad (\text{A.3.6})$$

## Appendix B

# The Green Function and Integral Equations

Here the integral equation relating the electric field on a closed boundary to any point enclosed by that boundary is derived. This integral equation is used in Section 2.3.4 as a near-field to far-field transformation and in Section 3.3 as a restriction on the field at the exterior boundary of the finite element domain. The integrand contains singularities when the integral equation is evaluated on the boundary and the integration over these singularities are also discussed.

### B.1 Integral Equation Derivation

Suppose the field  $E$  and its normal derivative is known on the boundary  $\Gamma_2$  separating two domains  $\Omega_1$  and  $\Omega_2$ . The domain  $\Omega_1$  is entirely enclosed by  $\Gamma_2$ , while the infinite domain  $\Omega_2$  is enclosed by  $\Gamma_2$  and a boundary at infinity  $\Gamma_\infty$ . The objective is to find the field at any point in  $\Omega_2$ . By multiplying the Helmholtz equation with the Green function and integrating over the infinite exterior domain this relation can be obtained as follows.

The Green function for a scalar field in two dimensions is defined as the solution to the differential equation

$$\nabla^2 G_0(\mathbf{x}, \mathbf{x}') + k_0^2 G_0(\mathbf{x}, \mathbf{x}') = -\delta(\mathbf{x} - \mathbf{x}') \quad (\text{B.1.1})$$

which has the solution

$$G_0(\mathbf{x}, \mathbf{x}') = \frac{1}{j^4} H_0^{(2)}(k_0 |\mathbf{x} - \mathbf{x}'|). \quad (\text{B.1.2})$$

By multiplying the free space homogeneous Helmholtz equation with this Green function and integrating over the infinite exterior region one obtains

$$\iint_{\Omega_2} G_0(\mathbf{x}, \mathbf{x}') [\nabla^2 E(\mathbf{x}') + k_0^2 E(\mathbf{x}')] d\Omega' = 0. \quad (\text{B.1.3})$$

The second scalar Green's theorem is then applied to yield

$$\begin{aligned} 0 &= \iint_{\Omega_2} E(\mathbf{x}') [\nabla^2 G_0(\mathbf{x}, \mathbf{x}') + k_0^2 G_0(\mathbf{x}, \mathbf{x}')] d\Omega' \\ &+ \oint_{\Gamma_2 + \Gamma_\infty} G_0(\mathbf{x}, \mathbf{x}') \frac{\partial E(\mathbf{x}')}{\partial n} - E(\mathbf{x}') \frac{\partial G_0(\mathbf{x}, \mathbf{x}')}{\partial n} d\Gamma'. \end{aligned} \quad (\text{B.1.4})$$

Since both the Green function and the field  $E$  satisfy the Sommerfeld radiation condition, the integral over  $\Gamma_\infty$  vanishes. It is also important to note that here the normal directional derivative points from  $\Omega_2$  towards  $\Omega_1$ . By choosing the normal direction on  $\Gamma_2$  from  $\Omega_1$  toward  $\Omega_2$  adds a negative sign to the integral over  $\Gamma_2$ . The left-hand side of (B.1.1) is recognised within the integral over  $\Omega_2$  and is replaced by  $-\delta(\mathbf{x} - \mathbf{x}')$

$$\begin{aligned} 0 &= \iint_{\Omega_2} -E(\mathbf{x}') \delta(\mathbf{x} - \mathbf{x}') d\Omega' \\ &+ \int_{\Gamma_2} E(\mathbf{x}') \frac{\partial G_0(\mathbf{x}, \mathbf{x}')}{\partial n} - G_0(\mathbf{x}, \mathbf{x}') \frac{\partial E(\mathbf{x}')}{\partial n} d\Gamma'. \end{aligned} \quad (\text{B.1.5})$$

Rearranging and using the definition of the Dirac delta function the desired transformation is obtained

$$E(\mathbf{x}) = \int_{\Gamma} \left( E(\mathbf{x}') \frac{\partial G_0(\mathbf{x}, \mathbf{x}')}{\partial n'} - G_0(\mathbf{x}, \mathbf{x}') \frac{\partial E(\mathbf{x}')}{\partial n'} \right) d\Gamma'. \quad (\text{B.1.6})$$

If instead of using the homogeneous Helmholtz equation to derive the integral equation the inhomogeneous equation is used the result is somewhat different. The inhomogeneous Helmholtz equation is

$$\nabla^2 E + k_0^2 E = j k_0 Z_0 J \quad (\text{B.1.7})$$

where  $Z_0$  is the free space impedance and  $J$  is some distributed current source density. By multiplying with the Green function and integrating over the exterior region one obtains

$$\iint_{\Omega_2} G_0(\mathbf{x}, \mathbf{x}') [\nabla^2 E(\mathbf{x}') + k_0^2 E(\mathbf{x}')] d\Omega' = \iint_{\Omega_2} G_0(\mathbf{x}, \mathbf{x}') jk_0 Z_0 J(\mathbf{x}') d\Omega'. \quad (\text{B.1.8})$$

The left-hand side of (B.1.8) is manipulated as above for the inhomogeneous Helmholtz equation, while the right-hand side is left in its current form to obtain after rearranging

$$\begin{aligned} E(\mathbf{x}) &= jk_0 Z_0 \iint_{\Omega_2} G_0(\mathbf{x}, \mathbf{x}') J(\mathbf{x}') d\Omega' \\ &+ \int_{\Gamma} \left( E(\mathbf{x}') \frac{\partial G_0(\mathbf{x}, \mathbf{x}')}{\partial n'} - G_0(\mathbf{x}, \mathbf{x}') \frac{\partial E(\mathbf{x}')}{\partial n'} \right) d\Gamma'. \end{aligned} \quad (\text{B.1.9})$$

The first term on the right-hand side of this equation is simply the field produced by the current source in region  $\Omega_2$  and can equivalently be represented by an incident field

$$E(\mathbf{x}) = E^{\text{inc}}(\mathbf{x}) + \int_{\Gamma} \left( E(\mathbf{x}') \frac{\partial G_0(\mathbf{x}, \mathbf{x}')}{\partial n'} - G_0(\mathbf{x}, \mathbf{x}') \frac{\partial E(\mathbf{x}')}{\partial n'} \right) d\Gamma'. \quad (\text{B.1.10})$$

## B.2 Integration over the Green Function Singularity

From the definition of the two-dimensional free space Green function and (A.1.9) it is clear that the Green function has a logarithmic singularity, which means integration across this singularity yields a finite value. Here an approximation to the double integral over a small length containing this singularity as used in Section 3.3.3 is derived.

Consider the double integral

$$I = \int_{-\frac{\delta}{2}}^{\frac{\delta}{2}} \int_{-\frac{\delta}{2}}^{\frac{\delta}{2}} f(x') G_0(x, x') dx' dx. \quad (\text{B.2.1})$$

Assuming that  $f(x)$  is slow varying and  $\delta$  small enough that  $f(x) \approx f(0)$  in

the above, and using the definition of the Green function gives

$$I = f(0) \int_{-\frac{\delta}{2}}^{\frac{\delta}{2}} \int_{-\frac{\delta}{2}}^{\frac{\delta}{2}} \frac{1}{j4} H_0^{(2)}(k_0|x-x'|) dx' dx. \quad (\text{B.2.2})$$

By the definition of the absolute value the inner integral is split into two sections

$$\begin{aligned} I &= f(0) \int_{-\frac{\delta}{2}}^{\frac{\delta}{2}} \left[ \int_{-\frac{\delta}{2}}^x \frac{1}{j4} H_0^{(2)}(k_0(x-x')) dx' + \int_x^{\frac{\delta}{2}} \frac{1}{j4} H_0^{(2)}(k_0(x'-x)) dx' \right] dx \\ &= f(0) \left[ \int_{-\frac{\delta}{2}}^{\frac{\delta}{2}} I_l dx + \int_{-\frac{\delta}{2}}^{\frac{\delta}{2}} I_u dx \right] \end{aligned} \quad (\text{B.2.3})$$

Substituting the approximation (A.1.9) for the Hankel function into the first inner integral gives

$$\begin{aligned} I_l &= \int_{-\frac{\delta}{2}}^x \frac{1}{j4} \left( 1 - j \frac{2}{\pi} \left[ \ln\left(\frac{1}{2}x\right) + \gamma \right] \right) dx' \\ &= \frac{x + \frac{\delta}{2}}{j4} - \frac{\gamma(x + \frac{\delta}{2})}{2\pi} - \frac{1}{2\pi} \int_{-\frac{\delta}{2}}^x \ln \left[ \frac{1}{2}k_0(x-x') \right] dx'. \end{aligned} \quad (\text{B.2.4})$$

Using the substitution  $u = \frac{1}{2}k_0(x-x')$  and simplifying yields

$$\begin{aligned} I_l &= \left( x + \frac{\delta}{2} \right) \left( \frac{1}{j4} - \frac{\gamma}{2\pi} \right) + \frac{1}{\pi k_0} \lim_{\tilde{u} \rightarrow 0} [u \ln(u) - u] \Big|_{\frac{1}{2}k_0(x+\frac{\delta}{2})}^{\tilde{u}} \\ &= \left( x + \frac{\delta}{2} \right) \left( \frac{1}{j4} + \frac{1-\gamma}{2\pi} - \frac{1}{2\pi} \ln \left[ \frac{1}{2}k_0 \left( x + \frac{\delta}{2} \right) \right] \right). \end{aligned} \quad (\text{B.2.5})$$

A similar result is obtained for the second inner integral

$$\begin{aligned} I_u &= \left( \frac{\delta}{2} - x \right) \left( \frac{1}{j4} - \frac{\gamma}{2\pi} \right) - \frac{1}{\pi k_0} \lim_{\tilde{u} \rightarrow 0} [u \ln(u) - u] \Big|_{\tilde{u}}^{\frac{1}{2}k_0(\frac{\delta}{2}-x)} \\ &= \left( \frac{\delta}{2} - x \right) \left( \frac{1}{j4} + \frac{1-\gamma}{2\pi} - \frac{1}{2\pi} \ln \left[ \frac{1}{2}k_0 \left( \frac{\delta}{2} - x \right) \right] \right). \end{aligned} \quad (\text{B.2.6})$$



Substituting  $I_l$  and  $I_u$  into (B.2.3) gives

$$\begin{aligned}
 I = & f(0) \left[ \int_{-\frac{\delta}{2}}^{\frac{\delta}{2}} \left( x + \frac{\delta}{2} \right) \left( \frac{1}{j^4} + \frac{1-\gamma}{2\pi} - \frac{1}{2\pi} \ln \left[ \frac{1}{2} k_0 \left( x + \frac{\delta}{2} \right) \right] \right) dx \right. \\
 & \left. + \int_{-\frac{\delta}{2}}^{\frac{\delta}{2}} \left( \frac{\delta}{2} - x \right) \left( \frac{1}{j^4} + \frac{1-\gamma}{2\pi} - \frac{1}{2\pi} \ln \left[ \frac{1}{2} k_0 \left( \frac{\delta}{2} - x \right) \right] \right) dx \right]. \quad (\text{B.2.7})
 \end{aligned}$$

Using the substitutions  $u = \frac{1}{2} k_0 \left( x + \frac{\delta}{2} \right)$  and  $u = \frac{1}{2} k_0 \left( \frac{\delta}{2} - x \right)$  in the first and second integrals, respectively, results in equivalent forms which are added to give

$$I = 2f(0) \int_0^{\frac{\delta k_0}{2}} \frac{4u}{k_0^2} \left( \frac{1}{j^4} + \frac{1-\gamma}{2\pi} - \frac{1}{2\pi} \ln(u) \right) du. \quad (\text{B.2.8})$$

Evaluating the above integral gives the final result

$$I = \frac{\delta^2}{j^4} \left( 1 - \frac{j^2}{\pi} \ln \left[ \frac{\delta k_0}{2} e^{\gamma - \frac{3}{2}} \right] \right) \quad (\text{B.2.9})$$

where the constant  $\frac{1}{2} e^{\gamma - \frac{3}{2}} = 0.1987054869$ .

### B.3 Integrating over the Green Function Derivative Singularity

From the definition in (B.1.2) and the approximation (A.1.10) it is clear that the derivative of the Green function has a singularity at zero. In Section 3.3.1 the integral on a closed contour containing this singularity is substituted with an integral excluding this singular point. Here it is shown that this is indeed valid.

Consider the integral equation

$$f(\mathbf{x}) = \int_{\Gamma_2} f(\mathbf{x}') \frac{\partial G_0(\mathbf{x}, \mathbf{x}')}{\partial n'} d\Gamma' \quad (\text{B.3.1})$$

obtained from (B.1.6) and discarding the term not containing the derivative of the Green function. Suppose  $\mathbf{x}$  lies on  $\Gamma_2$ , then at some point  $\mathbf{x} = \mathbf{x}'$  on the integration path the derivative of the Green function would become singular. This singular point is isolated by dividing the path of integration into two

sections

$$f(\mathbf{x}) = \text{P.V.} \int_{\Gamma_{\text{PV}}} f(\mathbf{x}') \frac{\partial G_0(\mathbf{x}, \mathbf{x}')}{\partial n'} d\Gamma' + \lim_{\epsilon \rightarrow 0} \int_{\Gamma_r} f(\mathbf{x}') \frac{\partial G_0(\mathbf{x}, \mathbf{x}')}{\partial n'} d\Gamma' \quad (\text{B.3.2})$$

where  $\Gamma_r$  is a small semi-circular path with radius  $\epsilon$  around the singular point and the first integral on the right is the principal value integral. The principal value integral can be defined as

$$\text{P.V.} \int_0^L Z(s) ds = \lim_{\epsilon \rightarrow 0} \left[ \int_0^{\tilde{x}-\epsilon} Z(s) ds + \int_{\tilde{x}+\epsilon}^L Z(s) ds \right] \quad (\text{B.3.3})$$

where  $L$  is the length of the integration path along  $\Gamma_2$  and the kernel of the integral in (B.3.1) is parameterised as  $Z(s)$  in terms of the arc length  $s$  along the path  $\Gamma_2$ . The singularity occurs at  $s = \tilde{x}$ . Note that as  $\epsilon \rightarrow 0$  the path  $\Gamma_r$  vanishes while  $\Gamma_{\text{PV}} \rightarrow \Gamma_2$ . Figure B.1 shows a segment of  $\Gamma$  near the singular point as well as the paths  $\Gamma_{\text{PV}}$  and  $\Gamma_r$ . Note that in the derivation of (B.1.6) it was assumed that the point  $\mathbf{x}$  lies in  $\Omega_2$ , which is why the path  $\Gamma_r$  is chosen as in Figure B.1, so that in the limit  $\mathbf{x}$  approaches  $\Gamma_2$  from the region  $\Omega_2$ .

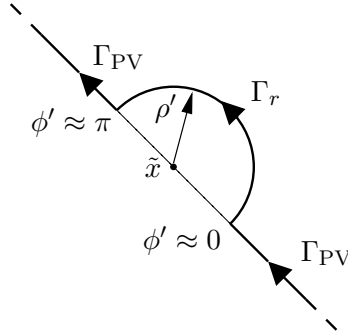


**Figure B.1:** Integration paths near a singularity of the derivative of the Green function.

Integration on the path  $\Gamma_r$  can be simplified by defining a local circular cylindrical coordinate system of which the origin coincides with the singular point. Let the radial and angular variables for this coordinate system be  $\rho'$  and  $\phi'$ , respectively. The distance  $|\mathbf{x} - \mathbf{x}'|$  is then simply the radius  $\rho'$  and the normal derivative is the negative of the radial derivative, in accordance with the convention of the normal direction in Section B.1. Using (A.1.8) and the

approximation (A.1.10) the derivative of the Green function is simply

$$\begin{aligned} \frac{\partial G_0(\mathbf{x}, \mathbf{x}')}{\partial n'} &= -\frac{\partial G_0(k_0 r)}{\partial \rho'} = \frac{k_0}{j^4} H_1^{(2)}(k_0 \rho') \\ &\approx \frac{k_0^2 \rho'}{j^8} + \frac{1}{2\pi \rho'}. \end{aligned} \quad (\text{B.3.4})$$

Using this expression in the integral along  $\Gamma_r$  and substituting the differential  $\Gamma'$  with  $\rho' d\phi$  gives

$$\int_{\Gamma_r} f(\mathbf{x}') \frac{\partial G_0(\mathbf{x}, \mathbf{x}')}{\partial n'} d\Gamma' = \int_0^{\phi_1} f(\mathbf{x}') \left( \frac{k_0^2 \rho'}{j^8} + \frac{1}{2\pi \rho'} \right) \rho' d\phi'. \quad (\text{B.3.5})$$

Now substituting  $\rho'$  with  $\epsilon$  and using  $f(\mathbf{x}') \approx f(\mathbf{x})$  for  $\epsilon \rightarrow 0$  obtains

$$\begin{aligned} \lim_{\epsilon \rightarrow 0} \int_0^{\phi_1} f(\mathbf{x}') \left( \frac{k_0^2 \epsilon^2}{j^8} + \frac{1}{2\pi} \right) d\phi' &= f(\mathbf{x}) \lim_{\epsilon \rightarrow 0} \int_0^{\phi_1} \left( \frac{k_0^2 \epsilon^2}{j^8} + \frac{1}{2\pi} \right) d\phi' \\ &= f(\mathbf{x}) \lim_{\epsilon \rightarrow 0} \left( \frac{k_0^2 \epsilon^2}{j^8} + \frac{1}{2\pi} \right) \phi \Big|_0^{\phi_1} \\ &= \frac{1}{2} f(\mathbf{x}) \end{aligned} \quad (\text{B.3.6})$$

where it is assumed the boundary  $\Gamma_2$  is smooth, so the upper limit of integration  $\phi_1 \rightarrow \pi$  as  $\epsilon \rightarrow 0$ . Finally, substituting this result into (B.3.2) and rearranging gives

$$\frac{1}{2} f(\mathbf{x}) = \int_{\Gamma_{\text{PV}}} f(\mathbf{x}') \frac{\partial G_0(\mathbf{x}, \mathbf{x}')}{\partial n} d\Gamma'. \quad (\text{B.3.7})$$

## Appendix C

# 2D Infinite Element Integrals

The integrals arising from evaluating the matrix entries for the two-dimensional infinite element in Section 3.4 are considered here. First the results for Galerkin weighted infinite elements are presented, followed by the results for complex conjugate weighted infinite elements.

### C.1 Elemental Integrals - Galerkin Weighted

In Section 3.4.3 the explicit expressions for the basis functions are given and are repeated here

$$\lambda_i = R_i(\rho)A_i(\phi) = e^{-jk_0(\rho-\rho_i)} \sum_{n=1}^{N_R} h_{in}\rho^{\frac{1}{2}-n}(a_i\phi + b_i). \quad (\text{C.1.1})$$

The angular functions  $A_i$  are simply linear interpolation functions and the integrals  $I_{ij}^{A1}$  in (3.4.23) and  $I_{ij}^{A2}$  in (3.4.24) are easily evaluated. Integrals concerning the radial functional are more complicated and warrant further discussion.

Taking the partial derivative of  $R_i$  with respect to  $\rho$  gives

$$\begin{aligned} \frac{dR_i}{d\rho} &= e^{-jk_0(\rho-\rho_i)} \sum_{n=1}^{N_R} \left[ h_{in} \left( \frac{1}{2} - n \right) \rho^{-\frac{1}{2}-n} - jk_0 h_{in} \rho^{\frac{1}{2}-n} \right] \\ &= e^{-jk_0(\rho-\rho_i)} \sum_{n=1}^{N_R} g_{in} \rho^{\frac{1}{2}-n} \end{aligned} \quad (\text{C.1.2})$$

where

$$g_{in} = \begin{cases} -jk_0 h_{in} & n = 1 \\ -jk_0 h_{in} + \left(\frac{3}{2} - n\right) h_{i(n-1)} & n = 2, 3, \dots, N_R \\ \left(\frac{3}{2} - n\right) h_{i(n-1)} & n = N_R + 1. \end{cases} \quad (\text{C.1.3})$$

The product  $R_i R_j$  is

$$\begin{aligned} R_i R_j &= p_{ij} e^{-j2k_0 \rho} \sum_{n=1}^{N_R} h_{in} \rho^{\frac{1}{2}-n} \sum_{n=1}^{N_R} h_{jn} \rho^{\frac{1}{2}-n} \\ &= p_{ij} e^{-j2k_0 \rho} \sum_{n=1}^{2N_R-1} s_n^{ij} \rho^{-n} \end{aligned} \quad (\text{C.1.4})$$

where

$$s_n^{ij} = \begin{cases} \sum_{m=1}^n h_{im} h_{j(n-m+1)} & n = 1, 2, \dots, N_R \\ \sum_{m=n-N_R}^{N_R-1} h_{i(m+1)} h_{j(n-m)} & n = (N_R + 1), (N_R + 2), \dots, (2N_R - 1) \end{cases} \quad (\text{C.1.5})$$

$$p_{ij} = e^{jk_0(\rho_i + \rho_j)} \quad (\text{C.1.6})$$

and the product of the derivatives of  $R_i$  and  $R_j$  is

$$\begin{aligned} \frac{dR_i}{d\rho} \frac{dR_j}{d\rho} &= p_{ij} e^{-j2k_0 \rho} \sum_{n=1}^{N_R+1} g_{in} \rho^{\frac{1}{2}-n} \sum_{n=1}^{N_R+1} g_{jn} \rho^{\frac{1}{2}-n} \\ &= p_{ij} e^{-j2k_0 \rho} \sum_{n=1}^{2N_R+1} f_n^{ij} \rho^{-n} \end{aligned} \quad (\text{C.1.7})$$

where

$$f_n^{ij} = \begin{cases} \sum_{m=1}^n g_{im} g_{j(n-m+1)} & n = 1, 2, \dots, (N_R + 1), \\ \sum_{m=n-N_R}^{N_R+1} g_{im} g_{j(n-m+1)} & n = (N_R + 2), (N_R + 3), \dots, (2N_R + 1). \end{cases} \quad (\text{C.1.8})$$

These products can now be substituted into the integrals of (3.4.19) through

(3.4.22) and the subfunctional for each infinite element can be calculated according to (3.4.18). Using the definitions

$$\tilde{L} = \lim_{\tilde{\rho} \rightarrow \infty} \left[ e^{-j2k_0\tilde{\rho}} \right] \quad (\text{C.1.9})$$

$$L^a = e^{-j2k_0\rho_a} \quad (\text{C.1.10})$$

the quantities  $I_{ij}^{R1}$ ,  $I_{ij}^{R2}$ ,  $I_{ij}^{R3}$  and  $I_{ij}^{R4}$  become

$$\begin{aligned} I_{ij}^{R1} &= \lim_{\tilde{\rho} \rightarrow \infty} \int_{\rho_a}^{\tilde{\rho}} \frac{dR_i}{d\rho} \frac{dR_j}{d\rho} \rho \, d\rho \\ &= p_{ij} \lim_{\tilde{\rho} \rightarrow \infty} \int_{\rho_a}^{\tilde{\rho}} e^{-j2k_0\rho} \sum_{n=1}^{2N_R+1} f_n^{ij} \rho^{1-n} \, d\rho \\ &= p_{ij} \lim_{\tilde{\rho} \rightarrow \infty} \left[ \frac{f_1^{ij}}{-j2k_0} \left( e^{-j2k_0\tilde{\rho}} - e^{-j2k_0\rho_a} \right) + \sum_{n=2}^{2N_R+1} \int_{\rho_a}^{\tilde{\rho}} e^{-j2k_0\rho} f_n^{ij} \rho^{1-n} \, d\rho \right] \\ &= p_{ij} \left[ -j\frac{1}{2}k_0 h_{i1} h_{j1} (\tilde{L} - L^a) + \sum_{n=2}^{2N_R+1} \frac{f_n^{ij}}{\rho_a^{n-2}} E_{(n-1)}(j2k_0\rho_a) \right] \quad (\text{C.1.11}) \end{aligned}$$

$$\begin{aligned} I_{ij}^{R2} &= \lim_{\tilde{\rho} \rightarrow \infty} \int_{\rho_a}^{\tilde{\rho}} R_i R_j \frac{1}{\rho} \, d\rho \\ &= p_{ij} \lim_{\tilde{\rho} \rightarrow \infty} \int_{\rho_a}^{\tilde{\rho}} e^{-j2k_0\rho} \sum_{n=1}^{2N_R-1} s_n^{ij} \rho^{-1-n} \, d\rho \\ &= p_{ij} \sum_{n=1}^{2N_R-1} \frac{s_n^{ij}}{\rho_a^n} E_{(n+1)}(j2k_0\rho_a) \quad (\text{C.1.12}) \end{aligned}$$

$$\begin{aligned} I_{ij}^{R4} &= \lim_{\tilde{\rho} \rightarrow \infty} [R_i R_j \tilde{\rho}] \\ &= p_{ij} \lim_{\tilde{\rho} \rightarrow \infty} \left[ e^{-j2k_0\tilde{\rho}} \sum_{n=1}^{2N_R-1} \frac{s_n^{ij}}{\tilde{\rho}^{n-1}} \right] \\ &= p_{ij} s_1^{ij} \lim_{\tilde{\rho} \rightarrow \infty} \left[ e^{-j2k_0\tilde{\rho}} \right] \\ &= p_{ij} h_{i1} h_{j1} \tilde{L} \quad (\text{C.1.13}) \end{aligned}$$

$$\begin{aligned}
I_{ij}^{R3} &= \lim_{\tilde{\rho} \rightarrow \infty} \int_{\rho_a}^{\tilde{\rho}} R_i R_j \rho \, d\rho \\
&= p_{ij} \lim_{\tilde{\rho} \rightarrow \infty} \int_{\rho_a}^{\tilde{\rho}} e^{-j2k_0\rho} \sum_{n=1}^{2N_R-1} s_n^{ij} \rho^{1-n} \, d\rho \\
&= p_{ij} \lim_{\tilde{\rho} \rightarrow \infty} \left[ \frac{s_1^{ij}}{-j2k_0} \left( e^{-j2k_0\tilde{\rho}} - e^{-j2k_0\rho_a} \right) + \sum_{n=2}^{2N_R-1} \int_{\rho_a}^{\tilde{\rho}} e^{-j2k_0\rho} s_n^{ij} \rho^{1-n} \, d\rho \right] \\
&= p_{ij} \left[ j \frac{1}{2k_0} h_{i1} h_{j1} (\tilde{L} - L^a) + \sum_{n=2}^{2N_R-1} \frac{s_n^{ij}}{\rho_a^{n-2}} E_{(n-1)}(j2k_0\rho_a) \right] \quad (C.1.14)
\end{aligned}$$

since all terms containing negative powers of  $\tilde{\rho}$  vanish in the limit  $\tilde{\rho} \rightarrow \infty$ .

According to (3.4.18) the infinite element matrix entries are

$$\begin{aligned}
K_{ij} &= I_{ij}^{R1} I_{ij}^{A1} + I_{ij}^{R2} I_{ij}^{A2} - k_0^2 I_{ij}^{R3} I_{ij}^{A1} + jk_0 I_{ij}^{R4} I_{ij}^{A1} \\
&= \left[ I_{ij}^{R1} - k_0^2 I_{ij}^{R3} + jk_0 I_{ij}^{R4} \right] I_{ij}^{A1} + I_{ij}^{R2} I_{ij}^{A2} \\
&= p_{ij} \left[ -jk_0 h_{i1} h_{j1} (\tilde{L} - L^a) + \sum_{n=2}^{2N_R+1} \frac{f_n^{ij}}{\rho_a^{n-2}} E_{(n-1)}(j2k_0\rho_a) \right. \\
&\quad \left. + k_0^2 \sum_{n=2}^{2N_R-1} \frac{s_n^{ij}}{\rho_a^{n-2}} E_{(n-1)}(j2k_0\rho_a) + jk_0 h_{i1} h_{j1} \tilde{L} \right] I_{ij}^{A1} \\
&\quad + p_{ij} \left[ \sum_{n=1}^{2N_R-1} \frac{s_n^{ij}}{\rho_a^n} E_{(n+1)}(j2k_0\rho_a) \right] I_{ij}^{A2} \quad (C.1.15)
\end{aligned}$$

where it becomes clear that the undefined oscillatory terms  $\tilde{L}$  cancel and after simplifying the matrix entries become

$$\begin{aligned}
K_{ij} &= p_{ij} \left[ \sum_{n=2}^{2N_R+1} \frac{f_n^{ij}}{\rho_a^{n-2}} E_{(n-1)}(j2k_0\rho_a) + k_0^2 \sum_{n=2}^{2N_R-1} \frac{s_n^{ij}}{\rho_a^{n-2}} E_{(n-1)}(j2k_0\rho_a) \right] I_{ij}^{A1} \\
&\quad + jk_0 p_{ij} h_{i1} h_{j1} L^a I_{ij}^{A1} + p_{ij} \left[ \sum_{n=1}^{2N_R-1} \frac{s_n^{ij}}{\rho_a^n} E_{(n+1)}(j2k_0\rho_a) \right] I_{ij}^{A2}. \quad (C.1.16)
\end{aligned}$$

## C.2 Elemental Integrals - Complex Conjugate Weighted

The integrals arising from complex conjugated weighting are very similar to those for Galerkin weighting except for the absence of the exponential factor.

Consequently the elemental matrix entries are somewhat simplified as it no longer requires computing the exponential integral and the integrals can be evaluated analytically.

The derivative of  $\bar{R}_j$  with respect to  $\rho$  is simply

$$\frac{\partial \bar{R}_j}{\partial \rho} = e^{jk_0(\rho - \rho_i)} \sum_{n=1}^{N_R} \bar{g}_{in} \rho^{\frac{1}{2} - n} \quad (\text{C.2.1})$$

where  $g_{in}$  has the same definition as in (C.1.3). The product  $R_i \bar{R}_j$  is

$$R_i \bar{R}_j = q_{ij} \sum_{n=1}^{2N_R - 1} s_n^{ij} \rho^{-n} \quad (\text{C.2.2})$$

where

$$q_{ij} = e^{jk_0(\rho_i - \rho_j)} \quad (\text{C.2.3})$$

and  $s_n^{ij}$  is still defined by (C.1.5). The product of the derivatives of  $R_i$  and  $\bar{R}_j$  is

$$\frac{dR_i}{d\rho} \frac{d\bar{R}_j}{d\rho} = q_{ij} \sum_{n=1}^{2N_R + 1} d_n^{ij} \rho^{-n} \quad (\text{C.2.4})$$

where

$$d_n^{ij} = \begin{cases} \sum_{m=1}^n g_{im} \bar{g}_{j(n-m+1)} & n = 1, 2, \dots, (N_R + 1), \\ \sum_{m=n-N_R}^{N_R+1} g_{im} \bar{g}_{j(n-m+1)} & n = (N_R + 2), (N_R + 3), \dots, (2N_R + 1). \end{cases} \quad (\text{C.2.5})$$

Substituting these products in the definitions (3.4.19) through (3.4.22) after



letting  $R_j \rightarrow \bar{R}_j$  gives

$$\begin{aligned}
I_{ij}^{R1} &= \lim_{\tilde{\rho} \rightarrow \infty} \int_{\rho_a}^{\tilde{\rho}} \frac{dR_i}{d\rho} \frac{d\bar{R}_j}{d\rho} \rho \, d\rho \\
&= q_{ij} \lim_{\tilde{\rho} \rightarrow \infty} \int_{\rho_a}^{\tilde{\rho}} \sum_{n=1}^{2N_R+1} d_n^{ij} \rho^{1-n} \, d\rho \\
&= q_{ij} \lim_{\tilde{\rho} \rightarrow \infty} \left[ d_1^{ij} (\tilde{\rho} - \rho_a) + d_2^{ij} \ln \left| \frac{\tilde{\rho}}{\rho_a} \right| + \sum_{n=3}^{2N_R+1} \frac{d_n^{ij}}{\rho_a^{n-1} (2-n)} \right] \quad (\text{C.2.6})
\end{aligned}$$

$$\begin{aligned}
I_{ij}^{R2} &= \lim_{\tilde{\rho} \rightarrow \infty} \int_{\rho_a}^{\tilde{\rho}} R_i \bar{R}_j \frac{1}{\rho} \, d\rho \\
&= q_{ij} \lim_{\tilde{\rho} \rightarrow \infty} \int_{\rho_a}^{\tilde{\rho}} \sum_{n=1}^{2N_R-1} s_n^{ij} \rho^{-1-n} \, d\rho \\
&= q_{ij} \sum_{n=1}^{2N_R-1} \frac{s_n^{ij}}{\rho_a^n n} \quad (\text{C.2.7})
\end{aligned}$$

$$\begin{aligned}
I_{ij}^{R3} &= \lim_{\tilde{\rho} \rightarrow \infty} \int_{\rho_a}^{\tilde{\rho}} R_i \bar{R}_j \rho \, d\rho \\
&= q_{ij} \lim_{\tilde{\rho} \rightarrow \infty} \int_{\rho_a}^{\tilde{\rho}} \sum_{n=1}^{2N_R-1} s_n^{ij} \rho^{1-n} \, d\rho \\
&= q_{ij} \lim_{\tilde{\rho} \rightarrow \infty} \left[ s_1^{ij} (\tilde{\rho} - \rho_a) + s_2^{ij} \ln \left| \frac{\tilde{\rho}}{\rho_a} \right| + \sum_{n=3}^{2N_R-1} \frac{s_n^{ij}}{\rho_a^{n-1} (2-n)} \right] \quad (\text{C.2.8})
\end{aligned}$$

$$\begin{aligned}
I_{ij}^{R4} &= \lim_{\tilde{\rho} \rightarrow \infty} [R_i \bar{R}_j \tilde{\rho}] \\
&= q_{ij} \lim_{\tilde{\rho} \rightarrow \infty} \left[ \sum_{n=1}^{2N_R-1} \frac{s_n^{ij}}{\tilde{\rho}^{n-1}} \right] \\
&= q_{ij} s_1^{ij}. \quad (\text{C.2.9})
\end{aligned}$$

Although the undefined oscillatory terms do not appear in these expressions as for the Galerkin weighted infinite elements, there are still unbounded terms. Fortunately these unbounded terms cancel in the summation of (C.1.15). Sub-

stituting the above expressions for  $I_{ij}^{R1}$  through  $I_{ij}^{R4}$  into (C.1.15) gives

$$\begin{aligned}
K_{ij} &= I_{ij}^{R1} I_{ij}^{A1} + I_{ij}^{R2} I_{ij}^{A2} - k_0^2 I_{ij}^{R3} I_{ij}^{A1} + j k_0 I_{ij}^{R4} I_{ij}^{A1} \\
&= \left[ I_{ij}^{R1} - k_0^2 I_{ij}^{R3} + j k_0 I_{ij}^{R4} \right] I_{ij}^{A1} + I_{ij}^{R2} I_{ij}^{A2} \\
&= q_{ij} \left[ (d_1^{ij} - k_0^2 s_1^{ij})(\tilde{\rho} - \rho_a) + (d_2^{ij} - k_0^2 s_2^{ij}) \ln \left| \frac{\tilde{\rho}}{\rho_a} \right| \right. \\
&\quad \left. + \sum_{n=3}^{2N_R+1} \frac{d_n^{ij}}{\rho_a^{n-1}(2-n)} - k_0^2 \sum_{n=3}^{2N_R-1} \frac{s_n^{ij}}{\rho_a^{n-1}(2-n)} + j k_0 q_{ij} s_1^{ij} \right] I_{ij}^{A1} \\
&\quad + q_{ij} \left[ \sum_{n=1}^{2N_R-1} \frac{s_n^{ij}}{\rho_a^n n} \right] I_{ij}^{A2}. \tag{C.2.10}
\end{aligned}$$

By using the definitions (C.1.5) and (C.1.8) it is shown that the unbounded terms cancel out since

$$d_1^{ij} = g_{i1} \bar{g}_{j1} = k_0^2 h_{i1} h_{j1} = k_0^2 s_1^{ij} \tag{C.2.11}$$

$$d_2^{ij} = g_{i1} \bar{g}_{j2} + g_{i2} \bar{g}_{j1} = k_0^2 (h_{i1} h_{j2} + h_{i2} h_{j1}) = k_0^2 s_2^{ij} \tag{C.2.12}$$

and the expression for the matrix entries is simplified to

$$\begin{aligned}
K_{ij} &= q_{ij} \left[ \sum_{n=3}^{2N_R+1} \frac{d_n^{ij}}{\rho_a^{n-1}(2-n)} - k_0^2 \sum_{n=3}^{2N_R-1} \frac{s_n^{ij}}{\rho_a^{n-1}(2-n)} + j k_0 q_{ij} s_1^{ij} \right] I_{ij}^{A1} \\
&\quad + q_{ij} \left[ \sum_{n=1}^{2N_R-1} \frac{s_n^{ij}}{\rho_a^n n} \right] I_{ij}^{A2}. \tag{C.2.13}
\end{aligned}$$

## Appendix D

# 3D Infinite Element Integrals

In this section the explicit expressions for the three-dimensional infinite element matrix entries are given. The numerical integration used to evaluate some of the integrals and some singularities that arise are also discussed.

### D.1 Integrand Evaluations

In Section 5.4.3 the explicit expressions for the basis functions are given and are repeated here

$$\mathbf{N}_i = \begin{cases} e^{-jk_0(r-r_i)} \sum_{m=1}^{N_R} h_{im}^{(1)} r^{-m} \left( (s_i + t_i\phi)\hat{i}_\theta + (u_i + v_i\theta)\hat{i}_\phi \right) \ell_i & i = 1, 2, 3 \\ e^{-jk_0(r-r_i)} \sum_{m=1}^{N_R} h_{im}^{(2)} r^{-1-m} (A_i + B_i\theta + C_i\phi)\hat{i}_r & i = 4, 5, 6. \end{cases} \quad (\text{D.1.1})$$

The elemental matrix entries are calculated according to (5.3.5) by substituting the appropriate basis functions  $\mathbf{N}_i$  and  $\mathbf{N}_j$  into

$$\begin{aligned} K_{ij} &= \iiint_{\Omega_2} (\nabla \times \mathbf{N}_i) \cdot (\nabla \times \mathbf{N}_j) - k_0^2 \mathbf{N}_i \cdot \mathbf{N}_j \, d\Omega \\ &+ jk_0 \iint_{\Gamma_\infty} (\hat{i}_r \times \mathbf{N}_i) \cdot (\hat{i}_r \times \mathbf{N}_j) \, d\Gamma. \end{aligned} \quad (\text{D.1.2})$$

The curl operator in spherical coordinates is

$$\begin{aligned}\nabla \times \mathbf{N} &= \frac{1}{\sin(\theta)} \left[ \frac{\partial (\sin(\theta)N^\phi)}{\partial \theta} - \frac{\partial N^\theta}{\partial \phi} \right] \hat{i}_r \\ &+ \frac{1}{r} \left[ \frac{1}{\sin(\theta)} \frac{\partial N^r}{\partial \phi} - \frac{\partial (rN^\phi)}{\partial r} \right] \hat{i}_\theta \\ &+ \frac{1}{r} \left[ \frac{\partial (rN^\theta)}{\partial r} - \frac{\partial N^r}{\partial \theta} \right] \hat{i}_\phi\end{aligned}\quad (\text{D.1.3})$$

and taking the curl of the basis functions gives

$$\begin{aligned}\nabla \times \mathbf{N}_i &= \ell_i e^{-jk_0(r-r_i)} \sum_{m=1}^{N_R} h_{im}^{(1)} r^{-1-m} \left[ V_i f(\theta) + U_i \cos(\theta) \right] \hat{i}_r \\ &- \ell_i e^{-jk_0(r-r_i)} \sum_{m=1}^{N_R+1} g_{im}^{(1)} r^{-m} (u_i + v_i \theta) \hat{i}_\theta \\ &+ \ell_i e^{-jk_0(r-r_i)} \sum_{m=1}^{N_R+1} g_{im}^{(1)} r^{-m} (s_i + t_i \phi) \hat{i}_\phi\end{aligned}\quad (\text{D.1.4})$$

for  $i = 1, 2, 3$  and

$$\begin{aligned}\nabla \times \mathbf{N}_i &= e^{-jk_0(r-r_i)} \sum_{m=1}^{N_R} h_{im}^{(2)} r^{-2-m} \frac{C_i}{\sin(\theta)} \hat{i}_\theta \\ &- e^{-jk_0(r-r_i)} \sum_{m=1}^{N_R} h_{im}^{(2)} r^{-2-m} B_i \hat{i}_\phi\end{aligned}\quad (\text{D.1.5})$$

for  $i = 4, 5, 6$ . The function  $f(\theta) = 1 + \sin(\theta) + \theta \cos(\theta)$  and the coefficients  $g_{im}^{(1)}$  are given by

$$g_{im}^{(1)} = \begin{cases} -jk_0 h_{im}^{(1)} & m = 1, 2 \\ -jk_0 h_{im}^{(1)} - (m-2)h_{1(m-1)}^{(1)} & m = 3, 4, \dots, N_R \\ -(m-2)h_{i(m-1)}^{(1)} & m = N_R + 1. \end{cases}\quad (\text{D.1.6})$$

Using  $p_{ij} = e^{jk_0(r_i+r_j)}$  the dot-product  $(\nabla \times \mathbf{N}_i) \cdot (\nabla \times \mathbf{N}_j)$  becomes

$$\begin{aligned} (\nabla \times \mathbf{N}_i) \cdot (\nabla \times \mathbf{N}_j) &= \ell_i \ell_j p_{ij} e^{-j2k_0 r} \left[ \sum_{m=1}^{2N_R-1} {}^{(11)}H_m^{ij} r^{-3-m} g_1^{ij}(\theta) \right. \\ &\quad \left. + \sum_{m=1}^{2N_R+1} {}^{(11)}G_m^{ij} r^{-1-m} g_2^{ij}(\theta) \right] \end{aligned} \quad (\text{D.1.7})$$

for  $i, j = 1, 2, 3$

$$(\nabla \times \mathbf{N}_i) \cdot (\nabla \times \mathbf{N}_j) = -\ell_i p_{ij} e^{-j2k_0 r} \sum_{m=1}^{2N_R} {}^{(12)}F_m^{ij} r^{-3-m} g_3^{ij}(\theta, \phi) \quad (\text{D.1.8})$$

for  $i = 1, 2, 3$  and  $j = 4, 5, 6$

$$(\nabla \times \mathbf{N}_i) \cdot (\nabla \times \mathbf{N}_j) = -\ell_j p_{ji} e^{-j2k_0 r} \sum_{m=1}^{2N_R} {}^{(12)}F_m^{ji} r^{-3-m} g_3^{ji}(\theta, \phi) \quad (\text{D.1.9})$$

for  $i = 4, 5, 6$  and  $j = 1, 2, 3$  and

$$(\nabla \times \mathbf{N}_i) \cdot (\nabla \times \mathbf{N}_j) = p_{ij} e^{-j2k_0 r} \sum_{m=1}^{2N_R-1} {}^{(22)}H_m^{ij} r^{-5-m} g_4^{ij}(\theta, \phi) \quad (\text{D.1.10})$$

for  $i, j = 4, 5, 6$ . In the above the coefficients  ${}^{(11)}H_m^{ij}$ ,  ${}^{(22)}H_m^{ij}$ ,  ${}^{(11)}G_m^{ij}$  and  ${}^{(12)}F_m^{ij}$  are defined as

$${}^{(11)}H_m^{ij} = \begin{cases} \sum_{n=1}^m h_{in}^{(1)} h_{j(m-1+1)}^{(1)} & m = 1, 2, \dots, N_R \\ \sum_{n=m-N_R+1}^{N_R} h_{in}^{(1)} h_{j(m-1+1)}^{(1)} & m = (N_R + 1), \dots, (2N_R - 1) \end{cases} \quad (\text{D.1.11})$$

$${}^{(22)}H_m^{ij} = \begin{cases} \sum_{n=1}^m h_{in}^{(2)} h_{j(m-1+1)}^{(2)} & m = 1, 2, \dots, N_R \\ \sum_{n=m-N_R+1}^{N_R} h_{in}^{(2)} h_{j(m-1+1)}^{(2)} & m = (N_R + 1), \dots, (2N_R - 1) \end{cases} \quad (\text{D.1.12})$$

$${}^{(11)}G_m^{ij} = \begin{cases} \sum_{n=1}^m g_{in}^{(1)} g_{j(m-1+1)}^{(1)} & m = 1, 2, \dots, (N_R + 1) \\ \sum_{n=m-N_R}^{N_R+1} g_{in}^{(1)} g_{j(m-1+1)}^{(1)} & m = (N_R + 2), \dots, (2N_R + 1) \end{cases} \quad (\text{D.1.13})$$

$${}_{(12)}F_m^{ij} = \begin{cases} \sum_{n=1}^m g_{in}^{(1)} h_{j(m-1+1)}^{(2)} & m = 1, 2, \dots, N_R \\ \sum_{n=m-N_R+1}^{N_R+1} g_{in}^{(1)} h_{j(m-1+1)}^{(2)} & m = (N_R + 1), \dots, (2N_R) \end{cases} \quad (\text{D.1.14})$$

and the functions

$$\begin{aligned} g_1^{ij}(\theta) &= \frac{1}{\sin^2(\theta)} \left[ f^2(\theta) v_i v_j + f(\theta) \cos(\theta) (v_i u_j - v_j u_i) + \cos^2(\theta) u_i u_j \right] \\ g_2^{ij}(\theta, \phi) &= (u_i u_j + s_i s_j) + (u_i v_j + u_j v_i) \theta + (s_i t_j + s_j t_i) \phi + v_i v_j \theta^2 + t_i t_j \phi^2 \\ g_3^{ij}(\theta, \phi) &= \frac{(u_i + v_i \theta) C_j}{\sin(\theta)} + (s_i + t_i \phi) B_j \\ g_4^{ij}(\theta, \phi) &= \frac{C_i C_j}{\sin^2(\theta)} + B_i B_j. \end{aligned} \quad (\text{D.1.15})$$

The dot-product  $\mathbf{N}_i \cdot \mathbf{N}_j$  is

$$\mathbf{N}_i \cdot \mathbf{N}_j = \begin{cases} \ell_i \ell_j p_{ij} e^{-j2k_0 r} \sum_{m=1}^{2N_R-1} {}_{(11)}H_m^{ij} r^{-1-m} g_2^{ij}(\theta, \phi) & i, j = 1, 2, 3 \\ 0 & i = 1, 2, 3 \quad j = 4, 5, 6 \\ 0 & i = 4, 5, 6 \quad j = 1, 2, 3 \\ p_{ij} e^{-j2k_0 r} \sum_{m=1}^{2N_R-1} {}_{(22)}H_m^{ij} r^{-3-m} g_5^{ij}(\theta, \phi) & i, j = 4, 5, 6 \end{cases} \quad (\text{D.1.16})$$

where

$$\begin{aligned} g_5^{ij}(\theta, \phi) &= A_i A_j + (A_i B_j + A_j B_i) \theta + (A_i C_j + A_j C_i) \phi \\ &+ (B_i C_j + B_j C_i) \theta \phi + B_i B_j \theta^2 + C_i C_j \phi^2. \end{aligned} \quad (\text{D.1.17})$$

The cross-product  $\hat{i}_r \times \mathbf{N}_i$  is

$$\hat{i}_r \times \mathbf{N}_i = \begin{cases} \ell_i e^{-jk_0(r-r_i)} \sum_{m=1}^{N_R} h_{im}^{(1)} r^{-m} \left[ (s_i + t_i \phi) \hat{i}_\phi - (u_i + v_i \theta) \hat{i}_\theta \right] & i = 1, 2, 3 \\ 0 & i = 4, 5, 6 \end{cases} \quad (\text{D.1.18})$$

which means the dot-product  $(\hat{i}_r \times \mathbf{N}_i) \cdot (\hat{i}_r \times \mathbf{N}_j)$  becomes

$$(\hat{i}_r \times \mathbf{N}_i) \cdot (\hat{i}_r \times \mathbf{N}_j) = \begin{cases} \ell_i \ell_j p_{ij} e^{-j2k_0 r} \sum_{m=1}^{2N_R-1} {}^{(11)}H_m^{ij} r^{-1-m} g_2^{ij}(\theta, \phi) & i, j = 1, 2, 3 \\ 0 & i, j \neq 1, 2, 3. \end{cases} \quad (\text{D.1.19})$$

Finally the above expressions can be substituted into the integrals in (D.1.2). For  $i, j = 1, 2, 3$  and substituting the spherical differentials  $d\Gamma \rightarrow r^2 \sin(\theta) d\theta d\phi$  and  $d\Omega \rightarrow r^2 \sin(\theta) d\phi d\theta dr$  gives

$$\begin{aligned} K_{ij} = & \ell_i \ell_j p_{ij} \lim_{\tilde{r} \rightarrow \infty} \left\{ \int_{r_a}^{\tilde{r}} e^{-j2k_0 r} \sum_{m=1}^{2N_R-1} {}^{(11)}H_m^{ij} r^{-1-m} dr \iint_S g_1^{ij}(\theta) \sin(\theta) d\theta d\phi \right. \\ & + \left[ \int_{r_a}^{\tilde{r}} e^{-j2k_0 r} \left( \sum_{m=1}^{2N_R+1} {}^{(11)}G_m^{ij} r^{1-m} - k_0^2 \sum_{m=1}^{2N_R-1} {}^{(11)}H_m^{ij} r^{1-m} \right) dr \right. \\ & \left. \left. + jk_0 e^{-j2k_0 r} \sum_{m=1}^{2N_R-1} {}^{(11)}H_m^{ij} r^{1-m} \right] \iint_S g_2^{ij}(\theta, \phi) \sin(\theta) d\theta d\phi \right\} \quad (\text{D.1.20}) \end{aligned}$$

where  $S$  is the solid angle between the vertices of the triangular footprint of the infinite element. Using  $I_f^S$  to denote the integral of the function  $f(\theta, \phi)$  over the solid angle  $S$  and the definition of the  $E_n$  function (A.2.3) gives

$$\begin{aligned} K_{ij} = & \ell_i \ell_j p_{ij} \left\{ I_{g_1^{ij}}^S \sum_{m=1}^{2N_R-1} \frac{{}^{(11)}H_m^{ij}}{r_a^m} E_{(m+1)}(j2k_0 r_a) \right. \\ & + I_{g_2^{ij}}^S \left[ \sum_{m=2}^{2N_R+1} \frac{{}^{(11)}G_m^{ij}}{r_a^{m-2}} E_{(m-1)}(j2k_0 r_a) \right. \\ & \left. - k_0^2 \sum_{m=1}^{2N_R-1} \frac{{}^{(11)}H_m^{ij}}{r_a^{m-2}} E_{(m-1)}(j2k_0 r_a) \right] \\ & + \lim_{\tilde{r} \rightarrow \infty} e^{-j2k_0 \tilde{r}} \left[ \frac{{}^{(11)}G_1^{ij}}{-j2k_0} - k_0^2 \frac{{}^{(11)}H_1^{ij}}{-j2k_0} + jk_0 {}^{(11)}H_1^{ij} \right] I_{g_2^{ij}}^S \\ & \left. - e^{-j2k_0 r_a} \left[ \frac{{}^{(11)}G_1^{ij}}{-j2k_0} - k_0^2 \frac{{}^{(11)}H_1^{ij}}{-j2k_0} \right] I_{g_2^{ij}}^S \right\}. \quad (\text{D.1.21}) \end{aligned}$$

Evaluation of the terms inside the square brackets inside the limit show that the entire factor is zero. Thus it is shown that the undefined oscillatory terms

cancel. Finally an expression is obtained for  $K_{ij}$  where  $i, j = 1, 2, 3$

$$\begin{aligned}
K_{ij} = & \ell_i \ell_j p_{ij} \left\{ I_{g_1^S}^{ij} \sum_{m=1}^{2N_R-1} \frac{{}^{(11)}H_m^{ij}}{r_a^m} E_{(m+1)}(j2k_0 r_a) \right. \\
& - I_{g_2^S}^{ij} \left[ e^{-j2k_0 r_a} j k_0 h_{i1} h_{j1} - \sum_{m=2}^{2N_R+1} \frac{{}^{(11)}G_m^{ij}}{r_a^{m-2}} E_{(m-1)}(j2k_0 r_a) \right. \\
& \left. \left. + k_0^2 \sum_{m=1}^{2N_R-1} \frac{{}^{(11)}H_m^{ij}}{r_a^{m-2}} E_{(m-1)}(j2k_0 r_a) \right] \right\}. \tag{D.1.22}
\end{aligned}$$

For  $i = 1, 2, 3$  and  $j = 4, 5, 6$  substitution of the basis functions into the expression for  $K_{ij}$  gives

$$\begin{aligned}
K_{ij} = & -\ell_i p_{ij} \lim_{\tilde{r} \rightarrow \infty} \int_{r_a}^{\tilde{r}} e^{-j2k_0 r} \sum_{m=1}^{2N_R} {}^{(12)}F_m^{ij} r^{-1-m} dr \iint_S g_3^{ij}(\theta, \phi) \sin(\theta) d\theta d\phi \\
= & -\ell_i p_{ij} I_{g_3^S}^{ij} \sum_{m=1}^{2N_R} \frac{{}^{(12)}F_m^{ij}}{r_a^m} E_{(m+1)}(j2k_0 r_a) \tag{D.1.23}
\end{aligned}$$

and for  $i = 4, 5, 6$  and  $j = 1, 2, 3$  the indices  $i$  and  $j$  are simply swapped in the above. Finally, for  $i, j = 4, 5, 6$  the matrix entries are

$$\begin{aligned}
K_{ij} = & p_{ij} \lim_{\tilde{r} \rightarrow \infty} \int_{r_a}^{\tilde{r}} e^{-j2k_0 r} \sum_{m=1}^{2N_R-1} {}^{(22)}H_m^{ij} r^{-3-m} dr \iint_S g_4^{ij}(\theta, \phi) \sin(\theta) d\theta d\phi \\
& - k_0^2 p_{ij} \lim_{\tilde{r} \rightarrow \infty} \int_{r_a}^{\tilde{r}} e^{-j2k_0 r} \sum_{m=1}^{2N_R-1} {}^{(22)}H_m^{ij} r^{-1-m} dr \iint_S g_5^{ij}(\theta, \phi) \sin(\theta) d\theta d\phi \\
= & p_{ij} I_{g_4^S}^{ij} \sum_{m=1}^{2N_R-1} \frac{{}^{(22)}H_m^{ij}}{r_a^{m+2}} E_{(m+3)}(j2k_0 r_a) \\
& - p_{ij} I_{g_5^S}^{ij} k_0^2 \sum_{m=1}^{2N_R-1} \frac{{}^{(22)}H_m^{ij}}{r_a^m} E_{(m+1)}(j2k_0 r_a). \tag{D.1.24}
\end{aligned}$$

The elemental matrix entries are now in a form that can be evaluated using standard numerical integration techniques.



## D.2 Gauss-Legendre Quadrature on Triangular Elements

From the results of the previous section it is clear that some of the integrals that have to be evaluated cannot be solved analytically and a numerical integration scheme has to be employed. Gauss-Legendre integration is employed to this end and the method is briefly discussed here.

In order to evaluate the angular integrals of (D.1.22) through (D.1.24) numerically the integrals over the solid angle  $S$  subtended by the base of the infinite elements are first written in a simpler form

$$I_g^S = \iint_S g(\theta, \phi) \sin(\theta) d\phi d\theta = \iint_S h(\theta, \phi) d\phi d\theta \quad (\text{D.2.1})$$

where the integrand is now  $h(\theta, \phi)$ . In this form the integral over  $S$  is equivalent to a planar triangular surface. This triangular surface is mapped to a standard triangle as shown in Figure D.1. The mapping function is easily obtained using simplex coordinates on the triangular surface defined in terms of  $(\theta, \phi)$  and by letting  $x$  and  $y$  equal the simplex which evaluate to unity at  $(\theta_3, \phi_3)$  and  $(\theta_2, \phi_2)$ , respectively. Defining the forward transformations as

$$x = T_x(\theta, \phi) = A_x + B_x\theta + C_x\phi \quad (\text{D.2.2})$$

$$y = T_y(\theta, \phi) = A_y + B_y\theta + C_y\phi \quad (\text{D.2.3})$$

the backward transformations can easily be found by solving for  $\theta$  and  $\phi$  which gives

$$\theta = T_\theta(x, y) = A_\theta + B_\theta x + C_\theta y \quad (\text{D.2.4})$$

$$\phi = T_\phi(x, y) = A_\phi + B_\phi x + C_\phi y \quad (\text{D.2.5})$$

$$J_{xy}(x, y) = \left\| \frac{\partial(\theta, \phi)}{\partial(x, y)} \right\| = B_\theta C_\phi - B_\phi C_\theta. \quad (\text{D.2.6})$$

Now the integral over  $S$  becomes

$$\begin{aligned} \iint_S h(\theta, \phi) d\phi d\theta &= \int_0^1 \int_0^{1-x} h\left(T_\theta(x, y), T_\phi(x, y)\right) J_{xy}(x, y) dx dy \\ &= \int_0^1 \int_0^{1-x} H(x, y) dx dy. \end{aligned} \quad (\text{D.2.7})$$

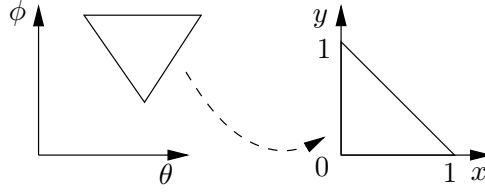


**Figure D.1:** Mapping from arbitrary triangle to standard triangle.

Following the procedure described in [48] the triangular surface in Figure D.1 is mapped to a square centred about the origin as shown in Figure D.2 using the transformation

$$x = U_x(\xi, \eta) = \frac{1 + \xi}{2} \quad (\text{D.2.8})$$

$$y = U_y(\xi, \eta) = \left(\frac{1 - \xi}{4}\right) (1 + \eta) \quad (\text{D.2.9})$$

$$J_{\xi\eta}(\xi, \eta) = \left\| \frac{\partial(x, y)}{\partial(\xi, \eta)} \right\| = \frac{1 - \xi}{8}. \quad (\text{D.2.10})$$

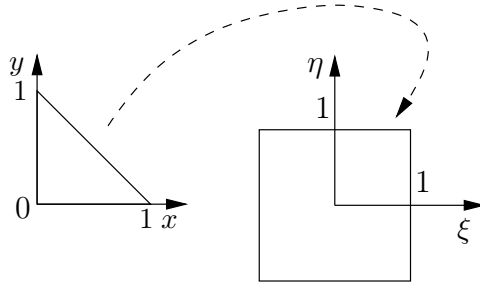


**Figure D.2:** Mapping from standard triangle to standard square.

Using these definitions for  $x$  and  $y$  in (D.2.7) and using an  $M$ -point quadrature rule for each variable gives

$$\begin{aligned} \iint_S h(\theta, \phi) d\phi d\theta &= \int_{-1}^1 \int_{-1}^1 H\left(U_x(\xi, \eta), U_y(\xi, \eta)\right) J_{\xi\eta}(\xi, \eta) d\xi d\eta \\ &= \sum_i^M \sum_j^M w_i w_j H\left(U_x(\xi_i, \eta_j), U_y(\xi_i, \eta_j)\right) J_{\xi\eta}(\xi_i, \eta_j) \\ &= \sum_{k=1}^{N=M \times M} c_k H(x_k, y_k) \end{aligned} \quad (\text{D.2.11})$$

where each  $k$  corresponds to a unique pair  $(ij)$  and

$$c_k = w_i w_j J_{\xi\eta}(\xi_i, \eta_j) \quad (\text{D.2.12})$$

$$x_k = U_x(\xi_i, \eta_j) \quad (\text{D.2.13})$$

$$y_k = U_y(\xi_i, \eta_j). \quad (\text{D.2.14})$$

The weights  $w_i, w_j$  and sample points  $\xi_i, \eta_j$  are chosen using Gauss-Legendre quadrature. Legendre polynomials are especially suited for this method as the zeros of these polynomials of all orders are all in the range  $(-1, 1)$ . That is, an arbitrary order quadrature rule can be applied. The sample points  $\xi_i$  for  $M$ -point quadrature are then simply the zeros of the polynomial  $P_M(\xi)$  and the optimal weight  $w_i$  associated with each of the roots  $\xi_i$  is given by

$$w_i = \frac{2(1 - \xi_i^2)}{(n+1)^2 [P_{M+1}(\xi_i)]^2}. \quad (\text{D.2.15})$$

Similarly the sample points  $\eta_j$  and corresponding weights  $w_j$  are determined.

The roots of the Legendre-polynomial are found using Laguerre's method [49] which converges to a complex root of a polynomial from any starting point. This method proceeds as follows. For an  $n$ th order polynomial  $f_n(x)$ , define

$$G(x) = \frac{f'_n(x)}{f_n(x)} \quad (\text{D.2.16})$$

$$H(x) = \left[ \frac{f'_n(x)}{f_n(x)} \right]^2 - \frac{f''_n(x)}{f_n(x)}. \quad (\text{D.2.17})$$

The distance from the root  $x_r$  to the current guess  $x_i$  is assumed to be

$$\alpha = x_r - x_i \quad (\text{D.2.18})$$

where  $\alpha$  can also be expressed as

$$\alpha = \frac{n}{\max \left( G \pm \sqrt{(n-1)(nH - G^2)} \right)}. \quad (\text{D.2.19})$$

Starting with an initial guess  $x_0$ , initial values for  $G(x_0)$  and  $H(x_0)$  are obtained which gives a first value for  $\alpha$ . Consequently the next guess  $x_1$  can be obtained using (D.2.18). The approximation to the root  $x_r$  is considered accurate when  $\alpha$  becomes sufficiently small.

### D.3 Integration of Singular Functions

From the definitions in (D.1.7) and (D.1.15) it is clear that the integrands of  $I_{g_1^{ij}}^S$  and  $I_{g_4^{ij}}^S$  become singular at  $\theta = 0, \pi$ . As in [3] where the numeric integration of similar singularities is discussed, it is shown here that these integrals evaluate to a finite value.

The singular integrands are of the form

$$f(\theta) = \frac{1}{\sin(\theta)} (1 + \cos(\theta) + \theta \cos(\theta) + \cos^2(\theta) + \theta^2 \cos^2(\theta)). \quad (\text{D.3.1})$$

Using the approximations  $\sin(\theta) \approx \theta$  and  $\cos(\theta) \approx 1$  for small  $\theta$  the singular integrands reduce to the simplified form

$$f(\theta) \approx \frac{1}{\theta}. \quad (\text{D.3.2})$$

Now consider integrating this function over a triangular surface  $A$  with one vertex at the origin. The integral becomes

$$\iint_A f(\theta) \, d\phi \, d\theta = \int_0^1 \int_0^\theta \frac{1}{\theta} \, d\phi \, d\theta. \quad (\text{D.3.3})$$

By a simple substitution  $\phi = \theta u$  this integral is transformed to an integral over a square as the limits become  $(0, \theta) \rightarrow (0, 1)$  and the singularity is removed since  $d\phi = \theta \, du$

$$\iint_A f(\theta) \, d\phi \, d\theta = \int_0^1 \int_0^1 \, du \, d\theta = 1. \quad (\text{D.3.4})$$

Similarly the singularity at  $\theta = \pi$  can be removed.

Since the singularity is assumed to be at a vertex of the triangle, using Gauss-Legendre quadrature never results in sampling the integrand at the singular point. Table D.1 gives the numerical values obtained for integrating (D.3.3) using Gauss-Legendre quadrature of varying orders. Using a five-point quadrature rule (as for the implementation discussed in Section 5.4.5) results in an error of less than 3% and this is considered sufficiently accurate.

Quadrature order	Result	Percentage error
3	0.9361	6.39%
5	0.9738	2.62%
7	0.9858	1.42%
9	0.9912	0.88%

**Table D.1:** Accuracy of Gauss-Legendre quadrature over a triangle with a singularity at a vertex.

# Bibliography

- [1] P. P. Silvester and G. Pelosi, *Finite Elements for Wave Electromagnetics*. Piscataway, NJ: IEEE Press, 1994.
- [2] R. L. Courant, “Variational methods for the solution of problems of equilibrium and vibration.” *Bulletin of the American Mathematical Society*, vol. 49, pp. 1–23, 1943.
- [3] J. M. Jin, *The Finite Element Method in Electromagnetics*, 2nd ed. New York, NY: Wiley, 2002.
- [4] P. P. Silvester, “Finite-element solution of homogeneous waveguide problems.” *Alta Frequenza*, vol. 38, pp. 313–317, 1969.
- [5] O. C. Zienkiewicz, *The Finite Element Method*. London, UK: McGraw-Hill, 1977.
- [6] P. P. Silvester and R. L. Ferrari, *Finite Elements for Electrical Engineers*. Cambridge, UK: Cambridge University Press, 1983.
- [7] D. B. Davidson, *Computational Electromagnetics for RF and Microwave Engineering*. Cambridge, UK: Cambridge University Press, 2005.
- [8] C. A. Balanis, *Advanced Engineering Electromagnetics*, 1st ed. Hoboken, NJ: Wiley, 1989.
- [9] G. S. Smith, *An Introduction to Classical Electromagnetic Radiation*. Cambridge, UK: Cambridge University Press, 1997.
- [10] P. P. Silvester and M.-S. Hsieh, “Finite-element solution of 2-dimensional exterior-field problems.” *PROC. IEE*, vol. 118, no. 12, pp. 1743–1747, Dec. 1971.

- [11] B. H. McDonald and A. Wexler, "Finite-element solution of unbounded field problems." *IEEE Trans. Microwave Theory Tech.*, vol. 20, no. 12, pp. 841–847, Dec. 1972.
- [12] M. J. McDougall and J. P. Webb, "Infinite elements for the analysis of open dielectric waveguides." *IEEE Trans. Microwave Theory Tech.*, vol. 37, no. 11, pp. 1724–1731, Nov. 1989.
- [13] M. S. Towers, A. McCowen, and J. A. R. Macnab, "Electromagnetic scattering from an arbitrary inhomogeneous 2D object - a finite and infinite element solution." *IEEE Trans. Antennas Propagat.*, vol. 41, no. 6, pp. 770–777, June 1993.
- [14] S. Gratkowski, L. P. Pichon, and A. Razek, "New infinite elements for a finite element analysis of 2D scattering problems." *IEEE Trans. Magn.*, vol. 32, no. 3, pp. 882–885, May 1996.
- [15] P. P. Silvester, D. A. Lowther, C. J. Carpenter, and E. A. Wyatt, "Exterior finite elements for 2-dimensional exterior-field problems." *IEE Proceedings-H*, vol. 118, pp. 1267–1270, 1977.
- [16] B. Engquist and A. Majda, "Absorbing boundary conditions for the numerical simulation of waves." *Math. Comput.*, vol. 31, pp. 629–651, July 1977.
- [17] A. Bayliss and E. Turkel, "Radiation boundary conditions for wave-like equations." *Communications on Pure and Applied Mathematics*, vol. 33, no. 6, pp. 707–725, Nov. 1980.
- [18] A. F. Peterson and S. P. Castillo, "A frequency-domain differential equation formulation for electromagnetic scattering from inhomogeneous cylinders." *IEEE Trans. Antennas Propagat.*, vol. 37, no. 5, pp. 601–607, May 1989.
- [19] J.-P. Berenger, "A perfectly matched layer for the absorption of electromagnetic waves." *J. Comp. Phys.*, vol. 114, no. 2, pp. 185–200, Oct. 1994.
- [20] A. F. Peterson, "'Interior resonance' problem associated with surface integral equations of electromagnetics: Numerical consequences and a survey of remedies." *Electromagnetics*, vol. 10, no. 3, 1990.

- [21] A. J. Poggio and E. K. Miller, "Integral equation solutions of three-dimensional scattering problems," in *Computer Techniques for Electromagnetics*, R. Mittra, Ed. Braunschweig, Germany: Pergammon Press, 1973.
- [22] A. Sommerfeld, "Partial differential equations in physics," in *Pure and Applied Mathematics*, P. A. Smith and S. Eilenberg, Eds. New York, NY: Academic Press Inc., 1957, vol. 1.
- [23] J. K. Byun and J. M. Jin, "A comparative study of infinite elements for two-dimensional electromagnetics scattering analysis." *Electromagnetics*, vol. 24, no. 4, pp. 219–236, May/June 2004.
- [24] A. Charles, M. S. Towers, and A. McCowen, "A general infinite element for terminating finite element meshes in electromagnetic scattering prediction." *IEEE Trans. Magn.*, vol. 34, no. 5, pp. 3367–3370, Sept. 1998.
- [25] A. Young and D. B. Davidson, "A comparison of mesh termination schemes for 2D scattering analysis using the finite element method." in *Proc. IEEE AFRICON 2007*, Windhoek, Namibia, Sept. 2007.
- [26] R. Lee and A. C. Cangellaris, "A study of discretization errors in the finite element approximation of wave solutions." *IEEE Trans. Antennas Propagat.*, vol. 40, no. 5, pp. 542–549, May 1992.
- [27] P. A. Raviart and J. M. Thomas, "A mixed finite element method for 2nd order elliptic problems." in *Lecture Notes on Mathematics*, I. Galligani and E. Mayera, Eds. New York, NY: Springer-Verlag, 1977, vol. 606, pp. 293–315.
- [28] J. C. Nedelec, "Mixed finite elements in  $\mathbb{R}^3$ ." *Numerische Mathematik*, vol. 35, pp. 315–341, 1980.
- [29] A. Bossavit and J. C. Verite, "Mixed FEM-BIEM method to solve 3-D eddy-current problems." *IEEE Trans. Magn.*, vol. MAG 18, no. 2, pp. 431–435, Mar. 1981.
- [30] M. L. Barton and Z. J. Cendes, "New vector finite elements for three-dimensional magnetic field computation." *J. Appl. Phys.*, vol. 61, no. 8, pp. 3919–3921, Apr. 1987.



- [31] J. P. Webb, "Edge elements and what they can do for you." *IEEE Trans. Magn.*, vol. 29, no. 2, pp. 1460–1465, Mar. 1993.
- [32] Z. J. Cendes, "Vector finite elements for electromagnetic field computation." *IEEE Trans. Magn.*, vol. 27, no. 5, pp. 3958–3966, Sept. 1991.
- [33] J. P. Webb, "Hierarchical vector basis functions of arbitrary order for triangular and tetrahedral finite elements." *IEEE Trans. Antennas Propagat.*, vol. 47, no. 8, pp. 1244–1253, Aug. 1999.
- [34] A. F. Peterson, "Absorbing boundary conditions for the vector wave equation." *Microwave and Optical Letters*, vol. 1, no. 2, pp. 62–64, Apr. 1988.
- [35] J.-P. Berenger, "Three-dimensional perfectly matched layer for the absorption of electromagnetic waves." *J. Comp. Phys.*, vol. 127, no. 2, pp. 363–379, Sept. 1996.
- [36] X. Yuan, D. R. Lynch, and J. W. Strohbehn, "Coupling of finite element and moment methods for electromagnetic scattering from inhomogeneous objects." *IEEE Trans. Antennas Propagat.*, vol. 38, no. 3, pp. 386–393, Mar. 1990.
- [37] J. K. Byun and J. M. Jin, "Finite element analysis of scattering from a complex BOR using spherical infinite elements." *Electromagnetics*, vol. 25, no. 4, pp. 267–204, May/June 2005.
- [38] K. Gerdes and L. Demkowicz, "Solution of 3D-Laplace and Helmholtz equations in exterior domains using *hp*-infinite elements." *Comp. Methods Appl. Mech. Engrg.*, vol. 137, pp. 239–273, Nov. 1996.
- [39] W. Cecot, W. Rachowicz, and L. Demkowicz, "An *hp*-adaptive finite element method for electromagnetics. Part 3: A three-dimensional infinite element for Maxwell's equations." *Int. J. Numer. Meth. Engng*, vol. 57, no. 7, pp. 899–921, June 2003.
- [40] A. Young and D. B. Davidson, "A three-dimensional infinite element compatible with tetrahedral vector finite elements." *IEEE Trans. Antennas Propagat.*, to be submitted.
- [41] D. S. Jones, *The Theory of Electromagnetism*. New York, NY: Pergamon Press, 1964.

- [42] D. B. Davidson and M. M. Botha, "Evaluation of a spherical PML for vector FEM applications." *IEEE Trans. Antennas Propagat.*, vol. 55, no. 2, pp. 494–498, Feb. 2007.
- [43] E. W. Weisstein. (2007, Aug.) Bessel function. Mathworld, Wolfram Research. Champaigne, IL. [Online]. Available: <http://mathworld.wolfram.com/BesselFunction.html>
- [44] ——. (2007, Aug.) Hankel function. Mathworld, Wolfram Research. Champaigne, IL. [Online]. Available: <http://mathworld.wolfram.com/HankelFunction.html>
- [45] ——. (2007, Aug.) Riccati-bessel functions. Mathworld, Wolfram Research. Champaigne, IL. [Online]. Available: <http://mathworld.wolfram.com/Riccati-BesselFunctions.html>
- [46] ——. (2007, Aug.) En-function. Mathworld, Wolfram Research. Champaigne, IL. [Online]. Available: <http://mathworld.wolfram.com/En-Function.html>
- [47] ——. (2007, Aug.) Legendre polynomial. Mathworld, Wolfram Research. Champaigne, IL. [Online]. Available: <http://mathworld.wolfram.com/LegendrePolynomial.html>
- [48] H. T. Rathod, K. V. Nagaraja, B. Venkatesudu, and N. L. Ramesh, "Gauss legendre quadrature over a triangle." *J. Indian Inst. Sci.*, vol. 84, no. 5, pp. 183–188, Sept./Oct. 2004.
- [49] E. W. Weisstein. (2007, Aug.) Laguerre's method. Mathworld, Wolfram Research. Champaigne, IL. [Online]. Available: <http://mathworld.wolfram.com/LaguerresMethod.html>